2017

QUANTUM INSPIRED SYMMETRIES IN LASER ENGINEERING

Mohammad Hosain Teimourpour
Michigan Technological University, mteimour@mtu.edu

QUANTUM INSPIRED SYMMETRIES IN LASER ENGINEERING

By

Mohammad Hosain Teimourpour

A DISSERTATION

Submitted in partial fulfillment of the requirements for the degree of

DOCTOR OF PHILOSOPHY

In Applied Physics

MICHIGAN TECHNOLOGICAL UNIVERSITY

2017

This dissertation has been approved in partial fulfillment of the requirements for the Degree of DOCTOR OF PHILOSOPHY in Applied Physics.

Department of Physics

Dissertation Advisor:	*Prof. Ramy El-Ganainy*
Committee Member:	*Prof. Miguel Levy*
Committee Member:	*Prof. Jae Yong Suh*
Committee Member:	*Prof. Durdu Guney*
Department Chair:	*Prof. Ravindra Pandey*

Dedication

To my beloved parents, who taught me to read.

Mom! my heart will always be tied to yours.

In the memory of my father who passed away ...

Contents

List of Figures

List of Tables

Acknowledgments

I would like to extend my sincerest gratitude and appreciation to my parents for their endless love, patience, sacrifice, and efforts in my life and education path. All the support they have provided me over the years was the greatest gift anyone has ever given me. It is just due to their hard work, unlimited persistence and dedication to my education that I achieved one of the highest level of education. It is impossible to thoroughly thank those patient souls who helped me to accomplish my dreams and no words can express my sincere appreciations. To them I am greatly indebted forever.

I would like to express my appreciations to my uncle Saeed who played an important role in my life and especially education. He taught me how to be strong, dedicated, and organized in every aspect of life. He is the one who showed me the beauty of science, when I was just a kid. To him all my love and sincerest acknowledgments.

I also appreciate all my brothers who were always my real friends. I am grateful for all their love, supports and friendships.

I would like to especially thank my adviser Professor Ramy El-Ganainy for everything he taught me. His dedication, patience, drive and kindness makes him unique among all of my teachers. He is not just my scientific adviser but also my brother and

caring friend. He is the one who helped and supported me whenever I needed. In all scientific projects that he involved me, we had very fruitful discussions and he was always entangled in all details from initiating the idea, developing the theory to even performing the numerical simulations.

My especial thanks also goes to Professor Demetrios Christodoulides for his patience in answering my questions and always treating me like a son during my interaction with him.

I also appreciate Professor Ravindra Pandey, chair of Physics Department at Michigan Technological University and Professor Jacek Borysow coordinator of Henes Center for Quantum Phenomena, for their supports during my PhD.

Finally, I thank all faculty and staff of Physics Department at Michigan Technological University for their great efforts in helping and supporting me. They all deserve a special thanks because they have been like a second family to me.

Abstract

In this thesis, quantum inspired symmetries including Parity-Time (PT) symmetry and Supersymmetry (SUSY) have been studied in the context of non-Hermitian engineered laser systems. This thesis starts with a short review of semiconductor lasers theory in second chapter, followed by an introduction to quantum inspired symmetries: PT symmetry and SUSY in optics and photonics in chapter three.

In chapter four, we have studied the robustness and mode selectivity in PT symmetric lasers. We investigate two important aspects of PT symmetric photonic molecule lasers, namely the robustness of their single longitudinal mode operation against instabilities triggered by spectral hole burning effects, and the possibility of more versatile mode selectivity. Our results, supported by numerically integrating the nonlinear rate equations and performing linear stability analysis, reveals the following: (1) In principle a second threshold exists after which single mode operation becomes unstable, signaling multimode oscillatory dynamics, (2) For a wide range of design parameters, single mode operation of PT lasers having relatively large free spectral range (FSR) can be robust even at higher gain values, (3) PT symmetric photonic molecule lasers are more robust than their counterpart structures made of single microresonators; and (4) Extending the concept of single longitudinal mode operation based on PT symmetry in millimeter long edge emitting lasers having smaller FSR can

be challenging due to instabilities induced by nonlinear modal interactions. Finally we also present a possible strategy based on loss engineering to achieve more control over the mode selectivity by suppressing the mode that has the highest gain (i.e. lies under the peak of the gain spectrum curve) and switch the lasing action to another mode.

In chapter five a new scheme for building two dimensional laser arrays that operate in the single supermode regime is proposed. This is done by introducing an optical coupling between the laser array and a lossy pseudo-isospectral chain of photonic resonators. The spectrum of this discrete reservoir is tailored to suppress all the supermodes of the main array except the fundamental one. This spectral engineering is facilitated by employing the Householder transformation in conjunction with discrete supersymmetry. The proposed scheme is general and can in principle be used in different platforms such as VCSEL arrays and photonic crystal laser arrays.

Finally, in chapter six we have investigated the laser self-termination (LST) in trimer photonic molecules. It is shown that under the appropriate conditions, LST can exist in complex discrete structures made of three-cavity photonic molecule lasers. We have shown that the phenomenon of LST is a purely linear effect associated with avoided level crossings. Furthermore, our simulations show that the predicted behavior is persistent when gain saturation nonlinearity is taken into account.

Conclusion remarks and future works are discussed in the last chapter.

Chapter 1

Introduction

The research field of optics and photonics has been one of the most active areas in the past several decades. The invention of lasers, fiber optics and the experimental progress in nonlinear and quantum optics along with the unprecedented progress in fabrication technology has put this field at the forefront of science and engineering. In the last two decades, considerable efforts have been dedicated to develop new concepts and material systems such as photonic crystals, plasmonics, metamaterial and exciton-polariton platforms. Recently, a new paradigm for engineering new photonics structures with novel functionalities has emerged. The corner stone of these new research direction is the formal analogies between Schrodinger equation and Maxwells equations under certain conditions. Particularly, even though the former is concerned with describing the microscopic world and the latter describe classical light, both share

the same underlying mathematics of wave phenomena. This correspondence has been recently utilized to map and test some concepts from condensed matter physics to optics. This mapping provide several advantages: (1) it allows the observation of new phenomena that could be otherwise hindered by many-body interactions in solid state systems; (2) Allows for the control of these interactions to investigate even more complex scenarios; and (3) Provide new avenues for engineering new photonic functionalities. Examples of such mapping in the past are Bloch oscillations and Anderson localization. Very recently, two new concepts that originated from quantum mechanics have been employed in optics, namely parity time (PT) symmetry and supersymmetry. This in turn led to intense activities to explore the potential of these notions to engineer novel photonic devices and controlling light-matter interactions in ways that would have been impossible (or at least difficult) otherwise. Emerging applications in microlaser, sensing and laser arrays are just few examples.

In this thesis we have investigated some of these concepts in along with some of their potential applications. This thesis is organized as follows. In chapter 2 we present a brief overview of semiconductor laser physics and engineering. In chapter 3 we review the mathematics of PT symmetry and supersymmetry along with some of the related concepts in laser theory. In Chapter 4, we present our work dealing with the robustness and mode selectivity in PT symmetric microring lasers. Our work on the utilization of supersymmetry to engineer two dimensional phase-locked laser arrays operating in the single mode regime is the topic of chapter 5. The curious phenomena

of laser self-termination in complex photonic molecules is studied in chapter 6. Finally, chapter 7 presents a conclusion and outlook for future work.

Chapter 2

Semiconductor lasers theory

In this chapter we review the fundamental and basic concepts of laser theory as they apply to semiconductor lasers [1, 2, 3, 4]. Generally a laser is an externally pumped self-sustained oscillator which is consist of an active (gain) medium placed inside an optical resonator to provide a positive feedback. Different types of laser varies only in their choice of cavity geometry, suitable active medium and pumping mechanism. In semiconductor lasers a semiconductor material is electrically pumped using a forward-biased p-n junction and carriers injected into a narrow active layer provides the optical gain. In edge emitting semiconductor lasers there is no need for an external cavity since cleaved facets of the semiconductor gain medium itself provides enough optical feedback.The injected electric current density J controls the strength of external pumping. The threshold of a laser at which J reaches a critical value J_{th}

when the gain is sufficient to overcome the cavity losses. Any further increase of J leads to light emission through stimulated emission. The main goal of this chapter is to review the fundamentals of semiconductor lasers and their rate equations.

This chapter is organized as follows [1]: we first start with Maxwell's equations and definition of the optical parameters needed to describe the laser, for example dielectric constant, the refractive index, and the absorption coefficients. Secondly, we proceed by finding lasing threshold through plane wave solution of the wave equation in one dimensional semiconductor cavity. Next, we study the lateral and transverse filed confinement in laser cavity. Finally, laser rate equations including carriers and filed are derived. This chapter concludes with description of the light-current curve of semiconductor lasers.

2.1 Maxwell's Equations

We start our discussion by Maxwell's equations in detail. In the MKS system of units we have

$$\nabla \times E = -\frac{\partial B}{\partial t} \tag{2.1}$$

$$\nabla \times H = J + \frac{\partial D}{\partial t} \tag{2.2}$$

$$\nabla . D = \rho_f \tag{2.3}$$

$$\nabla.B = 0 \tag{2.4}$$

where, E and H are the electric and magnetic field vectors, respectively, and D and B are the corresponding electric and magnetic flux densities. Here, J represents current density vector and ρ_f is the free charge density. For nonmagnetic dielectric materials the electric and magnetic flux densities are related to their corresponding fields through following relationships

$$D = \epsilon_0 E + P \tag{2.5}$$

$$B = \mu_0 H \tag{2.6}$$

$$J = \sigma E \tag{2.7}$$

where ϵ_0 and μ_0 are the vacuum permittivity and permeability, respectively and σ is the conductivity of the medium. In order to calculate the induced electric polarization P one requires to investigate the quantum mechanics features of the semiconductors such as Bloch wave functions and the density of states for the conduction and valance bands.

The wave equation that describes the propagation of the optical field inside a laser can be obtained by Maxwell's equations. We start by taking the curl of Eq. (2.1) to obtain

$$\nabla \times \nabla \times E = -\mu_0 \frac{\partial}{\partial t}(\nabla \times H) \tag{2.8}$$

where we used Eq. (2.6). By making use of Eqs. (2.2), (2.5), and (2.7), we can eliminate H, J, and D in favor of E and P to obtain

$$\nabla \times \nabla \times E = -\mu_0 \sigma \frac{\partial E}{\partial t} - \mu_0 \epsilon_0 \frac{\partial^2 E}{\partial t^2} - \mu_0 \frac{\partial^2 P}{\partial t^2} \tag{2.9}$$

the left hand side of Eq. (2.9) can be simplified with the help of following vector identity

$$\nabla \times \nabla \times E = \nabla(\nabla.E) - \nabla^2 E \tag{2.10}$$

In the absence of free charges, $\rho_f = 0$, and from Eq. (2.3) and Eq. (2.5) we have

$$\nabla.D = \epsilon_0 \nabla.E + \nabla.P = 0 \tag{2.11}$$

we can neglect $\nabla.P$ in most of the practical interest and as a result $\nabla.E = 0$. Consequently Eq. (2.9) reads

$$\nabla^2 E - \frac{\sigma}{\epsilon_0 c^2} \frac{\partial E}{\partial t} - \frac{1}{c^2} \frac{\partial^2 E}{\partial t^2} = \frac{1}{\epsilon_0 c^2} \frac{\partial^2 P}{\partial t^2} \tag{2.12}$$

where c is speed of light in vacuum

$$c = \frac{1}{\epsilon_0 \mu_0} \tag{2.13}$$

The wave equation (2.12) is valid for any arbitrary time varying fields and since

any field can be decomposed into its Fourier components we use following complex notation to describe the optical field with harmonic time variation as follows

$$E(x, y, z, t) = Re[\tilde{E}(x, y, z, t)exp(-i\omega t)] \tag{2.14}$$

$$P(x, y, z, t) = Re[\tilde{P}exp(-i\omega t)] \tag{2.15}$$

where $\omega = 2\pi\nu$ is the angular frequency and $\nu = c/\lambda$ is the oscillation frequency of optical field at the vacuum wavelength λ. The notation Re represents the real part of the bracket expression. By substituting equations (2.14) and (2.15) in Eq. (2.12), we obtain

$$\nabla^2\tilde{E} + k_0^2[1 + i\sigma/(\epsilon_0\omega)]\tilde{E} = -(k_0^2/\epsilon_0)\tilde{P} \tag{2.16}$$

where $k_0 = \omega/c$ is the vacuum wave number. Note that in the rest of this chapter we dropped tilde symbol ($\sim$) for simplicity. Under steady-state condition we have

$$P = \epsilon_0\chi(\omega)E \tag{2.2.17}$$

where $\chi(\omega)$ represents the dispersive susceptibility of the medium. It is useful to decompose χ into two parts

$$\chi = \chi_0 + \chi_p \tag{2.17}$$

where χ_0 represents the medium susceptibility in the absence of external pumping and χ_p is th additional contribution to susceptibility related to the strength of pumping

(for example in semiconductor lasers it is a function of the current injection). If we substitute Eq. (2.2.17) in Eq. (2.16) we obtain

$$\nabla^2 E + \epsilon k_0^2 E = 0 \tag{2.18}$$

where we defined the complex dielectric constant

$$\epsilon = \epsilon' + i\epsilon'' = \epsilon_b + iIm(\chi_0) + \chi_p + i\sigma/(\epsilon_0\omega) \tag{2.19}$$

here $\epsilon_b = 1 + Re(\chi_0)$ corresponds to the background dielectric constant of the unpumped material and is real, as defined. The notation Im stands for the imaginary part.

A considerable insight can be obtained by considering a plane-wave solutions of the wave equation (2.18) although these are not the spacial mode of the semiconductor laser. Under complex definition of the dielectric constant expressed by equation (2.19), the propagation of a plane wave in a medium are described in term of two optical constant: refractive index μ and absorption coefficient α. If we consider a plane wave propagating in the z direction with amplitude E_0 as follows

$$E = E_0 exp(i\tilde{\beta}z) \tag{2.20}$$

where $\tilde{\beta}$ represents the propagation constant and is given by

$$\tilde{\beta} = k_0\sqrt{\epsilon} = k_0\tilde{\mu} \tag{2.21}$$

where $\tilde{\mu}$ is the complex index of refraction as follows

$$\tilde{\mu} = k_0\sqrt{\epsilon} = k_0\tilde{\mu} \tag{2.22}$$

here complex refractive index $\tilde{\mu}$ can be written as

$$\tilde{\mu} = \mu + i(\alpha/2k_0) \tag{2.23}$$

where μ is the refractive index and α is the power absorption coefficient, and usually $\alpha << \mu k_0$. By making use of $\epsilon = \tilde{\mu}^2$ and Eq.(2.19) we obtain

$$\mu = \sqrt{\epsilon'} = [\epsilon_b + Re(\chi_p)]^{1/2} \tag{2.24}$$

$$\alpha = \frac{k_0\epsilon''}{\mu} = \frac{k_0}{\mu}[Im(\chi_0 + \chi_p) + \sigma/(\epsilon_0\omega)] \tag{2.25}$$

these equations show that how external pumping of semiconductor materials affects the index of refraction and the net absorption coefficient.

2.2 Threshold condition and longitudinal modes

In th previous section we described the plane wave solution of the wave equation and claimed that it can be used to estimate the laser frequency and lasing threshold. It has to be mentioned that the lasing modes are never plane waves, nonetheless, the derived value for the optical gain required for the lasing is reasonably accurate and is really helpful in understanding the fundamental physical aspects of the lasing process. We start by considering a laser cavity of length L as illustrated in Fig. 2.1. Where two cleaved facets construct the laser Fabry-Perot FP cavity. Here the z axes is the propagation direction of the plane wave along the cavity length

$$E = E_0 exp(i\tilde{\beta}z) \tag{2.26}$$

where from Eqs. (2.21) and (2.22) the propagation constant $\tilde{\beta}$ reads

$$\tilde{\beta} = \mu k_0 + i\alpha/2 \tag{2.27}$$

As we discussed before pumping of a semiconductor changes the refractive index of the material (μ) and this in turn changes the the propagation constant $\tilde{\beta}$. In general,

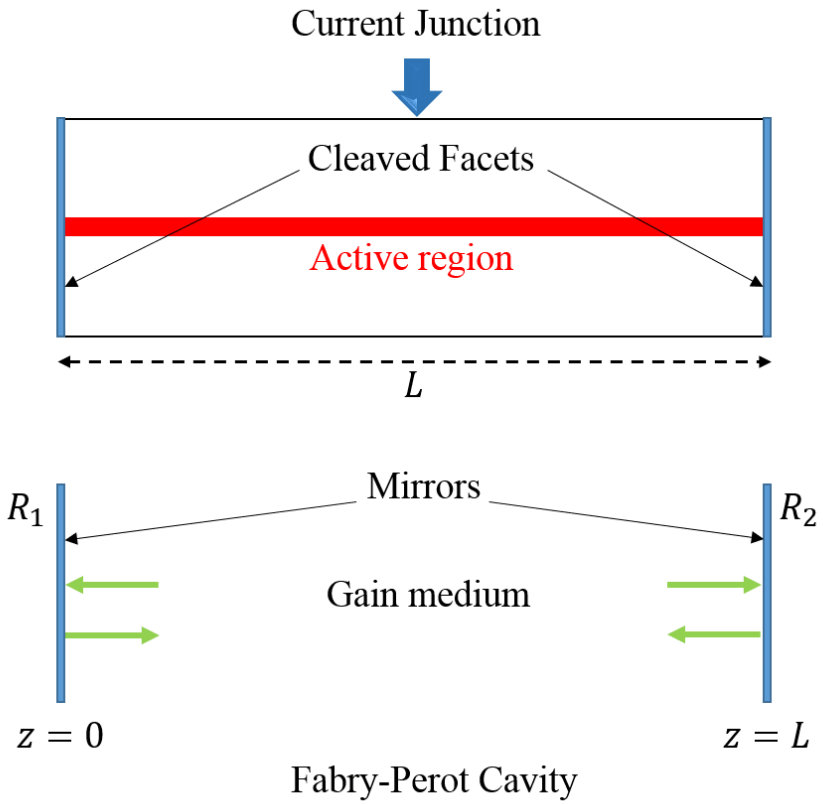

Figure 2.1: (a) Schematic of a laser cavity of length L. (b) Fabry-Perot (FP) cavity associated to the cavity in (a), where R_1 and R_2 represent the reflection coefficient of each cleaved facet.

however, $|Re(\chi_p)| << \epsilon_b$, and Eq. (2.23) can be approximated by

$$\mu \simeq \mu_b + \Delta\mu_p \tag{2.28}$$

where μ_b is the background refractive index of the unpumped material and $\Delta\mu_p$ is the refractive index change due to the presence of charge carriers (electrons and holes) is as follows

$$\Delta\mu_p \simeq Re(\chi_p)/2\mu_b \tag{2.29}$$

Nothing that usually $Re(\chi_p)$ is negative which makes $\Delta\mu_p$ negative. Although this reduction in the refractive index is very small (less than 1%) it dramatically affects the static, dynamics and spectral characteristics of the semiconductor lasers. This is a unique feature of the semiconductor lasers in contrast to other type of laser such as gas laser that $\Delta\mu_p \simeq 0$.

Next we consider three different sources of absorption in semiconductor materials. In Eq.(2.23) the term $Im(\chi_0)$ corresponds to material absorption while $Im(\chi_p)$ accounts for its reduction due to external pumping. Usually, the net gain g is defined as combination of these two terms

$$g = -\frac{k_0}{\mu_b} Im(\chi_0 + \chi_p) \tag{2.30}$$

The last term in Eq. (2.23) represents the internal losses that usually occur in a semiconductor laser (such as free carrier absorption and scattering at heterostructure interfaces) and accounted for $\alpha_{int} = k_0\sigma/(\epsilon_0\omega\mu)$. The net absorption coefficient reads

$$\alpha = -\Gamma g + \alpha_{int} \tag{2.31}$$

The coefficient Γ is known as the confinement factor and here phenomenologically added and its use will be justified in the section (2.5). This factor accounts for the fraction of mode energy confined in the gain medium.

In order to find the lasing threshold condition, the optical field in the cavity needs to reproduce itself after each cycle at steady state or continuous wave operation condition. This leads to

$$(R_1R_2)^{1/2}exp(2i\tilde{\beta}L) = 1 \tag{2.32}$$

where R_1 and R_2 are reflectivities of the facets on the two ends. By separating the real and imaginary parts of this equation and using Eq. (2.27) we obtain

$$(R_1R_2)^{1/2}exp(-\alpha L) = 1 \tag{2.33}$$

$$sin(2\mu k_0 L) = 0 \tag{2.34}$$

The threshold can be obtained from Eq. (2.33) by using Eq. (2.31) as follows

$$\Gamma g_{th} = \alpha_m + \alpha_{int} \tag{2.35}$$

where

$$\alpha_m = \frac{1}{2L} ln(\frac{1}{R_1R_2}) \tag{2.36}$$

is the mirror loss due to the radiation escaping from FP cavity. To obtain the lasing frequency we use Eq. (2.34) and by taking into account the periodic nature of trigonometric function, multiple solutions can be found

$$2\mu k_0 L = 2m\pi \tag{2.37}$$

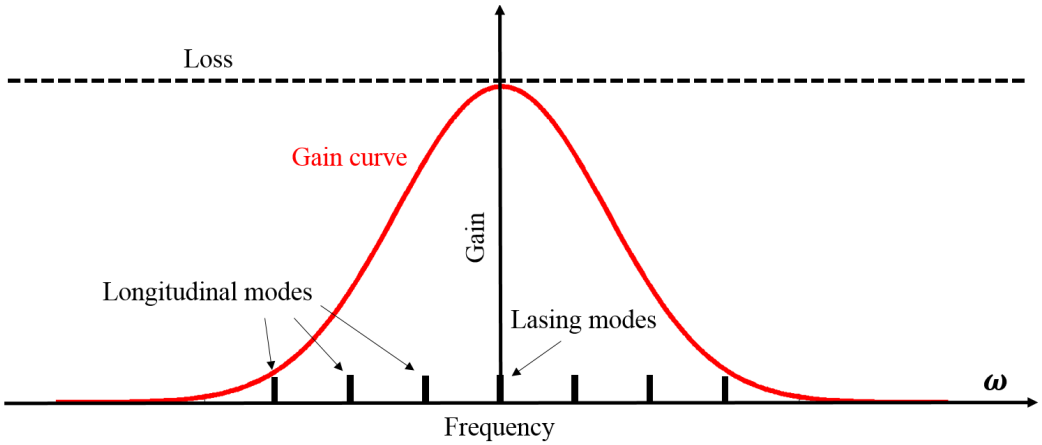

Figure 2.2: Schematic illustration of the gain curve and longitudinal modes of a semiconductor laser. The lasing threshold is reached when gain equals loss for the lasing mode in the vicinity of the gain peak.

here m is an integer. One can easily use $k_0 = 2\pi\nu/c$ and obtain the lasing frequencies

$$\nu = \nu_m = mc/(2\mu L) \tag{2.38}$$

where ν_m is the cavity resonance frequency. This means that the laser tends to lase (oscillates) at a frequency that is a longitudinal mode supported by FP cavity. Interestingly, reaching to the lasing threshold for one or more longitudinal modes depends on the characteristics of gain curve including the gain width and the gain broadening mechanism (whether homogeneous or inhomogeneous, see [1]). In the case of homogeneous broadening, only one longitudinal mode, which its frequency coincide with the gain-peak frequency, reaches threshold and the laser remains in the single mode operation regime even in the above threshold regime, Fig. 2.2.

Next we calculate the intermode spacing, to do so we have to take it into account

that refractive index μ varies with the frequency ν thus

$$\Delta(\mu\nu) = \mu(\Delta\nu) + \nu(\Delta\mu) \tag{2.39}$$

where Δ corresponds to small change, the intermode spacing is given by

$$\Delta\nu = c/(2\mu_g L) \tag{2.40}$$

where

$$\mu_g = \mu + v(\partial\mu/\partial\nu) \tag{2.41}$$

is the group index of the dispersive semiconductor material. This is a unique feature of this type of laser that the longitudinal frequencies and their separation vary with the external pumping, because of the refractive index modulation. To have a rough estimate of semiconductor lasers parameters mentioned above, let us consider an InGaAsP semiconductor laser with cavity length $L = 250\mu m$. For this material at wavelength $1.3 - 1.6\mu m$, refractive index is $\mu \simeq 3.4$ and group index is $\mu_g \simeq 4$. Thus the longitudinal mode separation can be found through Eq. (2.40) to be $\Delta\nu \simeq 150$ GHz or $\Delta\lambda = \lambda^2\Delta\nu/c \simeq 1$ nm. For cleaved facets with $R_1 = R_2 \simeq 0.32$ the facet loss from Eq. (2.36) is $\alpha_m \simeq 45\ cm^{-1}$. Taking into account usual values for $\Gamma \simeq 0.5$ and $\alpha_{int} \simeq 30\ cm^{-1}$ in Eq. (2.35) a material gain of $g_{th} = 150\ cm^{-1}$ is needed to achieve lasing threshold.

2.3 Gain and stimulated emission

In general a phenomenological approach can be used to describe a semiconductor laser and it has proven to be extremely accurate. This phenomenological approach is based on assumption of a linear relation between carrier density n and gain g at the lasing frequency (corresponding to the gain value at which gain spectrum peaks for a given current density J). Thus the gain g can be described as follows

$$g(n) = a(n - n_0) \tag{2.42}$$

where a is the gain coefficient and n_0 represents the carrier density needed to achieve transparency (the onset of population inversion). Note that an_0 corresponds to the absorption coefficient of the unpumped material. In order to complete this phenomenological approach, it is also assumed that the index of refraction varies linearly with the carrier density; i.e. $\Delta\mu_p$ in Eqs.(2.28) and (2.29) is given by

$$\Delta\mu_p = bn \tag{2.43}$$

where $b = \partial\mu/\partial n$ and is determined experimentally. By comparing Eqs. (2.42) and Eq. (2.43) with Eqs. (2.29) and (2.30), one can see that the in this model a linear

variation of the complex susceptibility χ_p with the density of carrier n, is assumed

$$\chi_p = \mu_b(2b - ia/k_0)n \tag{2.44}$$

Here it is quite useful to define the following parameter

$$\beta_c = \frac{Re(\chi_p)}{Im(\chi_p)} = -\frac{2k_0 b}{a} = -k_0(\frac{\partial \mu_g/\partial n}{\partial g/\partial n}) \tag{2.45}$$

where β_c is called line-width enhancement factor or antiguiding parameter and often used instead of b in phenomenological description of semiconductor lasers. Since b is a negative parameter, β_c is positive dimensionless number.

To complete the phenomenological description of semiconductor laser, the carrier density n should be related to the pumping source which is current density J. In general the carrier density rate equation that incorporates all mechanisms by which carriers are generated and lost inside the active material is given by

$$\frac{\partial n}{\partial t} = D(\nabla^2 n) + \frac{J}{qd} - R(n) \tag{2.46}$$

The first term on the right hand side, corresponds to carrier diffusion and D is the diffusion coefficient. The second term represents the rate at which the carrier (electrons or holes) are injected into the active layer via external electrical pumping where q is the electron charge and d is the thickness of the active layer. The last term $R(n)$

account for the carrier loss due to various recombination processes, both radiative and nonradiative. Note that Eq. (2.46) can be regressively derived through density matrix approach. Depending on the laser geometry, term corresponds to diffusion effect can be ignored, this is the case for strongly index guided lasers where the diffusion length is often larger than the active region dimension. Thus we can ignore the diffusion term, since in this lasers the carrier density does not vary significantly in the active region. In the steady state where $\partial n/\partial t = 0$ and we obtain

$$J = qdR(n) \tag{2.47}$$

It has to be noted that, this situation is entirely different for gain-guided semiconductor lasers where carrier diffusion causes the lateral variation of the carriers density and this in turn makes the gain in Eq. (2.42) specially inhomogeneous and increase the optical mode confinement. Thus the diffusion term should be considered in these type of semiconductor lasers. One can use the threshold condition Eq. (2.35) together with Eqs. (2.42) and (2.47) to model the light-current characteristics of semiconductor lasers. In the final step and in order to complete the laser description, we need to determine an appropriate form for recombination rate $R(n)$ appeared in Eq. (2.32). This recombination process may leads to either spontaneous or stimulated emission. A reasonable form for $R(n)$ is given by

$$R(n) = A_{nr}n + Bn^2 + Cn^3 + R_{st}N_{ph} \tag{2.48}$$

where it is assumed that injected current density is well above the doping level of the active layer. The first term $A_{nr}n$ accounts for nonradiative recombination. The second quadratic term takes into account the spontaneous radiative recombination, where an electron recombine a hole and a photon is spontaneously emitted. The cubic term Cn^3 is due to nonradiative Auger recombination process, which plays an important role in long-wavelength semiconductor lasers. The last term $R_{st}N_{ph}$ is due to stimulated recombination which leads to coherent emission of laser light. This term is directly related to the intracavity photon density N_{ph} and net rate of recombination emission

$$R_{st} = (c/\mu_g)g(n) \tag{2.49}$$

here $g(n)$ is the optical gain given by Eq. (2.42)

2.4 Waveguide modes

In semiconductor lasers output is in the form of a narrow optical beam with an elliptical cross section. This well defined optical mode is a solution of the wave equation (2.18) that satisfies all boundary conditions imposed by laser structure. Optical modes are usually denoted by E_{pqm} where the subscript m stands for longitudinal or axial mode index defined in Sec. (2.3). The subscripts p and q are integer numbers and they denote the transverse and lateral mode indexes, specifying the field

distribution in the directions perpendicular and parallel to the heterostructure plane, junction plane, respectively. It is crucial to understand the number of laser modes since it is often desired to have a laser emission predominantly in a single mode operating regime. On the other hand, near- and far-field widths and other important characteristics of the lasers depends on details of laser modes.

In heterostructure semiconductor lasers there is a reasonable refractive index discontinuity between the active and cladding layers and this in turn leads to mode confinement in the transverse direction, perpendicular to the junction plane, through index guiding or dielectric waveguiding. On the other hand, mode confinement in lateral direction is not always due to the index guiding. Depending on the field confinement mechanism in lateral direction, semiconductor laser are categorized as gain-guided or index-guided whether it is lateral variation of the gain or refractive index confines the mode. index-guided lasers can be further categorized as weakly or strongly index guided depending on the lateral index step. Figure. 2.3 schematically illustrates these three type of semiconductor lasers.

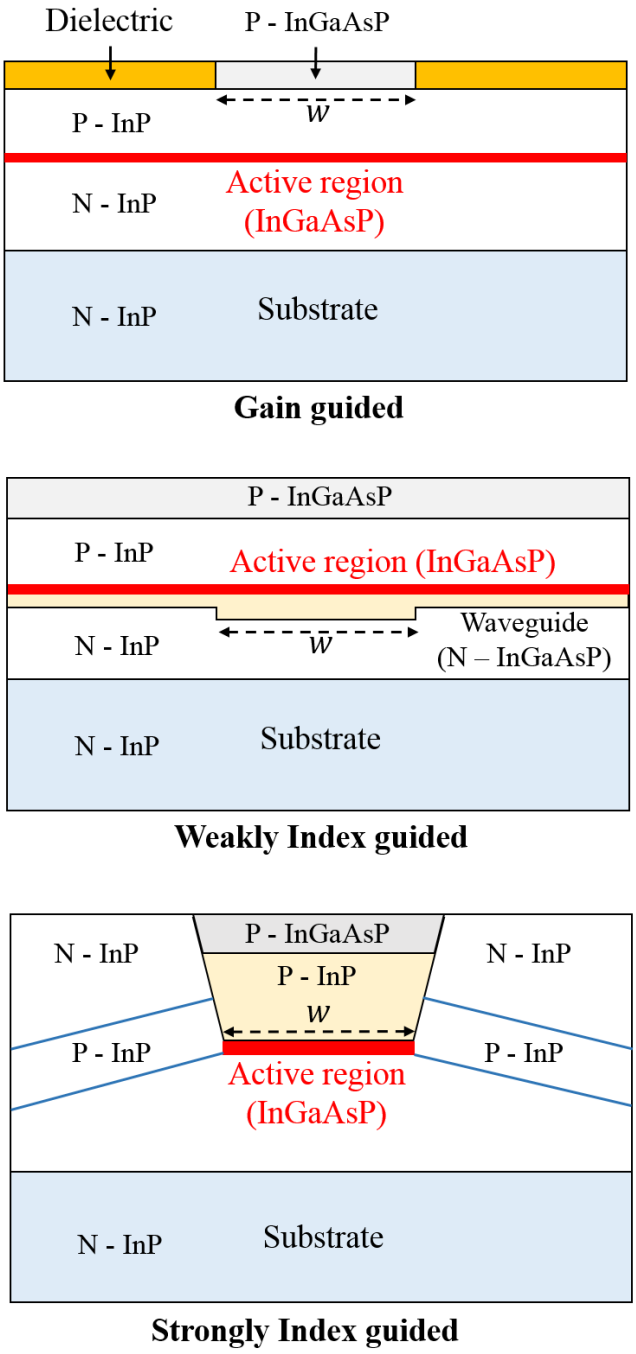

Figure 2.3: Schematic illustration of three kind of semiconductor lasers. The active-layer material (shaded area) surrounded by cladding material.

2.4.1 Effective index approximation

To describe the laser modes, the time independent wave equation has to be solved

$$\nabla^2 E + \epsilon(x, y) k_0^2 E = 0 \tag{2.50}$$

where specific harmonic time evolution at frequency ω corresponding to longitudinal mode is assumed. The dielectric constant is in the following general form

$$\epsilon(x, y) = \epsilon_j(x) \tag{2.51}$$

where the subscript j corresponds to different layers in the heterostructure laser. In general dielectric constant ϵ_j is a complex to account for loss in each layer; furthermore, in the active layer it is a function of external pumping (see Eq. (2.19)).

In fact, solving Eq. (2.50) and obtaining the exact solution is not an easy task, however, an alternative approach is to use effective index approximation. In this approach instead of solving the two dimensional wave equation, the problem is divided into two one-dimensional wave equations which are relatively easier to solve. This method is practically successful for both gain-guided and index-guided lasers because the dielectric constant is often a slowly varying function in the lateral x direction compared to its variation in the transverse y direction. As a result to a good approximation the

slab waveguide problem in y direction can be solved for each x and then the resulting solution can then be used to obtain the lateral variation. Thus the electric field in Eq. (2.50) is approximately given by

$$E \simeq \hat{e}\phi(y;x)\psi(x)exp(i\beta z) \tag{2.52}$$

where β is propagation constant of the mode and $\hat{e}$ is the unit vector in the polarization direction ogf the mode. After substituting this solution in wave equation (2.50)) we find

$$\frac{1}{\psi}\frac{\partial^2\psi}{\partial x^2} - \frac{1}{\phi}\frac{\partial^2\phi}{\partial y^2} + [\epsilon(x,y)k_0^2 - \beta^2] = 0 \tag{2.53}$$

in this method the transverse field distribution $\phi(y;x)$ for a fixed value of x is found by solving

$$\frac{\partial^2\phi}{\partial y^2} + [\epsilon(x,y)k_0^2 - \beta_{eff}^2]\phi = 0 \tag{2.54}$$

where β_{eff} is the effective propagation constant for given x value. Then the lateral field distribution can be found by solving

$$\frac{\partial^2\psi}{\partial x^2} + [\beta_{eff}^2 - \beta^2]\psi = 0 \tag{2.55}$$

For any given laser structure Eqs. (2.54)) and (2.55)) can be solved to obtain the field distribution in both transverse and lateral direction, respectively. Note that $\epsilon(x,y)$ is in general complex thus β_{eff} is also complex. The effective refractive index is defined

as follows

$$\mu_{eff} = \beta_{eff}/k_0 \tag{2.56}$$

In general Eq. (2.54)) is a one dimensional eigenvalue problem and can be solved through developed method for solving one dimensional waveguides. although in these method in general it is possible to consider gain or loss in each layer, it is not an easy task. The alternative way is to consider the effect of gain or loss in each layer as a small perturbation to the unperturbed eigenvalue problem. This is justified because field confinement in the transverse y direction is basically due to refractive index step at the heterostructure interfaces. Thus the dielectric constant $\epsilon(x, y)$ is given by

$$\epsilon(x, y) = \mu_b^2 + \Delta\epsilon(x, y) \tag{2.57}$$

where μ_b is the background refractive index and $\Delta\epsilon(x, y) << \mu_b^2$ is the small perturbation due to loss or gain. Next, we use first order perturbation theory to find effective refractive index

$$\mu_{eff} = \mu_e(x) + \Delta\mu_e \tag{2.58}$$

where μ_e is the effective refractive index for the unperturbed system

$$\frac{\partial^2\phi}{\partial y^2} + k_0^2[\mu_b^2 - \mu_e^2]\phi = 0 \tag{2.59}$$

the perturbation $\Delta\mu_e$ is given by

$$2\mu_e\Delta\mu_e = \frac{\int_{-\infty}^{\infty}\Delta\epsilon(x,y)\phi^2(y;x)dy}{\int_{-\infty}^{\infty}\phi^2(y;x)dy} \tag{2.60}$$

Since $\Delta\epsilon(x,y)$ is a constant in each layer, Eq. (2.60) can be simplified as follows

$$\Delta\mu_e = \frac{1}{2\mu_e}\sum_j \Gamma_j(x)\Delta\epsilon_j(x) \tag{2.61}$$

where sum is over all layers in the lateral direction and $\Delta\epsilon_j(x)$ is the dielectric perturbation of jth layer. Finally, $\Gamma_j(x)$ is referred to as confinement or filling factor , since it indicates the extend in which mode is confined in the active regime. It is given by

$$\Gamma_j(x) = \frac{\int_{d_j}\phi^2(y;x)dy}{\int_{-\infty}^{\infty}\phi^2(y;x)dy} \tag{2.62}$$

2.4.2 Transverse modes

The transverse mode of the system are obtained by solving the Eq. (2.59) and it is directly dependent on the structure of laser including thickness and the refractive index of each layer. To have a very simple intuitive picture of semiconductor lasers one can consider just a three layer slab waveguide shown schematically in Fig. 2.4. The active layer of thickness d is sandwiched by two cladding layers. This assumption

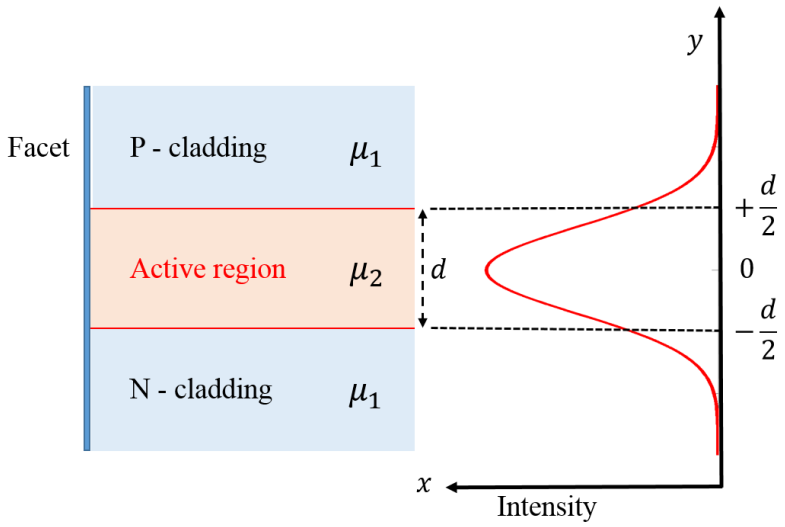

Figure 2.4: Left: schematic illustration of planar waveguide made of active and cladding layers with refractive indexes μ_1 and μ_2, respectively, where $\mu_1 < \mu_2$. Fundamental mode of this waveguide is also plotted on the right side.

is correct if the cladding layers are thick enough to confine light in the active layer with very small evanescent tail in other layers. The planar waveguide problem has been studied in details and it is found that a slab waveguide can support two kind of modes: transverse electric (TE) and transverse magnetic (TM), where for TE (TM) mode electric (magnetic) field is polarized along the heterojunction plane, i.e., the polarization vector in Eq. (2.52) is along the x axis. In both of these cases the same equation (2.59) should be solved to find the field distribution. The boundary conditions requires the continuity of tangential components of fields at boundaries. This corresponds to the continuity of ϕ and $\partial\phi/\partial y$ at boundaries $|y| = d/2$. The other boundary condition for guided modes is that the field $\phi(y)$ should vanishes as y tends to infinity.

Here we just present some of the most important results and concluding remarks of the mode analysis for illustrated structure in Fig. 2.3 and we do not concentrate on details and their derivation. The first important statement is the single-transverse mode condition (for a waveguide that supports only the lowest order, fundamental TE mode)

$$d < \frac{\lambda}{2}(\mu_2^2 - \mu_1^2)^{-1/2} \tag{2.63}$$

in other words a heterostructure semiconductor laser can be fabricated in such a way that it supports and emit light in a single transverse mode if its thickens satisfies Eq. (2.63). Note that typically $d \lesssim 0.2\mu m$ single mode condition is almost always satisfied in practical semiconductor lasers.

As we discussed before, transverse confinement Γ_T is an important factor in heterostructure semiconductor laser, because it corresponds to to the fraction of laser mode energy within the active layer and it can intract with injected current carriers. For the fundamental transverse mode a simple expression was found

$$\Gamma_T \cong D^2/(2 + D^2) \tag{2.64}$$

where $D = k_0(\mu_2^2 - \mu_1^2)^{1/2}d$ is normalized waveguide thickness. For an InGaAsP laser with $d = 0.15\mu m$ thickness of active layer, $D \cong 1$ and $\Gamma_T \cong 1/3$.

2.4.3 Lateral modes

To obtain the lateral modes one has to solve Eq. (2.55) and after substituting Eqs. (2.56) and (2.58) in it becomes

$$\frac{\partial^2\psi}{\partial x^2} + [k_0^2[\mu_e(x) + \Delta\mu_e(x)]^2 - \beta^2]\psi = 0 \tag{2.65}$$

Depending on the laser type either gain-guided or index-guided, the lateral-mode behavior in semiconductor lasers is different. In the gain guided lasers $\mu_e(x)$ is a constant (can be found by solving the unperturbed eigenvalue problem, Eq. (2.59), for transverse mode). On the other hand, for index-guided lasers the slab-waveguide problem should be solved in two regions as follows

$$\mu_e(x) = \begin{cases} \mu_e^{in}, & \text{if } |x| \leq w/2 \\ \mu_e^{out}, & \text{otherwise} \end{cases} \tag{2.66}$$

Here we just consider strongly index guided semiconductor lasers. The mode-propagation constant for this system is given by $\beta = k_0\bar{\mu} + i\bar{\alpha}/2$, where $\bar{\mu}$ and $\bar{\alpha}$ are effective refractive index and absorption of rectangular waveguide of width w and thickness d. The lateral mode can be found by solving the three layer slab waveguide

system

$$\frac{\partial^2\psi}{\partial x^2} + [k_0^2[\mu_e^2(x) - \bar{\mu}^2]\psi = 0 \tag{2.67}$$

By making use of first order perturbation theory, the mode absorption $\bar{\alpha}$ can be found

$$\bar{\alpha} = \frac{k_0}{\bar{\mu}} Im\Big(\frac{\int 2\mu_e(x)\Delta\mu_e(x)\psi^2(x)dy}{\int \psi^2(x)dy}\Big) \tag{2.68}$$

It can be shown that the waveguide supports the lowest-order lateral mode if the active layer width satisfies the following criteria

$$w \leq \lambda/(8\mu_e\Delta\mu_L)^{1/2} \tag{2.69}$$

where $\Delta\mu_L = \mu_e^{in} - \mu_e^{out}$ is lateral index step and μ_e is the average effective index. Similar to transverse confinement factor, here we can find the lateral mode confinement Γ_L for fundamental lateral mode

$$\Gamma_L \cong W^2/(2 + W^2) \tag{2.70}$$

where $W = k_0 w[(\mu_e^{in})^2 - (\mu_e^{out})^2]^{1/2}$ is the normalized waveguide width. It is shown that the mode loss $\bar{\alpha}$ can be be written as follows

$$\bar{\alpha} = -\Gamma g + \alpha_{int} \tag{2.71}$$

where $\Gamma = \Gamma_L \Gamma_T$ is the mode-confinement factor and α_{int} is the internal loss due to absorption in the cladding layer. The confinement factor corresponds to the fraction of the mode energy confined inside the active region. For typical strongly index-guided semiconductor lasers $w \cong 2\mu m$ and $\Gamma_L \cong 1$ and Γ_T can used for Γ. The internal loss in its general form should includes all sources of loss as follows

$$\alpha_{int} = \Gamma \alpha_a + (1 - \Gamma)\alpha_c + \alpha_{scat} \tag{2.72}$$

where α_a is the active-layer loss (mainly due to free carrier absorption), α_c is the cladding layer loss and α_{scat} corresponds to the scattering loss at heterostructure interfaces.

2.5 Semiconductor laser rate equations

The rate equations describe the interplay between photons and carriers in the semiconductor lasers and these governing equations can be used to describe the static, spectral and dynamic characteristic of these lasers. The starting point to find field rate equation is Maxwell's equations and considerable simplification can be achieved by assuming that the Eq. (2.12) holds even for time dependent fields

$$\nabla^2 E - \frac{1}{c^2}\frac{\partial}{\partial t}(\epsilon E) = 0 \tag{2.73}$$

This is justified for fast responding semiconductors, since their response time is relatively fast ($\sim 0.1ps$) compared to other time scales such as photons life time ($\sim 1ps$) and carriers recombination time. The optical mode E in general may includes many lateral, transverse and longitudinal modes oscillating at different frequencies. Furthermore, there are a large number standing modes along axial direction arising from a superposition of the forward and backward running waves. Here, for simplicity of notation we assume a single mode structure in all transverse, lateral and axial directions. Thus the electric field is given by

$$E(x,y,z,t) = \frac{1}{2}\hat{x}\psi(x)\phi(y)sin(kz)E(t)e^{-i\omega t} + c.c \tag{2.74}$$

here the wave number k is related to the cold cavity resonance frequency $\Omega = 2\pi\nu$ through Eq. (2.38) and $k = \mu\Omega/c$. The laser mode frequency ω is not determined yet but it is expected to be close to Ω. Next we substitute the electric field E given by Eq. (2.74) in the wave equation (2.73) and assuming that $E(t)$ varies slowly, and after some simplification and other assumptions which are not explained here, we obtain

$$\frac{dE}{dt} = \frac{i\bar{\mu}}{\mu_g}(\omega - \Omega)E + \frac{i\omega}{\mu_g}(\Gamma\Delta\mu_p + i\bar{\alpha}/2k_0)E \tag{2.75}$$

where μ_g is the group index corresponding to the mode index $\bar{\mu}$. Furthermore, $\Delta\mu_p$ is the carrier-induced index change (see Eq. (2.43)). The mode-absorption coefficient is given by $\bar{\alpha} = -\Gamma g + \alpha_{int} + \alpha_m$, which is generalized to include the loss due to

facets given by Eq. (2.36). It is useful to separate the real and imaginary parts of the electric field by defining $E = Ae^{-i\phi}$ and substituting it in Eq. (2.75), we obtain

$$\dot{A} = \frac{1}{2} v_g [\Gamma g - (\alpha_{int} + \alpha_m)] A \tag{2.76}$$

$$\dot{\phi} = -\frac{\bar{\mu}}{\mu_g}(\omega - \Omega) - \frac{\omega}{\mu_g}\Gamma \Delta\mu_p \tag{2.77}$$

where we and dot represents the time derivation. Here, $v_g = c/\mu_g$ is group velocity. Clearly, Eq. (2.77) shows that the carrier-induced change $\Delta\mu_p$ affects the lasing-mode frequency ω. These equations next to the carrier rate equation Eq. (2.46)

$$\frac{\partial n}{\partial t} = D(\nabla^2 n) + \frac{J}{qd} - R(n) \tag{2.78}$$

can be used to describe semiconductor lasers static and dynamics[1]. Nothing that these equations are coupled through $g(n) = a(n - n_0)$ and definition of $R(n)$ which is a function of photon numbers $R(n) = A_{nr}n + Bn^2 + Cn^3 + R_{st}N_{ph}$, see Eq. (2.48) .

2.6 Emission characteristics of semiconductor laser

Previous sections have discussed basic concepts of the semiconductor lasers and their governing rate equations. We now consider the emission characteristics which is used to study the performance of the semiconductor lasers. One of these fundamental features is the light-current characteristics.

A typical emitted power by one facet of the laser versus its injected current is plotted in Figure. 2.5 which is called light-current (L-I) curve and it is strongly temperature dependent. The turning point at which output emitted power increases dramatically is called lasing threshold and corresponds to threshold current I_{th}. For $I < I_{th}$ the light output is mainly because of spontaneous emission governed by Bn^2 in Eq. (2.48). On the other hand for $I > I_{th}$ stimulated emission has main contribution in the laser output power and it is expressed in the last term $R_{st}N_{ph}$ in Eq. (2.48). Lasing threshold basically corresponds to the point at which gain equals to loss and using Eqs. (2.35) and (2.44) one can see that:

$$n_{th} = n_0 + (\alpha_m + \alpha_{int})/(a\Gamma) \tag{2.79}$$

where n_0 is the transparency value at which population inversion occurs. By making

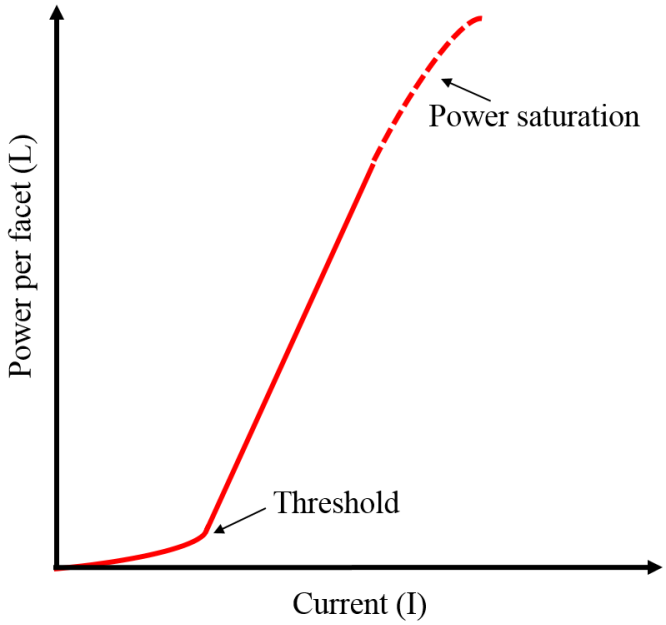

Figure 2.5: Typical Light - current of a semiconductor lasers.

use of Eqs. (2.47) and (2.48) the lasing threshold can be found:

$$J_{th} = qn_{th}/\tau_e(n_{th}) \tag{2.80}$$

where carrier - recombination time $\tau_e(n)$ is a function of n is given by

$$\tau_e(n) = (A_{nr} + Bn + Cn^2)^{-1} \tag{2.81}$$

Once the injected current reaches the lasing threshold the carrier density n remains constant to its threshold value n_{th} and any further increase of J leads to higher increase in laser output power through stimulated emission process. To find the

intracavity photon intensity one can use Eqs. (2.47) and (2.48)

$$N_{ph} = \eta_i(\tau_p/qd)(J - J_{th}) \tag{2.82}$$

where the internal quantum efficiency is added phenomenologically and

$$\tau_p^{-1} = v_g(\alpha_m + \alpha_{int}) \tag{2.83}$$

here $v_g = c/\mu_g$ is group velocity. Noting that Eq. (2.82) implies the fact that once the lasing threshold reaches, the intracanity photon density increases linearly with further increase of current density J. This equation can be also used to express the output power P_{out} in term of injected current I. Since $P_{out} = \frac{1}{2}h\nu v_g\alpha_m V N_{ph}$, and $V = Lwd$ is the volume of active region and also using $I = wlJ + I_L$ where I_L is the leakage current (depending on the laser geometry a part of total current may not pass through the active region) one can see that (above lasing threshold and before power saturation)

$$P_{out} = \frac{h\nu}{2q}\frac{\eta_i\alpha_m}{\alpha_m + \alpha_{int}}(I - I_{th} - \Delta I_L) \tag{2.84}$$

here ΔI_L corresponds to the possible increase of the leakage current with the current I. Nothing that $I_{th} = qVn_{th}/\tau_e + I_L$ is the threshold current. Eq. (2.84) represents the output power of laser as a function of the current I, clearly, this equation implies the fact that P_{out} varies linearly with I. It has to be mentioned that the slop of the L-I curve does not remain constant and power saturation may occur. In fact any of three

parameters I, I_{th} can contribute in power saturation effect. Consequently, at a laser oscillation well above lasing threshold the effect of gain saturation should be taken into account. The effect of gain saturation is usually added to the rate equations as follows

$$g = \frac{g_{th}}{1 + \epsilon_s |A|^2} \tag{2.85}$$

where ϵ_s is called gain saturation coefficient, for more details see [1, 2, 3].

References

[1] Agrawal, G. P. and Dutta, N. K. Semiconductor Lasers, (Springer Science and Business Media, 2013).

[2] Verdeyen J. T. Laser electronics, (Prentice-Hall, 1981).

[3] Ohtsubo, J. Semiconductor Lasers: Stability, Instability and Chaos, (Springer Berlin Heidelberg, 2005).

[4] Kapon, E. Semiconductor Lasers I: Fundamentals, (Academic Press, 1999).

[5] Ghafouri-Shiraz, H. Distributed Feedback Laser Diodes and Optical Tunable Filters, (John Wiley and Sons, 2004).

Chapter 3

Quantum inspired symmetries in optics: Parity-Time symmetry and Supersymmetry

Symmetries play an important role in quantum and classical physics [1, 2, 3, 4, 5]. In general, symmetries can be classified into continuous and discrete. Different symmetries are associated with conserved quantities or constants of motion. In this chapter we explore the concepts of parity-time reversal (PT) symmetry and supersymmetry in more details.

The peculiar concept of PT symmetry [6, 7, 8, 9, 10, 11] was recently mapped from

quantum mechanics to optics and photonics systems [15, 16] and substantially this so called Non-Hermitian engineering, has been both theoretically and experimentally expanded by many research groups. Results of these efforts led to many breakthroughs with application in ultra sensitive sensors, mode selectivity in laser systems, efficient wireless energy transport, and data processing that uses integrated devices in modern engineering [17, 18, 19, 20, 21, 22, 23, 24, 25, 26, 27, 28, 29, 30, 34]. PT symmetric lasers are among these interesting system in which judicious non-Hermitian engineering of the gain/loss in laser systems enables single mode operation. Particular goal in this thesis is to study non-Hermitian engineered laser systems. In this chapter one section is dedicated to review the main idea of PT symmetric lasers.

Quite a bit after birthday of PT symmetry in photonics, and more recently the marriage between SUSY and optics conceived as a powerful tool to engineer novel photonic structures. In contrast to more familiar approaches in integrated optics that rely on engineering the local properties of optical indices and magnetic permeabilities, SUSY is a framework that seeks to engineer certain global features of the system by collectively manipulating the associated eigenvalues and scattering coefficients. This unique top-down paradigm can allow for tailoring optical devices that facilitate parallel information processing and collective suppression or enhancement of nonlinear optical interactions with possible applications in optical communication and computing, transformation optics and laser engineering.

In this chapter we present an overview of these two symmetries in quantum mechanics and then their transformation into optics and photonics. Finally as mentioned before, the main goal is to see their potential application in laser technology.

3.1 Parity-Time symmetry in Quantum Mechanics

In 1998 Bender and Boettcher showed that even a non-Hermitian Hamiltonian can have a group of real eigenvalues [6]. In other words, the Hrmiticity of Hamiltonian is not a necessary condition for realness of the its eigenvalues. They have started with non-Hermitian Hamiltonians of the following form $\hat{H} = \hat{p}^2 + V(\hat{x}) = \hat{p}^2 + m^2\hat{x}^2 - (i\hat{x})^N$ where N is a real number, and it is demonstrated that eigenvalues of this Hamiltonian are real. In this work, it is shown that if Hamiltonian of any given non-Hermitian system commutes with $\hat{P}\hat{T}$ operator then one may expect a real spectrum for such a system:

$$[\hat{P}\hat{T}, \hat{H}] = 0 \tag{3.1}$$

where $\hat{P}$ and $\hat{T}$ are Parity and Time operators, respectively; and in term of position $\hat{x}$ and momentum $\hat{p}$ operators, they correspond to:

$$\begin{cases} \hat{P} : \hat{p} \Rightarrow -\hat{p} \; and \; \hat{x} \Rightarrow -\hat{x} \\ \\ \hat{T} : \hat{p} \Rightarrow -\hat{p}, \; \hat{x} \Rightarrow -\hat{x} \; and \; \hat{i} \Rightarrow -\hat{i} \end{cases} \tag{3.2}$$

note that $\hat{T}$ is inverting the time $t \rightarrow -t$. Immediate result of Eqs. (3.1 and 3.2) is that Hamiltonian $\hat{H} = \frac{p^2}{2m} + V(x)$ is PT symmetric if

$$\hat{H}(\hat{p}, \hat{x}, t) = \hat{H}^*(\hat{p}, -\hat{x}, -t) \;\; \rightarrow \;\; V(\hat{x}) = V^*(-\hat{x}) \tag{3.3}$$

which means that for given non-Hermitian Hamiltonian of the form $\hat{H} = \frac{p^2}{2m} + V_R(\hat{x}) + i\gamma V_I(\hat{x})$, real part $V_R(\hat{x})$ and imaginary part $V_I(\hat{x})$ of potential should be even and odd functions of $\hat{x}$, respectively. On the other hand, it turned out that only for certain values of $\gamma < \gamma_{EP}$, eigenvalues of the system are real which is called PT phase and for $\gamma > \gamma_{EP}$ system lives in broken PT phase and its eigenvalues are complex.

The critical point at which $\gamma = \gamma_{EP}$ is referred to as an exceptional point or spontaneous PT symmetry breaking point. These points in parameter space are also refereed to as non-Hermitian degeneracies at which eigenvalues and eigenvectors of the systems simultaneously coalesce [6, 7, 8, 9, 10, 11]. Phase transition between PT and broken PT phase at these points attracted a considerable attention in the recent decade just

because of their potential application in sensing, single mode laser operation, loss induced transparency, power transformation and many other applications in optics and photonics. In what follows a section is dedicated to describe the mapping of PT from quantum mechanics into paraxial optics and its implementation in integrated photonics.

3.2 Parity-Time symmetry in Optics

Interestingly, there is a correspondence between quantum mechanics and paraxial optics, which means that one can transport ideas from one to the other [12, 13]. Inspired by such an idea, in 2007 PT symmetry was mapped from quantum mechanics to optics [15] and then shortly confirmed by two experimental works [19, 20].

Figure. 3.1 scehmatically illustrates the main idea of this mapping in which the wave nature of particles in quantum mechanics is described by Schrodinger equation and the light wave propagation in paraxial optics approximation is governed by [14]

$$i\frac{\partial E}{\partial z} + \frac{1}{2k}\frac{\partial^2 E}{\partial x^2} + k_0[n_R(x) + in_I(x)]E = 0 \tag{3.4}$$

where E is electric field of the wave and x and z correspond to the transverse and

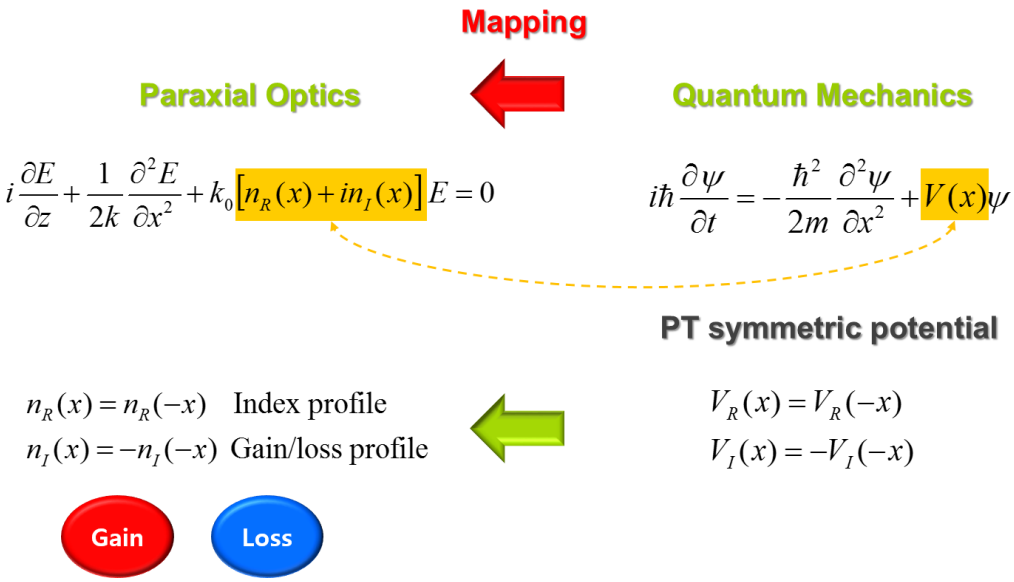

Figure 3.1: Schematic illustration of mapping the PT symmetry from quantum mechanics to paraxial optics. Here refractive index in optical systems plays the role of potential in quantum mechanics.

propagation directions, respectively. Clearly, in this figure optical system is represented as an isomorphic of its PT symmetric quantum counterpart, under a crucial condition at which: real $n_R(x)$ and imaginary $n_I(x)$ parts of the refractive index be an even and an odd function of position, respectively. Nothing that imaginary part of the refractive index corresponds to gain/loss. Next, we present the simplest implementation of a PT symmetric system in integrated photonics.

3.2.1 PT symmetry in coupled optical waveguides

One of the simplest example of PT symmetric systems in optics and especially integrated photonics is illustrated in Figure. 3.2. This system composed of two weakly

coupled waveguides and can be described based on coupled mode theory [14] as follows [15]

$$\begin{cases} i\frac{\partial E_1(z)}{\partial z} - i\gamma E_1(z) + \kappa E_2(z) = 0 \\ i\frac{\partial E_2(z)}{\partial z} + i\gamma E_2(z) + \kappa E_1(z) = 0 \end{cases} \tag{3.5}$$

where $E_1(z)$ and $E_2(z)$ represent electric fields in two coupled identical waveguides,

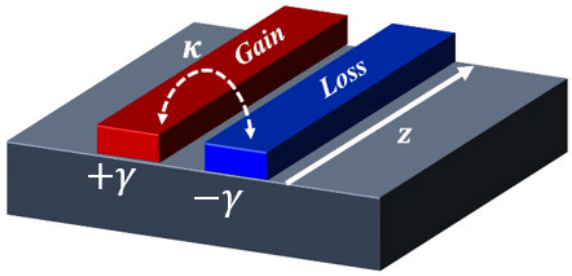

Figure 3.2: Schematic illustration of two weakly coupled waveguides with gain and loss. Here, κ represents the coupling coefficient between these waveguides.

with gain and loss, respectively. Left waveguide receives gain $+\gamma$ and right one has equal amount of loss $-\gamma$. Coupling coefficient between coupled waveguides is represented by κ. Clearly, this system respects the PT symmetry, since parity operator $\hat{P}$ switches the gain and loss waveguides and time operator $\hat{T}$ also converts gain into loss and loss into gain. Thus after applying $\hat{P}\hat{T}$ operator the system returns to its original form. Equation (3.5) can be written in the following matrix form:

$$i\frac{d}{dz}\begin{bmatrix} E_1(z) \\ E_2(z) \end{bmatrix} = \hat{H}\begin{bmatrix} E_1(z) \\ E_2(z) \end{bmatrix} \tag{3.6}$$

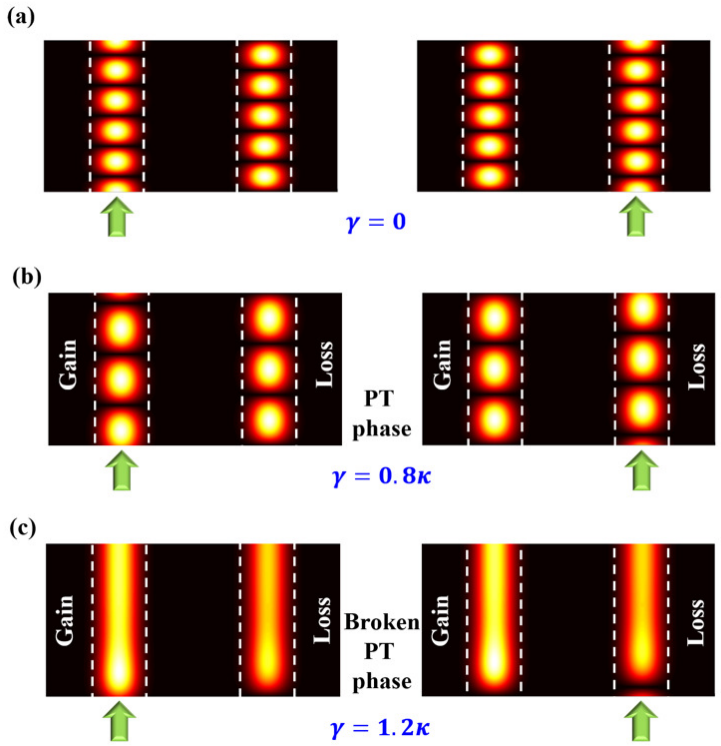

Figure 3.3: Light propagation in coupled waveguides for (a) passive system with $\gamma = 0$, (b) PT phase when $\gamma = 0.8\kappa$ and (c) Broken PT phase when $\gamma = 1.2\kappa$. Here we assumed κ=1.0. Noting that in order to avoid power inflation in (c) we have considered gain saturation effect: $\gamma \rightarrow \gamma/(1 + \alpha|E_1(z)|^2)$ with gain saturation factor $\alpha = 0.1$. Green arrow represents the excited waveguide via external input signal. Clearly, light propagation dynamics in broken PT regime is independent of initial excitation condition.

where

$$\hat{H} = \begin{bmatrix} +i\gamma & -\kappa \\ -\kappa & -i\gamma \end{bmatrix} \tag{3.7}$$

For this system of equation one can find a solution as follows:

$$\begin{cases} E_1(z) = E_1(0)(cos(\beta z) + \frac{\gamma}{\beta} sin(\beta z)) + iE_2(0)(\frac{\kappa}{\beta} sin(\beta z)) \\ E_2(z) = E_2(0)(-cos(\beta z) + \frac{\gamma}{\beta} sin(\beta z)) + iE_1(0)(\frac{\kappa}{\beta} sin(\beta z)) \end{cases} \tag{3.8}$$

where $E_{1,2}(0)$ are initial states corresponding to excitation in each waveguide and

$$\beta = \pm\sqrt{\kappa^2 - \gamma^2} \tag{3.9}$$

Equation (3.9) shows that for $\kappa > \gamma$ propagation constants of the system are real which is called PT phase. This implies a peculiar fact that even in the presence of gain and loss in the system, still one can expect a regime in which there is no amplification or damping, Figure. 3.3 (b). Here for comparison purpose we have illustrated the passive ($\gamma = 0$) case in Figure. 3.3 (a). On the other hand for $\kappa < \gamma$ system lives in broken PT phase and propagation constants is complex $\pm i\sqrt{\gamma^2 - \kappa^2}$ and obviously system undergoes amplification/attenuation, see Figure. 3.3 (c).

It is also very important to look at the eigenvalues and eigenvectors of the $\hat{H}$ in each of these regimes. In the PT phase where $\kappa > \gamma$ eigenvectors of the $\hat{H}$ are $(1, \mp e^{\mp i\theta})^T$ where $sin(\theta) = \gamma/\kappa$ and corresponding eigenvalues are $\pm\kappa cos(\theta)$. Here T represents the transpose operator. At Exceptional point where $\kappa = \gamma$ eigenvectors coalesce $(1, i)^T$ and eigenvalues are the same and equal to zero. Clearly, at EP the system's dimensionally reduced to one. Finally, in broken PT regime where $\kappa < \gamma$: eigenvectors are $(1, \pm ie^{\pm\theta})^T$ where $cosh(\theta) = \gamma/\kappa$ and corresponding eigenvalues are $\pm i\kappa sinh(\theta)$. More importantly, one can see that eigenvectors of this non-Hermitian system are not orthogonal, in other words, the basis is skewed [6, 7]. Figure. 3.4 illustrates the eigenvalues of the system versus (γ) gain/loss coefficient.

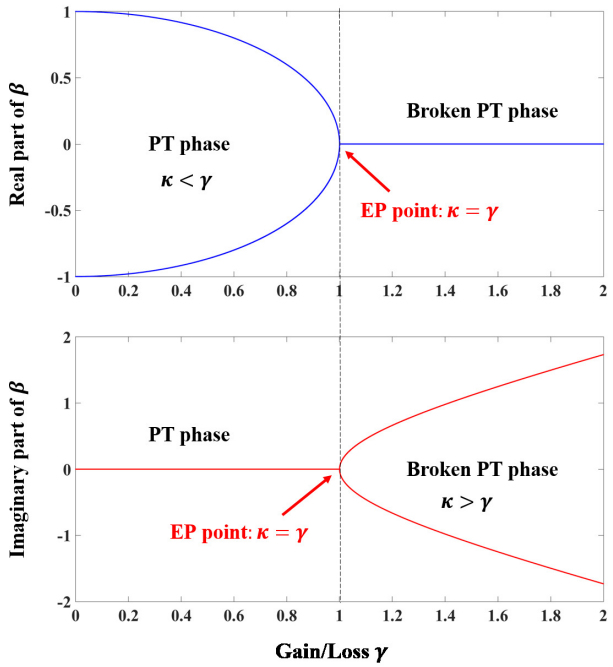

Figure 3.4: Real (top) and imaginary (bottom) parts of the eigenvalues of the system versus gain/loss γ. Here $\kappa = 1.0$ and dashed line passes through exceptional point at $\kappa = \gamma$. Clearly, PT/broken PT phases are on the left/right side of this line.

PT symmetry in optics was first realized in two different experiments where judiciously engineered coupled waveguides with loss/loss [19] or gain/loss [20] are fabricated to investigate the phase transition in parameter space between two identified PT and broken PT regimes. These two experiments actually paved the way for new generation of integrated photonics systems with many applications including single mode lasers [29, 30, 31] and more recently optical sensors [32] and robust wireless power transfer systems [33]. In this thesis, we are interested in single mode PT symmetric lasers and in general non-Hermitian engineered laser systems to achieve single mode operation. Thus in the next section, we shortly review one of the most relevant experimental work in single mode PT symmetric microlasers.

3.2.2 PT symmetric lasers

Single mode operation of laser systems was always one of the fundamental aims of laser designers. To accomplish this goal, there are many ways such as: coupling the laser cavity to another detuned external cavity, using distributed feedback gratings to introduce a dispersive element and suppress undesired modes or by modulation of the pump spatially [35, 36, 37, 38, 39]. Although each of these methods are very efficient but not all of them are compatible with every type of resonators and each of them has its own design and fabrication restrictions. Consequently, it is important to always find alternative schemes with less complexity and much more versatility. Recently, a single mode laser based on PT symmetry is theoretically [28] and experimentally presented [29, 30] and it is shown that PT symmetry breaking can be used to achieve single mode lasing operation in inherently multimoded microring lasers. Demonstrated system in [30] is consists of two identical coupled microrings, one cavity is passive (lossy) and the other one provides equal amount of gain through optical pumping. The main idea here is to design the system in such a way that all unwanted modes stay in PT phase and the only lasing mode lives in breaking PT phase, thus the lasing mode enjoys more gain than the other competing modes. On the other hand, in PT regime unwanted modes undergo the gain and loss equally without reaching to lasing threshold (neither amplification nor decay), as result they do not contribute in lasing. Noting that this idea is implemented in microring lasers

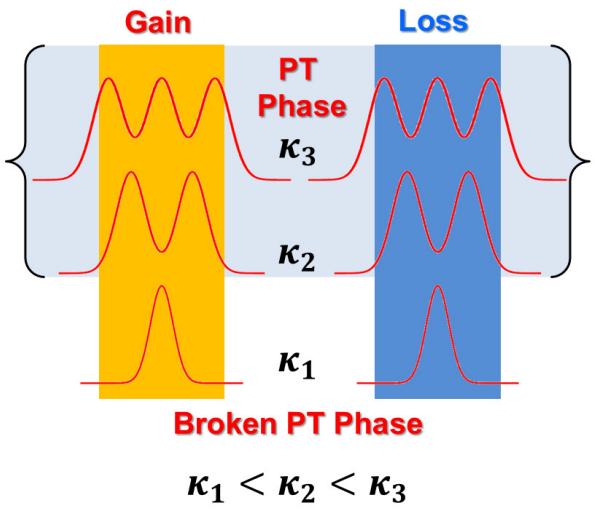

Figure 3.5: Schematic illustration two coupled laser cavities with gain and loss. For simplicity we just considered three modes in each cavity represented by $\omega_{1,2,3}$ and they all have the same gain/loss coefficient γ. The coupling coefficient is clearly different for each mode and $\kappa_1 < \kappa_2 < \kappa_3$. The system is engineered in such a way that $\kappa_1 < \gamma < \kappa_2 < \kappa_3$ thus fundamental mode lives in broken PT phase and the other modes in PT phase. This leads to single mode lasing in fundamental mode whereas the other modes do not contribute in lasing as long as $\kappa_1 < \gamma < \kappa_2 < \kappa_3$ is satisfied.

to suppress longitudinal [30] and transverse modes [31]. Here we shortly review the latter one.

In order to understand how PT symmetric laser works we consider an schematic laser system represented in Figure. 3.5. Here it is assumed that laser cavity supports three transverse modes and the goal is to suppress all of them except for the fundamental one. To do this, we consider an identical but lossy cavity which supports all modes of the laser cavity (with gain). Next, these two cavities should be placed close enough to introduce a coupling between modes and clearly, these coupling coefficients satisfy $\kappa_1 < \kappa_2 < \kappa_3$, since higher order modes have longer tail outside the cavity than the

fundamental one. Since this system respects PT symmetry eigenmodes of the system are given by (see Eq. (3.9))

$$\omega_n^{(\pm)} = \omega_n \pm \sqrt{\kappa_n^2 - \gamma_n^2} \tag{3.10}$$

where ω_n is resonance frequency of each mode and γ_n corresponds to its gain/loss. Now, for simplicity, let us assume that all modes have the same gain/loss coefficient and then by judicious engineering of the gain/loss coefficients (γ) in such a way that $\kappa_1 < \gamma < \kappa_2 < \kappa_3$ one can immediately see that both higher order modes live in PT phase which implies no amplification nor attenuation. Thus, for these modes, system undergoes neutral oscillations and supermodes are evenly distributed between gain and loss regions. On the other hand, the fundamental mode lives in the broken PT phase, thus for this mode system experiences amplification/attenuation, ($\omega_1^{(\pm)}$ are complex for fundamental modes, see Eq. (3.10)). Therefore only lasing mode is the one in broken PT phase and the other modes may not lase as long as they are in PT phase.

3.3 Suppersymmetry in Quantum Mechanics

Supersymmetry (SUSY) was first convinced in the context of high energy physics and it relates bosonic and fermionic particles [40, 41]. SUSY plays an important role in standard model, quantum field and string theories, astrophysics, low energy physics in nuclear physics, condensed matter, statistical mechanics, nonlinear dynamics and soliton theory as well as stochastic processes and BCS-type theories.

In 1981, E. Witten introduced the concept of SUSY in quantum mechanics [42]. He started with system of single particle Schrdinger equation in one dimension and introduced the notion of SUSY to quantum mechanics. His work, let to interesting results and attracted considerable attention and research activities.

In order to understand the concept of SUSY in quantum mechanics, let us start with a system composed of a bosonic and fermionic harmonic oscillators in the absence of any interactions. Hamiltonian of this system can be described based on the second quantization formalism, as follows:

$$H = H_b + H_f = \omega_b a^\dagger a + \omega_f f^\dagger f \tag{3.11}$$

where H_b and H_f are bosonic and fermionic Hamiltonians, respectively. Here, a and $a^\dagger$ are the bosonic annihilation and creation operators respecting the commutation

relations $[a, a^\dagger] = 1$ and $[a, a] = [a^\dagger, a^\dagger] = 0$; while c and $c^\dagger$ are the fermionic annihilation and creation operators obeying $\{f, f^\dagger\} = 1$ and $\{f, f\} = \{f^\dagger, f^\dagger\} = 0$. In the above [ ] and {} denote commutation and anticommutation operations, respectively and we have set $\hbar = 1$. In Eq. (3.11), $\omega_{b,f}$ are the frequencies associated with the bosonic and fermionic oscillators. Because of the different algebra of the the a and f operators, it is easy to see that each bosonic state can be populated by any number of bosons while each fermionic state can be occupied only by one fermion (Pauli exclusion principle). Wavefunction of this system can be described in Fock space as a direct tensor product of the bosonic and fermionic states: $|\psi_{m,n}>=|m,n>$ where $m = 0, 1, 2, ...$, while $n = 0, 1$. The associated eigenvalues (neglecting zero-point energy) are given by $E_{m,n} = \hbar(m\omega_b + n\omega_f)$. In Figure. 3.6 eigenstates of this system is categorized in two different possible sectors: the bosonic sector where there are no fermions $|\psi_{m,n=0}>$ and the fermionic sector where there is one fermion $|\psi_{m,n=1}>$. In the special case at which $\omega_b = \omega_f = \omega$, (which is technically called unbroken SUSY), it is easy to see that: $E_{m+1,n=0} = E_{m,n=1}$. Thus,except for the ground state $E_0,\ 0$, there is a correspondence between the eigenvalues of the bosonic and fermionic sectors.

It is also possible to describe the eigenstates associated with Eq. (3.11) using the operators $Q = \begin{pmatrix} 0 & 0 \\ A & 0 \end{pmatrix}$ and $Q^\dagger = \begin{pmatrix} 0 & A^\dagger \\ 0 & 0 \end{pmatrix}$, where $A = d/dx + \omega x$ and $A^\dagger = -d/dx + \omega x$. Easily, one can see that $\frac{1}{2}\{Q, Q^\dagger\} = \frac{1}{2}\begin{pmatrix} A^\dagger A & 0 \\ 0 & AA^\dagger \end{pmatrix} \equiv$

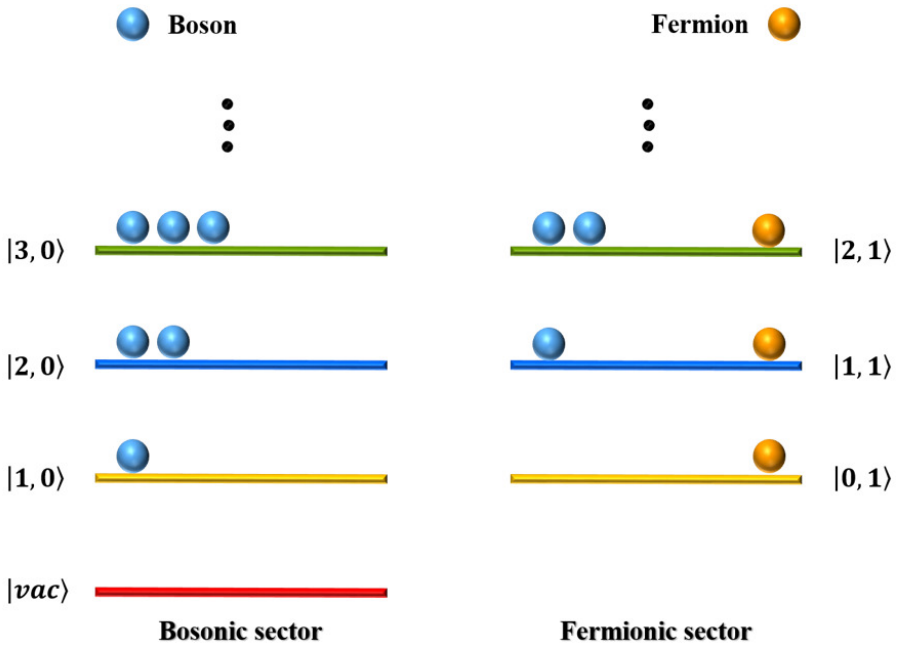

Figure 3.6: Schematic illustration of two superpartner systems in the contex of SUSY. On the left one system composed of Bosonic elements and on the right its Fermionic superpartner is shown.

$\begin{pmatrix} H_b & 0 \\ 0 & H_f \end{pmatrix} \equiv H$, together with the relations $\{Q, Q\} = \{Q^\dagger, Q^\dagger\} = \{Q, H\} = 0$. The above system of algebra that consists of commutations and anticommutations relations is called as super algebra with Q and $Q^\dagger$ called the supercharges and the Hamiltonian corresponding to the bosonic ($H_b \equiv \omega a^\dagger a$) and fermionic ($H_f \equiv \omega(a^\dagger a + 1)$) sectors are known as the superpartner Hamiltonians. It has to be mentioned that bosonic and fermionic Hamiltonians $H_{b,f}$ are related to each others through intertwining the order of operators A and $A^\dagger$. Shortly, it is explained that, this property leads to important consequences.

The above construction can be extended beyond harmonic oscillators by the generalization $A^\dagger = -d/dx + W(x)$ and $A = d/dx + W(x)$, where $W(x)$ is chosen to be a real function. By doing this, we find the new Hamiltonians: $H_b = -\frac{1}{2}\frac{-d^2}{dx^2} + V_1(x)$ and $H_f = -\frac{1}{2}\frac{-d^2}{dx^2} + V_2(x)$, where the potential functions $V_{1,2}(x) = \frac{1}{2}(W^2(x) \mp \frac{dW(x)}{dx})$ are known as the superpartner potentials. The above Hamiltonian can be written in a more compact format $H = (-\frac{1}{2}\frac{d^2}{dx^2} + \frac{W^2(x)}{2})I_2 + \frac{1}{2}\frac{dW(x)}{dx}\sigma_3$ with the identity matrix $I_2 = \begin{pmatrix} 1 & 0 \\ 0 & 1 \end{pmatrix}$ and Pauli matrix $\sigma_3 = \begin{pmatrix} 1 & 0 \\ 0 & -1 \end{pmatrix}$. This Hamiltonian interpreted by E. Witten as that of a spin $\frac{1}{2}$ particle moving in one dimension under the action of a potential $\frac{W^2(x)}{2}$ and a magnetic field $\frac{1}{2}\frac{dW(x)}{dx}$.

Let us now assume that $|\phi_b>$ is an eigenstate of H_b with an eigenvalue λ, i.e. $H_b|\phi_b> = A^\dagger A|\phi_b> = \lambda|\phi_b>$. It follows that $AH_b|\phi_b> = (AA^\dagger)A|\phi_b> = H_f A|\phi_b> = \lambda A|\phi_b>$. In other words, if $|\phi_b>$ is an eigenstate of H_b with an eigenvalue λ, then $|\phi_f> = A|\phi_b>$ is an eigenstate of H_f having the same eigenvalue. Thus, if $|\phi_f>$ is an eigenstate of H_f with an eigenvalue λ, then $|\phi_b> = A^\dagger|\phi_f>$ is an eigenstate of H_b with the same eigenvalue. Figure. 3.6 shows that only the ground state of H_b which is annihilated by the action of the operator A does not have a corresponding state in the fermionic sector. However, when SUSY is broken, the ground state can still have a corresponding state.

One may ask an interesting question: for any given potential $V_1(x)$, how can one finds its superpartner $V_2(x)$? To do so, one has to first find function $W(x)$ through

solving Reccati-type equation, or alternatively, one can show that $W(x) = -\frac{d}{dx}\ln(\psi_o)$ where ψ_o is the ground state wavefunction associated with $V_1(x)$. Then, it is straight forward to use $V_2(x) = \frac{1}{2}(W^2(x) + \frac{dW(x)}{dx})$ and find superpartner $V_2(x)$.

Further details on SUSY quantum mechanics and its various applications can be found in [40, 41].

3.4 SUSY in Optics

As we described earlier, there is a formal mathematical analogy between quantum mechanics and the paraxial equation of diffraction in optics. The concept of supersymmetric optics was first introduced in [43] and recently studied in details in [44, 45, 46, 47, 48, 49, 50, 51] in connection with applications in optical communications and laser engineering.

3.4.1 Continuous case

Let us start by considering the one dimensional propagation of transverse electric (TE) light across a refractive index profile $n(x)$ where x is the transverse coordinate (nothing that similar conclusions may apply for transverse magnetic (TM) case):

$(\partial_{xx} + \partial_{zz} + k_0^2 n^2(x))E_y(x,z) = 0$, where z is the propagation distance and E_y is the transverse electric component. One can describe the propagating modes in this system as $E_y(x,z) = G(x)\exp(i\beta z)$ where β is the propagation constant and $G(x)$ satisfies:

$$\begin{aligned} \mathcal{H}G(x) &= -\beta^2 G(x), \\ \mathcal{H} &\equiv -d^2/dx^2 - k_0^2 n^2(x) \end{aligned} \tag{3.12}$$

Lets assume that for any given refractive index profile $n^{(1)}(x)$, we express the fundamental optical mode (ground state) by $G^{(1)}(x)$ and its propagation constant by $\beta_1^{(1)}$. Thus, according to what we have studied in previous section, the supersymmetric refractive index (potential) partners read:

$$\begin{aligned} [k_o n_{1,2}(x)]^2 &= \left(\beta_1^{(1)}\right)^2 - W(x)^2 \pm \partial_x W(x), \\ W(x) &= -\frac{d}{dx}\ln(G_1^{(1)}(x)) \end{aligned} \tag{3.13}$$

The SUSY relation in Eq. (3.12) becomes more transparent if we note that $\mathcal{H}^{(1)} + (\beta_1^{(1)})^2 = B^\dagger B$ and $\mathcal{H}^{(2)} + (\beta_1^{(1)})^2 = BB^\dagger$ where $B = -d/dx + W(x)$ and $B^\dagger = d/dx + W(x)$. Except for minor sign conventions, these equations are similar to the ones studied in the previous section. Therefore, all above mentioned properties of the SUSY such as spectral isospectrality (due to the properties of intertwining operators) and all the results regarding reflection and transmission coefficients associated with superpartner potentials in quantum mechanics, can be mapped into optical systems.

3.4.2 Discrete case

In general, any optical system can be described by Maxwell's equations, however, coupled mode theory, which is also derived from Maxwell's equations, leads to considerable simplification in analysis of coupled discrete optical systems such as waveguides or cavities. In this approach a system of coupled first order differential equations describes the equation of motion for the optical amplitudes $\vec{e}(t)$ inside the cavities (or waveguides) as follows:

$$i\frac{d\vec{e}(t)}{dt} = \mathcal{D}^{(1)}\vec{e}(t), \tag{3.14}$$

where the discrete Hamiltonian $\mathcal{D}^{(1)}$ is an $N \times N$ tridiagonal symmetric matrix having the elements $\mathcal{D}^{(1)}_{i,j} = \Omega_i\delta_{i,j} + J_{i,j}\delta_{i,j+1} + J_{i,j}\delta_{i,j-1}$. In Eq. (3.14), Ω_i is the frequency of the i^{th} cavity and can be in general complex to indicate dissipation, while $J_{i,j} = J_{j,i}$ are the temporal coupling coefficients. The same formalism applies to the case of coupled waveguide arrays after the substitution $\Omega \to \beta$ and $J \to \kappa$, where $\beta's$ and $\kappa's$ are the propagation constants and the spatial coupling coefficients, respectively. We express the eigenvalues of $\mathcal{D}^{(1)}$ by λ_n with $n = 1, 2, ...N$. Now in order to map SUSY into this discrete system, we can use QR factorization method (see [52, 53]) to construct a superpartner discrete Hamiltonian $\mathcal{D}^{(2)}$ having all the eigenvalues except , say λ_m as follows: first to evaluate $\mathcal{D}^{(1)} - \lambda_m I_N = QR$, where I_N is the identity matrix of size $N \times N$. Second, we compute $\mathcal{D}^{(2)} = RQ + \lambda_m I_N$. One can show that the resultant

$N \times N$ matrix is composed of two uncoupled blocks: one has unit dimension and contains the element λ_m and the other is an $(N-1)\times(N-1)$ tridiagonal matrix that corresponds to $\mathcal{D}^{(2)}$ with eigenvalues identical to the the eigenvalues λ_n, $n \neq m$. This transformation is called discrete supersymmetry (DSUSY). The main characteristic of this method is that it construct a reduced *quasi-isospectral symmetric tridiagonal* matrix which can be optically realized by judicious engineered cavity or waveguide arrays. It has to be mentioned that, other decomposition techniques such as the Cholesky method can be also used (but with some constraints).

In the next section we review an interesting use of DSUSY in laser engineering to achieve single mode laser arrays.

3.4.3 Supersymmetric laser arrays

Since early days of laser invention achieving single mode high power laser was not an easy task and finding effective solutions for this issue has been always challenging. In semiconductor lasers, this issue has been also tackled by many research groups, however, using these proposed approaches is not always easy or even possible for every semiconductor laser platform [35, 36, 37, 38]. In general, increasing the pumping power leads to higher output power, however, after a certain threshold nonlinear effects due to inherent material nonlinearity and carrier diffusion dynamics may lead

to chaotic laser dynamics. Obviously, this issue can be solved by increasing the laser area thus lees laser power in cavity to avoid nonlinear effects. On the other hand, increasing the laser area leads to multimode laser cavity which can lead to multimode laser dynamics and this again degrades the laser output. Filamentation effect is a well-known issue in large area lasers caused by carrier dynamics of modulation instabilities. An alternative solution is to have an array of coupled lasers with small area [36]. For such an array of N coupled cavities there are N supermodes and immediately one can tell that all these modes will compete in lasing [36]. On the other hand if such a laser array, lases in its in-phase (fundamental mode) the output power at the far field is enhanced buy factor proportional to N^2.

Recently, it turned out that SUSY together with non-Hermitian engineering can be used to mitigate multimode laser operation and achieve single mode laser arrays in one and two dimensional systems [50, 51]. In this section we review the one dimensional sypersymmetric laser arrays and in chapter five we study the two dimensional case.

Figure. 3.7 schematically presents the main idea of this approach for 1D case in which an array of semiconductor lasers (edge-emitting waveguide resonators) is coupled to its lossy suppersymmetric partner. In the linear regime at the lasing threshold, once can construct such a super partner through DSUSY, in such a way it supports all supermodes of the main laser array except for its fundamental (in-phase) one. By introducing coupling between these arrays (the main one and its superpartner) all

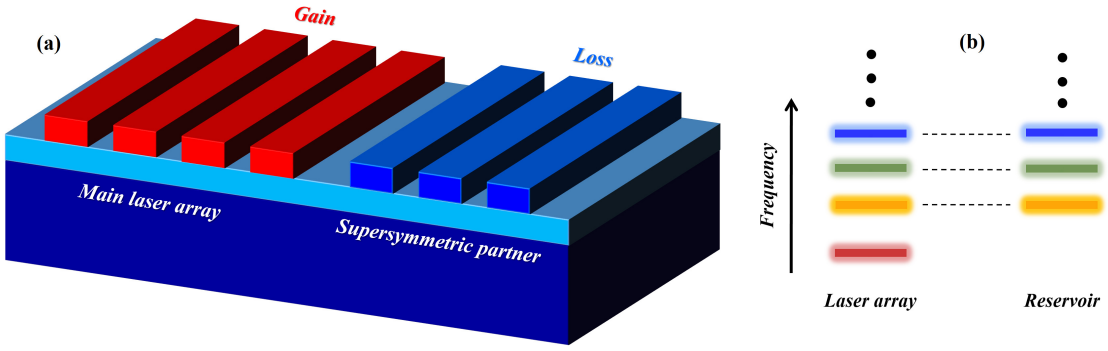

Figure 3.7: (a) Laser array is coupled to its dissipative superpartner. (b) Supersymmetric partner array designed to supports all modes of the main laser array ecxept for fundamental one. Thus quality factor of all of unwanted modes are spoiled except for fundamental inphase one. This leads to the single mode lasing in desired fundamental mode [50].

supermodes of the main array form doublets except for the fundamental mode which does not have a superpartner. Finally, introducing optical loss to the superpartner array spoils the quality factors of the all undesired higher order modes and force only the fundamental mode into lasing action via uniform pumping of the main laser array.

References

[1] Classical Mechanics (3rd Edition) H. Goldstein, ISBN-13: 978-0201657029 Pearson;(2001)

[2] Quantum Mechanics, Third Edition: Non-Relativistic Theory Quantum Mechanics, L. D. Landau, L. M. Lifshitz, ISBN-13: 978-0750635394, Butterworth-Heinemann; 3 edition (1981)

[3] Quantum Electrodynamics, Second Edition: Volume 4 (Course of Theoretical Physics) L. D. Landau, L. M. Lifshitz, ISBN-13: 978-0750633710, Butterworth-Heinemann; 3 edition (1982)

[4] Principles of Quantum Mechanics R. Shankar, ISBN 978-1-4757-0576-8, Springer (1994).

[5] Modern Quantum Mechanics (2nd Edition) J. J. Sakurai and Jim J. Napolitano, ISBN-13: 978-0805382914, Pearson (2010).

[6] C. M. Bender, and S. Boettcher, Real Spectra in Non-Hermitian Hamiltonians Having PT Symmetry Phys. Rev. Lett. 80, 5243 (1998).

[7] C. M. Bender, Making sense of non-Hermitian Hamiltonians, Phys Rep. Prog. Phys. 70, 947 (2007).

[8] A. Znojil, PT-symmetric square well, Phys. Lett. A 285, 7 (2001).

[9] Z. Ahmed , Real and complex discrete eigenvalues in an exactly solvable one-dimensional complex PT-invariant potential, Phys. Lett. A 282, 343 (2001).

[10] W. D. Heiss, M. Mller, and I. Rotter, Collectivity, phase transitions, and exceptional points in open quantum systems, Phys. Rev. E 58, 2894 (1998).

[11] W. D. Heiss, Exceptional points of non-Hermitian operators, J. Phys. A: Math. Gen. 37, 2455 (2004).

[12] M. Nazarathy and J. Shamir, Fourier optics described by operator algebra, Journal of the Optical Society of America Vol. 70, Issue 2, pp. 150-159 (1980).

[13] V.I Man ko and K.B. Wolf, Lie Methods in Optics II, Springer Lecture Notes in Physics, Vol. 352. Ed. by k. B. Wolf (Springer Verlag, Heidelberg, 1989).

[14] K. Okamoto , Fundamentals of Optical Waveguides, Second Edition (Optics and Photonics Series) 2nd Edition, ISBN-13: 978-0125250962, Academic Press (2005)

[15] R. El-Ganainy, K. G. Makris, D. N. Christodoulides, Z. H. Musslimani, Theory of coupled optical PT-symmetric structures, Opt. Lett. 32, 2632 (2007).

[16] K. G. Makris, R. El-Ganainy, D. N. Christodoulides, and Z. H. Musslimani, Beam Dynamics in PT-Symmetric Optical Lattices, Phys. Rev. Lett. 100, 103904 (2008).

[17] Z. H. Musslimani, K. G. Makris, R. El-Ganainy, D. N.Christodoulides, Optical Solitons in PT Periodic Potentials, Phys. Rev. Lett. 100, 030402 (2008).

[18] K. G. Makris, R. El-Ganainy, D. N. Christodoulides, and Z. H. Musslimani, PT -symmetric optical lattices, Phys. Rev. A 81, 063807 (2010).

[19] A. Guo, G. J. Salamo, D. Duchesne, R. Morandotti , M. Volatier Ravat, V. Aimez , G. A. Siviloglou and D. N. Christodoulides, Observation of PT Symmetry Breaking in Complex Optical Potentials Phys. Rev. Lett. 103, 093902 (2009).

[20] C. E. Ruter, K.G. Makris, R. El-Ganainy, D.N. Christodoulides, M. Segev, D. Kip, Observation of paritytime symmetry in optics, Nature Physics 6, 192 (2010).

[21] Z. Lin, H. Ramezani, T. Eichelkraut, T. Kottos, H. Cao, and D. N. Christodoulides, Unidirectional Invisibility Induced by PT-Symmetric Periodic StructuresPhys. Rev. Lett. 106, 213901 (2011).

[22] H. Ramezani, T. Kottos, R. El-Ganainy and D.N. Christodoulides, Unidirectional nonlinear PT-symmetric optical structuresPhys Rev. A. 82, 043803 (2010).

[23] E M Graefe, U Gnther, H J Korsch and A E Niederle, A non-Hermitian PT

symmetric BoseHubbard model: eigenvalue rings from unfolding higher-order exceptional points J. Phys. A: Math. Theor. 41 255206 (2008).

[24] X. Z. Zhang, L. Jin, and Z. Song, Perfect state transfer in PT-symmetric non-Hermitian networksPhys. Rev. A 85, 012106 (2012).

[25] A. Regensburger, C. Bersch, M. A. Miri, G. Onishchukov, D. N. Christodoulides, U. Peschel, Paritytime synthetic photonic lattices, Nature, 488, 167 (2012).

[26] B. Peng, S. K. Ozdemir, F. Lei, F. Monifi, M. Gianfreda, G. L. Long, S. Fan, F. Nori, C. M. Bender and L. Yang, Paritytime-symmetric whispering-gallery microcavities, Nature Physics, DOI: 10.1038/NPHYS2927.

[27] Teimourpour, M. H., El-Ganainy, R., Eisfeld, A., Szameit, A. and Christodoulides, D. N. Light transport in PT-invariant photonic structures with hidden symmetries. Physical Review A 90(5), 053817 (2014).

[28] M.A. Miri, P. LiKamWa, and D.N. Christodoulides, Large area single-mode paritytime-symmetric laser amplifiers, Optics Letters Vol. 37, Issue 5, pp. 764-766 (2012).

[29] Feng, L., Wong, Z. J., Ma, R., Wang, Y. and Zhang, X. Single-mode laser by parity-time symmetry breaking. Science 346, 972975 (2014).

[30] Hodaei, H., Miri, M. A., Heinrich, M., Christodoulides, D. N. and Khajavikhan, M. Parity-timesymmetric microring lasers. Science 346, 975978 (2014).

[31] H. Hodaei, M.A. Miri, Absar U. Hassan, W. E. Hayenga, M. Heinrich, Demetrios N. Christodoulides, M. Khajavikhan, Single mode lasing in transversely multi-moded PT-symmetric microring resonators

[32] Hodaei H, Hassan AU, Wittek S, Garcia-Gracia H, El-Ganainy R, Christodoulides DN, Khajavikhan M. Enhanced sensitivity at higher-order exceptional points, Nature 548(7666):187-191. doi: 10.1038/nature23280 (2017).

[33] Sid Assawaworrarit, Xiaofang Yu and Shanhui Fan, Robust wireless power transfer using a nonlinear paritytime-symmetric circuit, Nature Vol. 546, 387 (2017).

[34] MH Teimourpour, K zdemir, R El-Ganainy, Reverse PT phase transition across exceptional points of any order, EPL (Europhysics Letters) 119 (3), 34003 (2017).

[35] Agrawal, G. P. and Dutta, N. K. Semiconductor Lasers, (Springer Science and Business Media, 2013).

[36] Verdeyen J. T. Laser electronics, (Prentice-Hall, 1981).

[37] Ohtsubo, J. Semiconductor Lasers: Stability, Instability and Chaos, (Springer Berlin Heidelberg, 2005).

[38] Kapon, E. Semiconductor Lasers I: Fundamentals, (Academic Press, 1999).

[39] Ghafouri-Shiraz, H. Distributed Feedback Laser Diodes and Optical Tunable Filters, (John Wiley and Sons, 2004).

[40] Bijan Kumar Bagchi, Supersymmetry In Quantum and Classical Mechanics ISBN 9781420035810, CHAPMAN and HALL/CRC (2001).

[41] F. Cooper, Supersymmetry in Quantum Mechanics (World Scientific, 2002).

[42] Edward Witten Dynamical breaking of supersymmetry Nuclear Physics B Volume 188, Issue 3, 5 October 1981, Pages 513-554

[43] S. M. Chumakov and K. B. Wolf, Supersymmetry in Helmholtz optics, Phys. Lett. A 193, 51 (1994).

[44] Miri, M. A., Heinrich, M., El-Ganainy, R. and Christodoulides, D. N. Supersymmetric optical structures. Phys. Rev. Lett. 110, 233902-1 2339025 (2013).

[45] M. Heinrich, M. A. Miri, S. Sttzer, R. El-Ganainy, S. Nolte, A. Szameit, and D. N. Christodoulides, Supersymmetric mode converters, Nat. Commun. 5, 3698 (2014).

[46] M. A. Miri, M. Heinrich, and D. N. Christodoulides, SUSY-inspired one-dimensional transformation optics, Optica 1, 89 (2014).

[47] M. Heinrich, M. A. Miri, S. Sttzer, S. Nolte, D. N. Christodoulides, and A. Szameit, Observation of supersymmetric scattering in photonic lattices, Opt. Lett. 39, 6130 (2014).

[48] S. Yu, X. Piao, J. Hong, and N. Park, Bloch-like waves in random-walk potentials based on supersymmetry, Nat. Commun. 6, 8269 (2015).

[49] M. H. Teimourpour, D. N. Christodoulides and R El-Ganainy, Optical revivals in nonuniform supersymmetric photonic arrays, Optics letters 41 (2), 372-375 (2016).

[50] R. El-Ganainy, L. Ge, M. Khajavikhan, and D. N. Christodoulides, Supersymmetric laser arrays, Phys. Rev. A 92, 033818 (2015).

[51] Teimourpour, M. H., Ge, L., Christodoulides, D. N. and El-Ganainy, R. Non-Hermitian engineering of single mode two dimensional laser arrays. Sci. Rep. 6, 33253 (2016).

[52] V. Spiridonovdag and A. Zhedanovddag, Discrete-time Volterra chain and classical orthogonal polynomials, Journal of Physics A: Mathematical and General, Volume 30, Number 24 (1997).

[53] B. F. Samsonova and A.ASuzko, Discrete supersymmetries of the Schrdinger equation and nonlocal exactly solvable potentials, Volume 302, Issues 56, Pages 234-241 (2002).

Chapter 4

Robustness and mode selectivity in PT symmetric lasers

Semiconductor lasers are indispensable tools that play important roles in several applications such as fiber optics communication networks, optical memory, medical diagnosis and surgery, and sensing. Commercial semiconductor lasers fall into two main categories: surface and edge emitting devices [1, 2, 3], the design details of which can vary widely depending on the material system, photonic architecture, emission wavelength and operation environment. The former can be tailored to support only one longitudinal mode. The latter however, due to the relatively large gain bandwidth curve of semiconductors compared to atomic gas and the longer optical path of a full roundtrip inside the cavity, can be multimoded. Several strategies have been

developed to overcome this problem. One common techniques is based on distributed feedback mechanism which relies on periodic modulation of optical refractive index [4]. The quest for continuous miniaturization and lower power consumption (ideally threshold-less devices) has sparked interest in novel laser cavities such as microdiscs [5, 6, 7, 8, 9, 10, 11, 12], microrings [13, 14, 15], photonic crystals [16, 17] and plasmonics [18]. Although, several methods for achieving single mode emission in these geometries have been proposed [12, 13, 14], a commercially viable option is still lacking.

Recently, the novel concept of PT symmetry [19, 20] was recently introduced in optics and photonics [21, 22, 23, 24, 25], which subsequently led to intense investigations [26, 27, 28, 29, 30, 31, 32, 33, 34, 35, 36, 37, 38, 39, 40, 41, 42, 43]. Inspired by some of these recent activities, non-Hermitian engineering of laser emission near exceptional points have been theoretically investigated and experimentally reported by several research groups [44, 45, 46, 47, 48, 49, 50, 51, 52]. In particular the work in [45] demonstrated the possibility of single mode operation in PT symmetric photonic molecules made of microring resonators. Subsequent theoretical studies have investigated nonlinear interactions between the optical supermodes in these systems [53, 54, 55] assuming that each resonator supports only one optical mode (with the exception of [54] which also considered spatial hole burning effects in multimode cavities).

Motivated by these rapid developments, here we investigate PT symmetric photonic

molecule lasers (see Fig 4.1 (a)), taking into consideration the nonlinear interactions between the intrinsic single cavity modes (not just the supermodes). Our study, complementing previous works and providing insight into the operation dynamics of PT symmetric lasers, reveal the following important results: (1) PT symmetry can provide superior performance (in terms of single longitudinal mode operation) in microcavities having relatively large FSR, and (2) Extending the concept to millimeter long edge emitting lasers can be challenging due to nonlinear instabilities, and (3) More general loss engineering schemes can be used to achieve more control over mode selectivity. To this end, we start by considering a photonic molecule laser made of two

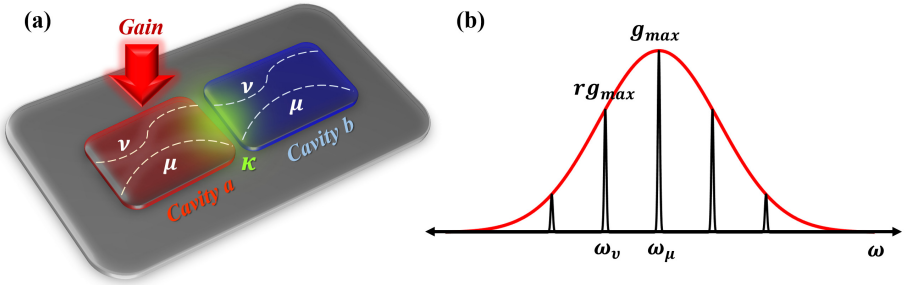

Figure 4.1: (a) A schematic of the photonic molecule laser investigated in this work. It consists of two identical coupled optical cavities (a and b), each of which supports in general many several modes (later we focus on only two modes). The coupling coefficients between each pair of the modes is assumed to be the same and equal κ. Moreover, pumping is applied only to cavity a. A typical semiconductor gain curve along with the assumed modal frequencies are shown in (b) where g_{max} and rg_{max} are gain values experienced by modes μ and ν respectively.

coupled isospectral optical cavities that support only one transverse mode and several longitudinal ones. We assume that the pumping (electrical or optical) is applied only to one cavity while the other remains passive as illustrated schematically in Fig. 4.1 (a). We denote the identical intrinsic loss coefficients of any mode n in either cavity by

α_n (which in general can include material and radiation loss as well as any mechanism for extracting laser light such as evanescent coupling to waveguides). Our model so far coincide with that presented in [45]. In order to demonstrate the possibility of engineering a more complex lasing selectivity, we depart from [45] (which treats only the case of cavities having equal loss) by assuming that the passive cavity can exhibit an extra contribution to the modal loss and we denote this additional part by γ_n. Under these conditions and by eliminating the fast carrier dynamics adiabatically from the rate equations, we arrive at:

$$\begin{aligned} i\frac{da_n}{dt} - (\omega_n - i\alpha_n)a_n - i\frac{g_n}{1+\sum_{m=1}^{N} s_{nm}|a_m|^2}a_n + \kappa_n b_n = 0. \\ i\frac{db_n}{dt} - (\omega_n - i\alpha_n - i\gamma_n)b_n + \kappa_n a_n = 0. \end{aligned} \tag{4.1}$$

In equation (4.1), a_n and b_n are the electric field amplitudes associated with mode n in cavities a and b respectively, and g_n is the gain coefficient in cavity a while κ_n is the coupling coefficient between modes n. Here, ω_n corresponds to resonance frequency of mode n. Finally, s_{nn} (s_{nm}) are the self (cross) gain saturation coefficient (usually $s_{nn} > s_{nm}$) [15]. Below or at the lasing threshold, the eigenvalues of the above system, as expressed in the basis $exp(-i\Omega_n t)$, are given by:

$$\Omega_n^{\pm} = \omega_n + i\frac{g_n - 2\alpha_n - \gamma_n}{2} \pm i\sqrt{(\frac{g_n + \gamma_n}{2})^2 - \kappa_n^2} \tag{4.2}$$

Above the lasing threshold, nonlinear interactions are crucial and must be taken into

consideration.

Having introduced the model, we now proceed to investigate the robustness and mode selectivity of single longitudinal mode PT symmetric lasers in the following sections. In the rest of this work, single mode operation refers to the longitudinal modes. Additionally, for illustration purpose and in order to gain insight into the physics of the problem, we will consider only two modes per cavity, denoted by $n = \mu$ (the mode corresponds to ω_μ that lies under the peak of the gain curve g_{max}) and the other mode indicated by ω_ν which experiences a gain rg_{max}. As the pump is increased, the value of g_{max} increases but we assume that the ratio $r < 1$ remains constant. Furthermore, we assumed $\kappa_\mu = \kappa_\nu \equiv \kappa$ [45].

4.1 Robustness and stability of single mode PT lasers

In this section, we study the robustness of single mode PT lasers against spectral hole burning effects that might trigger multimode operation. Here we assume that $\gamma_n = 0$ and $\alpha_\mu = \alpha_\nu \equiv \alpha$. According to equation (4.2), the system starts lasing in the broken PT phase if $\alpha > \kappa$. Under this condition, the lasing threshold is given by $g_\mu^{th} = \alpha + \kappa^2/\alpha$ [49]. To first demonstrate the possible different lasing regimes, we integrate equation (4.1) numerically for $\alpha = 1.5$, $\kappa = 1$, $r = 0.75$ and $g_{max} = 1$

or $g_{max} = 3.3$. This set of parameters are chosen to ensures that the first lasing mode μ starts in the broken phase while the other mode is still in the PT phase (equation (4.2). Our simulations indicates the existence of two regimes of operation: (I) a single mode steady state emission when $g_{\mu}^{th} < g_{max} < g_{\nu}^{th}$; and (II) a multimode oscillatory behavior when $g_{\nu}^{th} < g_{max}$, where g_{μ}^{th} is the lasing threshold and g_{ν}^{th} is the second (instability) threshold [1, 2]. Figures 4.2 (a) and (b) depict typical temporal behaviors corresponding to these two regimes, respectively. In plotting the results of Fig.4.2 we chose $\Delta\omega = \omega_{\mu} - \omega_{\nu} = 1$ for illustration purposes (note that the actual value of $\Delta\omega$ affects only the modal gain ratio r). Intuitively, one can understand the behavior observed in Fig. 4.2 by noting that, in our model, each cavity supports two modes. As the pump levels increase above the first threshold, the first mode starts to lase and both the modal gain ratio r and the cross gain saturation act together to suppresses the second lasing mode. However, as the pump is further increased, this steady state solution might become unstable which can then lead to multimode laser oscillations with beating effects.

Further simulations for different system's parameters shows that g_{ν}^{th} increases as $s_{\mu\nu}$ increases or r decreases. These parameters depend on the material system, cavity design (emission frequency and modal overlap), thus one expect different systems to enter the multimode regime at different pumping levels. In order to fully characterize this behavior, we use linear stability analysis. The steady state lasing solutions can be found by substituting: $a_{\mu\nu} = \eta_{1,3} exp(i\lambda t)$ and $b_{\mu\nu} = \eta_{2,4} exp(i\lambda t)$ to obtain: $\lambda\eta_{1-4} =$

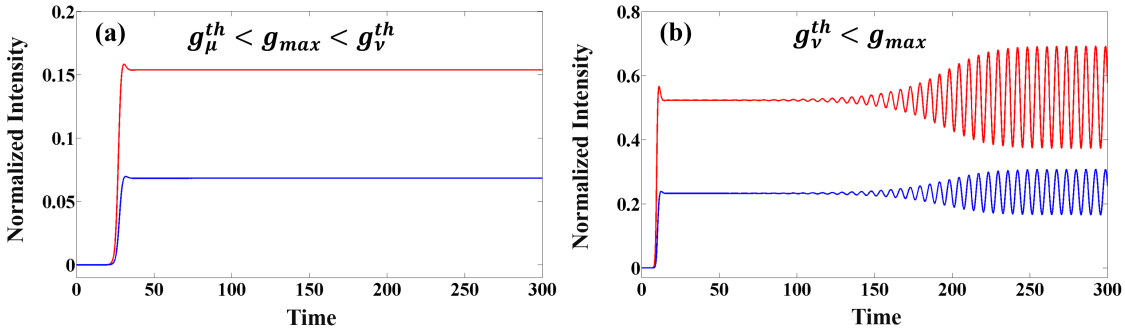

Figure 4.2: Lasing dynamics of the photonic laser molecule of Fig. 6.1 in the broken PT regime when (a) $g_{max} = 1.0$, and (b) $g_{max} = 3.3$. In both figures, red and blue lines correspond to $|a_\mu + a_\nu|^2$ and $|b_\mu + b_\nu|^2$, respectively. Here $s_{\mu\mu} = s_{\nu\nu} = 1$ and $s_{\mu\nu} = s_{\nu\mu} = 0.25$.

$f_{1-4}(\eta_{1-4})$, where the nonlinear functions f_{1-4} can be found from equation 4.1. Here we are interested in the case where only one mode is lasing, i.e. we set $\eta_{3,4} = 0$, to arrive at:

$$M\vec{\eta} = \lambda\vec{\eta},\ M = \begin{pmatrix} 0 & \kappa & 0 \\ \kappa & 0 & -\alpha \\ 0 & \alpha & 0 \end{pmatrix},\ \alpha\eta_{R1} - \frac{g_{max}}{1 + s_{\mu\mu}\eta_{R1}^2}\eta_{R1} + \kappa\eta_{I2} = 0 \tag{4.3}$$

where, $\vec{\eta} = [\eta_{R1}\ \eta_{R2}\ \eta_{I2}]^T$, with the subscript T denoting matrix transpose. In writing equation 4.3 we assumed that $\eta_{I1} = 0$ since only the relative phase between $\eta_{1,2}$ matters. This eigenvalue problem has two different solutions: (1) PT phase: $\lambda = \pm\sqrt{\kappa^2 - \alpha^2}$, $\eta_1 = \sqrt{(\frac{g_{max}}{2\alpha} - 1)/s_{\mu\mu}}$, $\eta_2 = (\frac{\lambda}{\kappa} + i\frac{\alpha}{\kappa})\eta_1$ (note that $(|\eta_1| = |\eta_2|)$; and (2) Broken PT phase (optimal for laser operation): $\lambda = 0$, $\eta_1 = \sqrt{(\frac{g_{max}}{\alpha + \kappa^2/\alpha} - 1)/s_{\mu\mu}}$, $\eta_2 = \frac{i\kappa}{\alpha}\eta_1$. Note that although these solutions always exist for any pump values, they might not be unique in certain regimes. The stability of these steady

state solutions, which determines the lasing characteristics can be found by performing linear stability analysis [2]. By introducing a small perturbation vector $\vec{\delta q} = (\delta\eta_{R1-R4}, \delta\eta_{I1-I4}))$ over any given solution, we obtain $\dot{\vec{\delta q}} = J.\vec{\delta q}$ where the Jacobian matrix $J = \frac{\partial(f_1,...,f_4)}{\partial(\eta_{R1},\eta_{I1},...,\eta_{R4},\eta_{I4})}$ is a function of that particular solution. Here the subscripts R, I indicate real and imaginary parts, correspondingly. If $max(Re(\theta)) > 0$, where θ are the eigenvalues of the matrix J, the perturbation grows and the solution is unstable. On the other hand, the solution is stable if $max(Re(\theta)) > 0$[2].

Figures 4.3 (a) and (b) show that stability maps of a PT symmetric laser when $\alpha = 1.5$, $s_{\mu\mu} = s_{\nu\nu} = 1$ and $s_{\mu\nu} = s_{\nu\mu} = 0.5$ as a function of the gain ratio r and the coupling coefficients κ for two different values of the maximum pumping gain $g_{max} = 5, 10$. As we can see from Fig. 4.3 (a) Starting from a low value of r, the single mode operation is found to be stable over a wide range of the coupling parameter κ (the regime below the white dashed line). As r is further increased, an intermediate domain (between the dashed white and black lines) with mixed stability features is entered. In this regime, the system is unstable for lower κ values and can be stabilized by increasing κ. Above a certain value for r, the laser becomes unstable for all κ's in the specific range. Similar behavior is also observed in Fig 4.3 (b) with the exception that the unstable domain is now expanded at the expense of stable and intermediate domains. Also the values of r at which the transitions between the different domains for fixed κ is down-shifted.

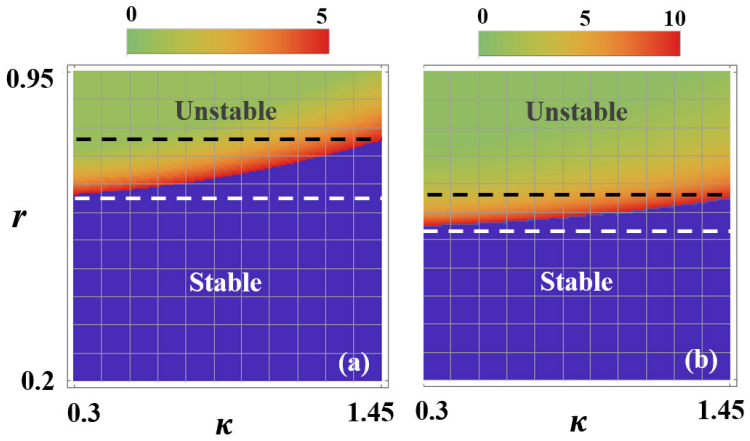

Figure 4.3: (a) Stability maps of a PT symmetric laser as a function of the gain ratio r and the coupling coefficients κ when $g_{max} = 5$. Starting from a low value of r, the single mode operation in both cases is found to be stable over a wide range of the coupling parameter κ (the regime below the white dashed line). As r is further increased, an intermediate domain (between the dashed white and black lines) with mixed stability features is entered. In this regime, the system is unstable for lower κ values and can be stabilized by increasing κ. Above a certain value for r, the laser becomes unstable for all κ's in the specific range. (b) Same as in (a) but for $g_{max} = 10$. Here, as expected, the unstable domain is larger and the values of r at which the transitions between the different domains for fixed κ is down-shifted. In both figures, the blue shaded areas represent the stable domain and the color map represent the values of g_{ν}^{th}.

Figures 4.4 (a) and (b), on the other hand depict the different stability regimes when $\kappa = 1$ as a function of r and $s_{\mu\nu}$ again for different pump values $g_{max} = 5, 10$. All other parameters are similar to those in Fig. 4.3. Here also one can identify three different operating regimes: stable, intermediate and unstable. As expected the area under the unstable domain increases as a function of g_{max}. In perfect agreement with our previous discussion, we find that the system can transit from a stable to an unstable operation as $s_{\mu\nu}$ decreases or as r increases.

Finally, for completeness, we present the stability maps for a single laser cavity (having

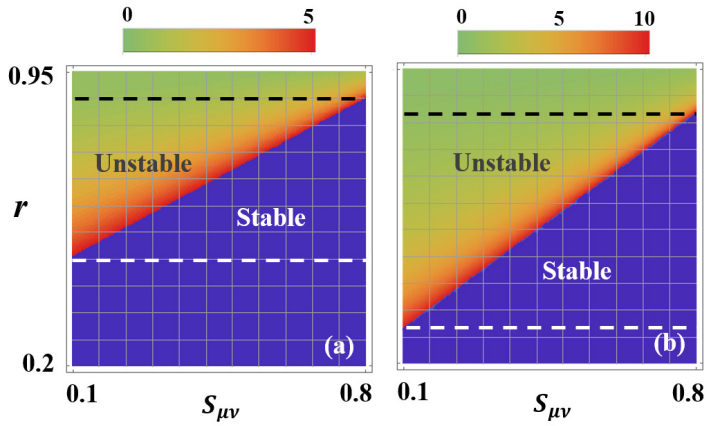

Figure 4.4: Stability maps as a function of r and $s_{\mu\nu}$ for the same parameters used in 4.3 when $\kappa = 1$ and (a) $g_{max} = 5$ and (b) $g_{max} = 10$. Here also one can identify three different operating regimes: stable, intermediate and unstable. As discussed in text smaller values for r and larger $s_{\mu\nu}$ lead to better stability features.

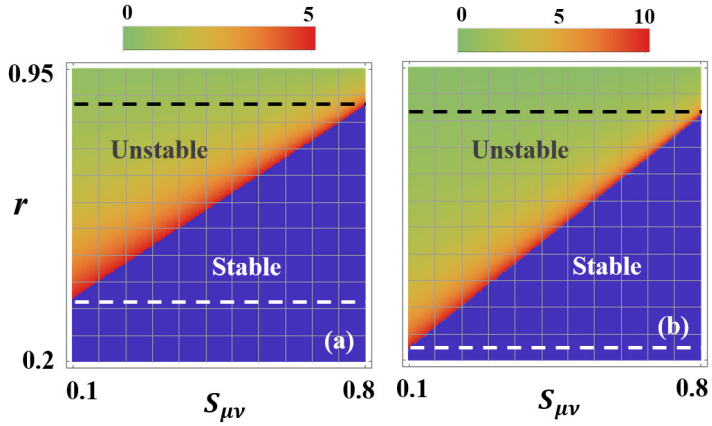

Figure 4.5: Stability maps for single cavity laser. All parameters are similar to those in Fig. 4.4. Evidently, in this case, the area under the unstable regime is larger, thus confirming the superior performance of PT symmetric lasers.

the same parameters as in Fig. 4.4) in Fig. 4.5 where we observe a noticeable expansion of the instability domain. This result indicate that, at least for small r values, PT symmetric lasers indeed exhibit superior performance over single cavity systems.

4.2 Mode selectivity via dissipation engineering

In multimode semiconductor laser systems, the lasing thresholds of different modes are determined by the cavity geometry and the central frequency/bandwidth of the gain curve. In the experimental work of [45], the two coupled cavities had identical loss coefficients (i.e. $\gamma_n = 0$). As a result, the first lasing mode was the one that falls under the peak of the gain curve (mode μ in Fig. 6.1). Here we explore whether a more general scheme can provide extra flexibility over the mode selectivity. For example let us assume that it is required to engineer the system properties to suppress mode μ and promote other mode ν to lase first, i.e $g_\nu^{th} < g_\mu^{th}$. To do so, we employ a technique similar to that demonstrated in [47, 48, 49] and, in contrast to the previous section, we assume a finite value for the asymmetric loss coefficients, i.e. $\gamma_{\mu,\nu} \neq 0$. By neglecting the nonlinear modal interactions for the moment, one can identify four different regimes of operation based on the classification of the lasing modes (either PT or broken PT (BPT)) according to the linear eigenvalues of Eq. (2): ((A) PT-PT if $(\gamma_\nu+2\alpha_\nu)/r < \gamma_\mu+2\alpha_\mu$, (B) PT-BPT if $(\gamma_\nu+2\alpha_\nu)/r < \alpha_\mu+\kappa^2/(\gamma_\mu+\alpha_\mu)$, (C) BPT-PT if $(\alpha_\nu+\kappa^2/(\gamma_\nu+\alpha_\nu))/r < \gamma_\mu+2\alpha_\mu$, and (D) BPT-BPT if $(\alpha_\nu+\kappa^2/(\gamma_\nu+\alpha_\nu))/r < \alpha_\mu + \kappa^2/(\gamma_\mu + \alpha_\mu)$. These criteria can be experimentally satisfied by using spatial and/or spectral loss distribution as we discuss in more details in the conclusion section.

As an example, Fig.4.6 depicts these domains as a function of $\gamma_{\nu,\mu}$ for the parameters

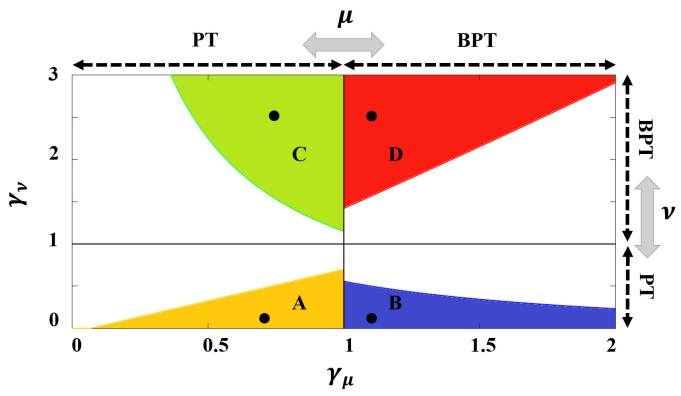

Figure 4.6: Different lasing regimes for photonic molecule laser as a function of γ_ν and γ_μ. The design parameters are chosen to be $\kappa = 1$, $\alpha_\nu = \alpha_\mu \equiv \alpha = 0.1$ and $r = 0.75$. The shaded and the white areas correspond to domains where mode ν and μ lases first, correspondingly.Vertical and horizontal lines mark the transition between PT and BPT phases for modes μ and ν, respectively. The black dots represents specific design parameters to investigated in more details. Importantly, the different lasing domains are broad enough which allows for large design and implementation tolerance.

mentioned in the caption. We note that although nonlinear interactions play a crucial role in the laser dynamics above thresholds, identifying the domains (A)-(D) based on linear analysis is important for choosing a suitable initial design parameters that allow mode ν to be the first lasing mode. By inspecting Fig. 4.6, we can draw several important conclusions. For example, in domain A, $\gamma_\mu > \gamma_\nu$ while the converse is true in C. At first glance, it might appear surprising in this last case that mode ν can be still the first lasing mode even when $\gamma_\mu < \gamma_\nu$. However by recalling that in this regime, mode ν is in the broken phase while μ is in the PT phase, it is straightforward to show that the modal loss of supermode formed by the hybridization of modes ν in both cavities is less than that associated with μ— a peculiar effect of broken PT phase after crossing exceptional points [44, 49, 54]. In order to further illustrate our

results, we plot the imaginary parts of eigenvalues associated with the lasing modes for four different points (each chosen to lie within one of the distinct domain of Fig. 4.6) as shown in Fig. 4.7.

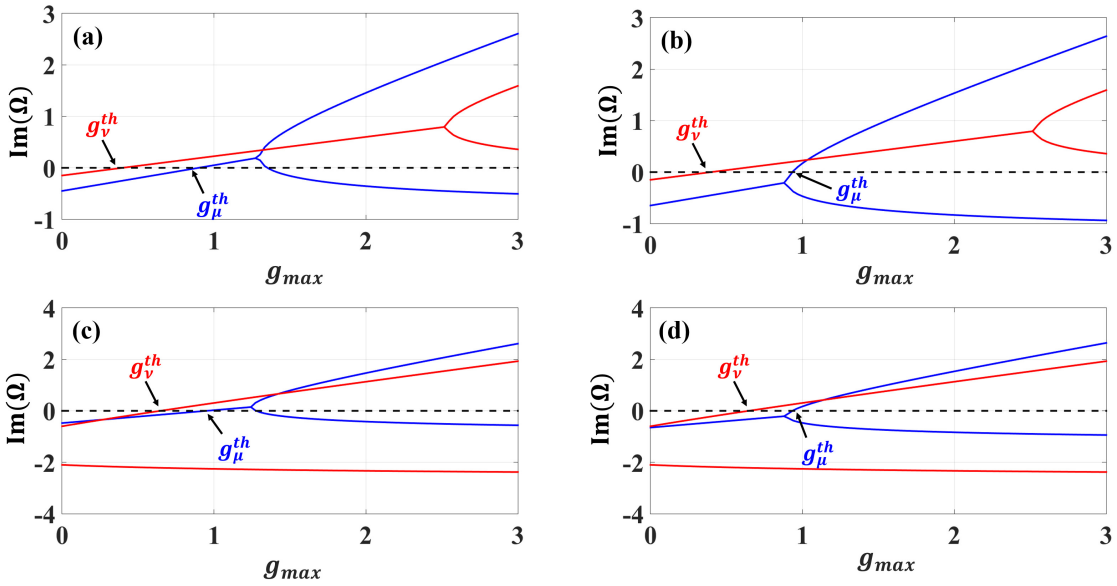

Figure 4.7: Imaginary part of the eigenvalues of Eq. (4.2) as a function of g_{max} are plotted for the different points indicated in each lasing regimes in Fig. 4.6: 4(a) Both modes lase in PT regime for: $\gamma_\nu = 0.1$ and $\gamma_\mu = 0.7$ (PT-PT), (b) Mode ν lases first in the PT regime followed by mode μ lases in broken PT regime for: $\gamma_\nu = 0.1$ and $\gamma_\mu = 1.1$ (PT-BPT), (c) The first lasing mode ν start to lase in broken PT phase then the second mode μ in PT regime for: $\gamma_\nu = 2.5$ and $\gamma_\mu = 0.75$ (BPT-PT), and (d) both modes lase in broken Pt phase $\gamma_\nu = 2.5$ and $\gamma_\mu = 1.1$ (BPT-BPT). Note that always $g_\nu^{th} < g_\mu^{th}$.

We have so far discussed the behavior of the linear model described by equation (4.1) and demonstrated the possibility for mode selectivity in photonic molecule PT lasers by applying pump only to one cavity while engineering the modal dissipation on the second cavity. In that analysis, we neglected nonlinear self gain saturation as well as nonlinear modal interaction via cross gain saturation. Here we study how these

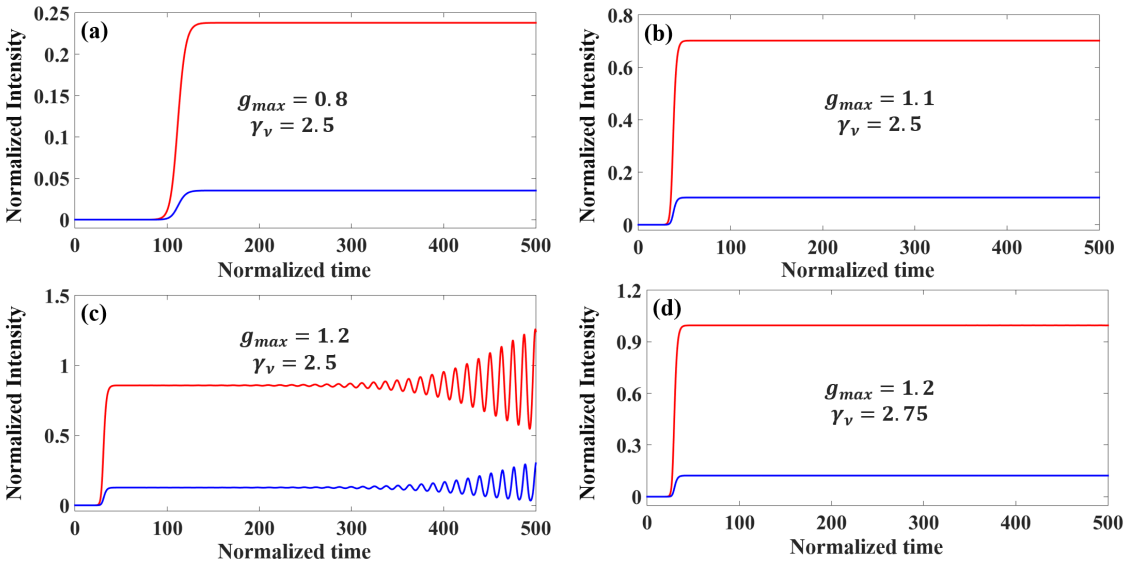

Figure 4.8: Lasing dynamics for the point shown in domain C of Fig. 4.6 under different conditions (a)-(d). In all simulations, we take $\gamma_\mu = 0.75$, $\alpha = 0.1$ $\kappa = 1$, $s_{\mu\mu} = 1$ and $s_{\mu\nu} = 0.25$. Red/blue lines represent the total intensity in the active/passive cavities, respectively. In (a),(b) and (d), only mode ν is lasing whereas in (c) multimode instabilities take place as g_{max} increases. This instabilities can be mitigated by exploring other values for γ_ν as shown in (d).

nonlinearities affect the lasing dynamics. To do so, we numerically integrate equation (4.1) for some initial noise. We are particularly interested in domain C where mode ν is in the broken phase (thus experiences more gain) while mode μ is in the PT phase where it experiences more loss. Fig. 4.8(a) plots the lasing dynamics (total intensity in each cavity) for the point indicated in domain C in Fig. 4.6. The system reaches its steady state after some transient response. We have inspected the intensity of the individual modes and found that indeed only mode ν is participating in the lasing action. In Fig. 4.8(b) we plot the field intensity under the same conditions as in (a) but for a higher gain value. Again single mode steady state lasing is observed. As the gain is further increased, the lasing action can undergo multimode instabilities

manifested by the oscillatory behavior in (c). However, the system can be driven back to its single mode stable operation by adjusting the losses as shown in (d). In practice, for every gain value, a stability map superimposed on Fig. 4.6 would determine the stable operation regimes.

References

[1] Agrawal, G. P. and Dutta, N. K. Semiconductor Lasers, (Springer Science and Business Media, 2013).

[2] Ohtsubo, J. Semiconductor Lasers: Stability, Instability and Chaos, Springer Berlin Heidelberg (2005).

[3] Kapon, E. Semiconductor Lasers I: Fundamentals, (Academic Press, 1999).

[4] Ghafouri-Shiraz, H. Distributed Feedback Laser Diodes and Optical Tunable Filters, (John Wiley and Sons, 2004).

[5] McCall, S. L., Levi, A. F. J., Slusher, R. E., Pearton, S. J., and Logan, R. A. Whispering gallery mode microdisk lasers. Appl. Phys. Lett. **60** 289-291 (1992)

[6] Kuwata-Gonokami, M. *et al.* Polymer microdisk and microring lasers. Opt. Lett. **20**, 2093-2095 (1995).

[7] Bayer, M. *et al.* Optical Modes in Photonic Molecules," Phys. Rev. Lett. **81**, 2582-2585 (1998).

[8] Fujita, M., Sakai, A., Baba, T. Ultrasmall and ultralow threshold GaInAsP-InP microdisk injection lasers: design, fabrication, lasing characteristics, and spontaneous emission factor. IEEE Journal of Selected Topics in Quantum Electronics **5**(3) 673 - 681 (1999).

[9] Fujita, M., Baba, T. Microgear laser. Applied Physics Letters **80** 2051-2053 (2002).

[10] Nakagawa, A., Satoru, I., Baba, T. Photonic molecule laser composed of GaInAsP microdisks. Applied Physics Letters **86** 041112 (2005).

[11] Ishii, S., and Baba, T. Bistable lasing in twin microdisk photonic molecules. Applied Physics Letters **87** 181102 (2005).

[12] Li, M. *et al.* Inversed Vernier effect based single-mode laser emission in coupled microdisks. Scientific Reports **5**, Article number: 13682 (2015).

[13] Nozaki, K., Nakagawa, A., Sano, D., and Baba, T. Ultralow threshold and single-mode lasing in microgear lasers and its fusion with quasi-periodic photonic crystals. IEEE J. Sel. Top. Quantum Electron. **9**, 13551360 (2003).

[14] Schlehahn, A. *et al.* Mode selection in electrically driven quantum dot microring cavities. Optics express **21**(13), 15951-15958 (2013).

[15] Sorel, M. *et al.* Operating regimes of GaAs-AlGaAs semiconductor ring lasers:

experiment and model. IEEE Journal of Quantum Electronics **39** 1187-1195 (2003).

[16] Painter, O. *et al.* Two-Dimensional Photonic Band-Gap Defect Mode Laser," Science **284** 1819-1821 (1999).

[17] Altug, H. and Vučković, J. Photonic crystal nanocavity array laser. Optics Express **13**(22) 8819-8828 (2005).

[18] Khajavikhan, M. *et al.* Thresholdless nanoscale coaxial lasers. Nature **482**, 204207 (2012).

[19] Bender, C. M., and Boettcher, S. Real Spectra in Non-Hermitian Hamiltonians Having PT Symmetry. Phys. Rev. Lett. **80**, 5243 (1998).

[20] Bender, C. M., Boettcher, S. Meisinger, P. PT-symmetric quantum mechanics. Journal of Mathematical Physics **40**, (5), 2201-2229 (1999).

[21] El-Ganainy, R., Makris, K. G., Christodoulides, D. N., and Musslimani, Z. H., Theory of coupled optical PT-symmetric structures. Optics letter **32**(17) 2632-2634 (2007).

[22] Musslimani, Z. H., Makris, K. G., El-Ganainy, R., and Christodoulides, D. N. Optical solitons in PT periodic potentials. Phys. Rev. Lett. **100**, 030402-1-4 (2008).

[23] Makris, K. G., El-Ganainy, R., Christodoulides, D. N., and Musslimani, Z. H. Beam dynamics in PT-symmetric optical lattices. Phys. Rev. Lett. **100**, 103904-1-4 (2008).

[24] Guo, A. *et al.* Observation of PT-symmetry breaking in complex optical potentials. Phys. Rev. Lett. **103**, 093902-1-4 (2009).

[25] Rüter, C. E. *et al.* Observation of parity-time symmetry in optics. Nature Phys. **6**, 192-195 (2010).

[26] Longhi, S. Peschel Bloch Oscillations in Complex Crystals with PT Symmetry. Phys. Rev. Lett. **103**, 123601 (2009).

[27] Chong, Y. D., Ge, L., Cao, H., and Stone, A. D. Coherent perfect absorbers: time-reversed lasers. Phys. Rev. Lett. **105**, 053901 (2010).

[28] Lin, Z. *et al.* Unidirectional invisibility induced by P T-symmetric periodic structures. Phys. Rev. Lett. **106** (21), 213901 (2011).

[29] Schindler, J. Li, A. Zheng, M. C., Ellis, F. M., Kottos, T. Experimental study of active LRC circuits with PT symmetries. Phys. Rev. A **84** (4), 040101 (2011).

[30] R. El-Ganainy, K.G. Makris, D.N. Christodoulides, Local PT invariance and supersymmetric parametric oscillators, Phys. Rev. A **86**, 033813 (2012)

[31] Schomerus, H., Topologically protected midgap states in complex photonic lattices. Optics Lett. **38**, 1912-1914 (2013).

[32] Teimourpour, M.H., El-Ganainy, R., Eisfeld, A., Szameit, A., and Christodoulides, D. N. Light transport in PT-invariant photonic structures with hidden symmetries. Physical Review A **90**, 5 053817 (2014).

[33] Wiersig, J., Enhancing the sensitivity of frequency and energy splitting detection by using exceptional points: application to microcavity sensors for single-particle detection. Phys. Rev. Lett. **112**, 203901 (2014).

[34] Peng, B. *et al.* Parity-time-symmetric whispering-gallery microcavities. Nature Physics **10**, 394-398 (2014).

[35] Jing, H. *et al.* PT-Symmetric Phonon Laser. Phys. Rev. Lett. **113**, 053604 (2014).

[36] Makris, K. G., Ge, L., and Treci, H. E. Anomalous transient amplification of waves in non-normal photonic media. Phys. Rev. X **4**, 041044 (2014).

[37] Zhang, J. *et al.* Giant nonlinearity via breaking parity-time symmetry: A route to low-threshold phonon diodes. Phys. Rev. B *92*, 115407 (2015).

[38] Liu, Z.P. *et al.* Metrology with PT-Symmetric Cavities: Enhanced Sensitivity near the PT-Phase Transition. Phys. Rev. Lett. **117**, 110802 (2016).

[39] Monifi, F. *et al.* Optomechanically induced stochastic resonance and chaos transfer between optical fields. Nature Photonics **10**, 399405 (2016).

[40] Doppler, J. *et al.* Dynamically encircling an exceptional point for asymmetric mode switching. Nature **537** (7618), 76-79 (2016)

[41] Jing, H. zdemir, .K., L, H., Nori, F. High-order exceptional points in optomechanics. Scientific Reports **7**, 3386 (2017).

[42] Ramezani, H. Non-Hermiticity-induced flat band. Phys. Rev. A **96**, 011802 (2017).

[43] Jahromi, A. K. et al. Transparent Perfect Mirror. ACS Photonics **4**, 1026-1032 (2017).

[44] Liertzer, M. *et al.* Pump-induced exceptional points in lasers.," Phys. Rev. Lett. **108** 173901-1-5 (2012).

[45] Hodaei, H., Miri, M. A., Heinrich, M., Christodoulides, D. N., and Khajavikhan, M. Parity-timesymmetric microring lasers. *Science* **346**, 975–978 (2014).

[46] Feng, L. Wong, Z. J., Ma, R. M., Wang, Y., and Zhang, X. Single mode laser by parity-time symmetry breaking. *Science* **346**, 972-975 (2014).

[47] Brandstetter, M. *et al.* Reversing the pump dependence of a laser at an exceptional point. Nat. Commun. **5**, 4034 (2014).

[48] Peng, B. *et al.* Loss-induced suppression and revival of lasing. Science **346**, 328 (2014).

[49] El-Ganainy, R., Khajavikhan, M., and Ge, L. Exceptional points and lasing self-termination in photonic molecules. Phys. Rev. A **90**, 013802 (2014).

[50] El-Ganainy, R., Khajavikhan, M., and Christodoulides, D. N. Supersymmetric laser arrays. Phys. Rev. A **92**, 033818 (2015)

[51] Teimourpour, M. H., Ge, L., Christodoulides, D. N., and El-Ganainy, R. Non-Hermitian engineering of single mode two dimensional laser arrays. Sci. Rep. **6**, 33253 (2016).

[52] Gu, Z. *et al.* Experimental demonstration of PT-symmetric stripe lasers Laser Photon. Rev. **10**, 588-594 (2016).

[53] Hassan, A. U., Hodaei, H., Miri, M. A., Khajavikhan, M., and Christodoulides, D. N., Nonlinear reversal of the PT-symmetric phase transition in a system of coupled semiconductor microring resonators. Phys. Rev. A **92**, 063807 (2015).

[54] Ge, L. and El-Ganainy, R. Nonlinear modal interactions in parity-time (PT) symmetric lasers. Sci. Rep. **6** 24889 (2016).

[55] Yange, J. Nonlinear behaviors of parity-time-symmetric lasers. arXiv:1607.06707.

[56] Gao, Z., Fryslie, S.T. M., Thompson, B. J., Carney, P. S., and Choquette, K. D. Parity-time symmetry in coherently coupled vertical cavity laser arrays. *Optica* **4**, 323-329 (2017).

Chapter 5

Non-Hermitian engineering of single mode two dimensional laser arrays

Over the last two decades, vertical cavity surface emitting lasers (VCSELs) have become a mature technology that finds several different applications [1, 2]. The output power of a VCSEL laser is proportional to the area of its active region. Increasing the emission power can be thus achieved by building large area VCSELs. This however introduces some difficulties such as filamentation [3] and multimode operation [4, 5, 6, 7]. An attractive alternative is to build an array of coupled VCSEL lasers. If all the elements in the array lase in the same phase, the output intensity at the focus

of the emitted laser beam can be enhanced by a factor proportional to the square of the number of the individual elements constituting the array. Today, VCSEL laser arrays can provide up to several watts of output powers and play important role in many applications in industry, communication networks, and multimedia to just mention a few [1]. Despite this tremendous success, laser arrays in general suffer from multimode operation. While several techniques for eliminating longitudinal modes of individual resonators exist [8, 9, 10, 11], suppressing the transverse supermodes is by no means an easy task [3, 4, 5, 6]. This can be explained by noting that these supermodes arise as a result of eigenfrequency splitting introduced by the coupling between the individual laser resonators. Given that the discrete spectral band associated with these supermodes is usually smaller than (or comparable to) the spectral gain bandwidth of typical semiconductor active media, lasing competition between these eigenmodes takes place. This can lead to a multimode operation that affects the stability of the laser output power as well the quality of the emitted laser beam [12]. While nonlinear gain saturation might favor some modes over others, a lack of precise control over the operation of these laser systems can present a practical challenge. Recently, a technique based on discrete supersymmetry (DSUSY) [13, 14, 15, 16, 17] was proposed in order to solve similar problems for one dimensional (1D) laser waveguide arrays [7]. In that work, a pseudoisospectral array, generated through DSUSY, was employed as a reservoir that spoils the quality factors of all higher order transverse collective modes while at the same time leaving the fundamental supermode

intact. This was possible primarily owing to a particular feature of DSUSY: the effective Hamiltonian matrix describing a 1D array with nearest neighbor coupling (NNC) is symmetric and tridiagonal and can be thus used with DSUSY to engineer a pseudo-isospectral reservoir [7]. Despite the appeal of this technique, it cannot be applied for two dimensional (2D) laser arrays for the following reason: unlike their 1D counterparts, 2D arrays cannot not be represented by tridiagonal matrix. Thus, blindfold application of 1D DSUSY to the effective Hamiltonian matrix of a 2D array results in a reservoir with complicated higher order couplings beyond NNC, which is not practical to implement. Thus, the following question naturally arise: can one find a variant of 1D DSUSY that can be applied for the 2D systems? In other words, can we engineer an implementable pseudo-isospectral reservoir that has an identical spectrum of a 2D laser array except for the fundamental supermode, in order to eliminate the multimode dynamics and achieve only single mode laser emission (as depicted schematically in Fig. 5.1)?

In this work we provide an answer to this question by using the Householder transformation method [19] in conjunction with discrete supersymmetry [7]. In particular, starting from the banded matrix that describes the 2D laser array, we first use the Householder method in order to obtain an isospectral tridiagonal matrix that can be implemented by a 1D chain of coupled resonators with only NNC. Note that due to the spectral degeneracies of 2D systems, and since degeneracy is not permitted in 1D systems [20] (see supplementary material A), the resultant isospectral 1D array will

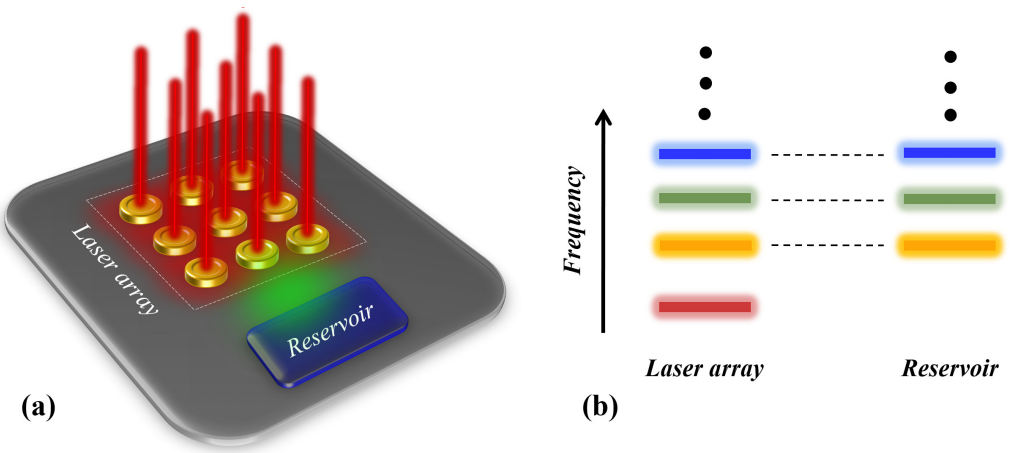

Figure 5.1: (a) A schematic of the photonic molecule laser investigated in this work. It consists of two identical coupled optical cavities (a and b), each of which support two modes. The coupling coefficients between each pair of the modes is assumed to be the same and equal κ. Moreover, pumping is applied only to cavity a. A typical semiconductor gain curve along with the assumed modal frequencies are shown in (b) where g_{max} and rg_{max} are gain values experienced by modes μ and ν respectively.

in general consists of a union of two different isolated chains. In terms of matrices, this means that applying the Householder transformation to a banded matrix that represents a 2D array will yield a tridiagonal matrix that exhibits several block diagonals, each of which has a non-degenerate spectrum. The next step is to apply DSUSY transformation to the 1D chain in order to create an auxiliary structure that shares all the eigenfrequencies of the original laser array except that associated with the fundamental supermode. By introducing optical losses to this 1D discrete reservoir (made of several independent 1D chains) and by engineering its coupling to the original 2D laser array, the quality factors of the higher order supermodes of the main 2D laser array are spoiled and as a result, their lasing thresholds are increased, all while leaving the lasing properties of the fundamental mode (threshold and profile) almost

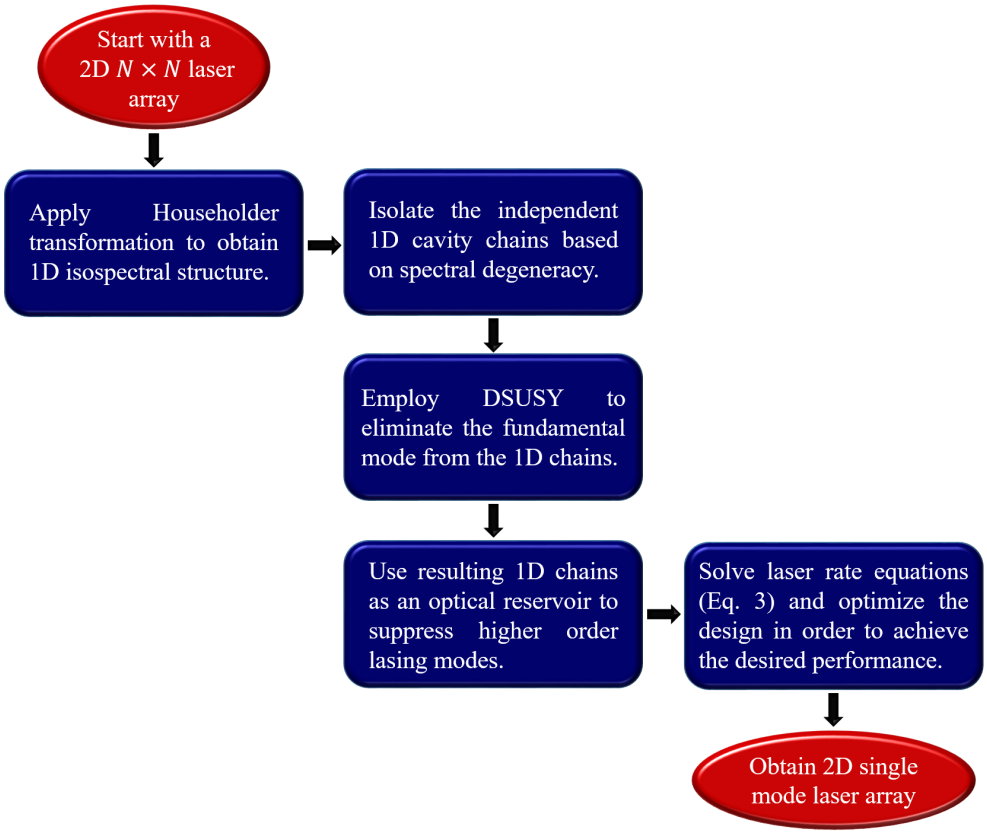

Figure 5.2: A flowchart that illustrates the main steps for designing 2D single mode laser arrays based on Householder transformation in conjunction with discrete supersymmetry techniques.

intact. Finally, by using the results of the last step as an initial starting point and by considering laser rate equations and assuming fast carrier dynamics, we optimize the design in order to achieve the desired performance under gain saturation nonlinearity- a model that has been shown to yield good results for analyzing PT symmetric lasers [21, 22]. These steps are summarized by the flowchart shown in Figure. 5.2.

5.1 Single mode operation in uniform square laser arrays

The Householder-DSUSY technique described in the introduction is very general and can be applied to any array topology. However, here we focus on square arrays due to their simple practical feasibility. In particular, we deal in this section with uniform square arrays having $N \times N$ optical cavity elements. Within the framework of coupled mode theory and before or just at lasing threshold where the system is linear:

$$i\frac{da_{m,n}}{dt} = (\omega_0 - i\gamma + ig)a_{m,n} + \sum_{m'.n'} \kappa_{m,n}^{m',n'} a_{m,n} \tag{5.1}$$

In equation (5.1), $a_{m,n}$ is the optical field amplitude in the cavity element characterized by the integer indices m and n , ω_0 is the uniform resonant frequency resonant modes of each isolated optical cavity, γ and g represent the optical loss (radiation and material) and gain, respectively while $\kappa_{m,n}^{m',n'}$ are the elements of the coupling matrix which are finite only for next neighboring coupling and zero otherwise and t represents time. In the model described by equation 5.1, we have neglected diagonal coupling between the resonators as well as other higher order couplings beyond NNC. This treatment is justified, for example, for closely packed cylindrical VCSEL arrays,

with the radius r of each cavity being much larger than their spacing d. As such, the diagonal distance between two cavities $2(\sqrt{2}-1)r+\sqrt{2}d$ is also much larger than d, indicating a negligible diagonal coupling when compared with NNC. We note however that our proposed method can be still applied without any restrictions if higher order couplings are taken into account.

Equation (5.1) can be recast in a Hamiltonian form:

$$i\frac{d\vec{a}}{dt} = H\vec{a} \tag{5.2}$$

where $\vec{a} = [a_1 a_2 ... a_{N^2}]^T$ is the optical amplitude vector and T denote matrix transpose. The subscript l in a_l is related to the double indices notation by $l = N \times (m-1) + n$. Note that, written in a frame rotating with an angular velocity of ω_0, the diagonal elements of the Hamiltonian matrix H contain only imaginary numbers that represent the optical loss of each cavity. As we have discussed earlier, since H describes a 2D array, its structure is not tridiagonal.

Thus the DSUSY method used in [7] cannot be applied here to achieve single mode lasing. However, this difficulty can be alleviated by first applying the Householder transformation to generate a tridiagonal matrix $\hat{H}$, which is isospectral to H and can be then used in conjunction with DSUSY to engineer the quality factors of the higher order modes in order to ensure single mode operation. We note that the Householder

method has been employed recently for studying eigenvalue statistics in networks with reduced dimensions [23].

Based on our discussion so far, one might anticipate that the reservoir should at least consist of $N^2 - 1$ optical resonators in order to kill all the higher order lasing eigenmodes. However, this is not necessarily correct since, unlike 1D arrays, 2D structures can exhibit spectral degeneracies. In particular, as we show in supplementary material, the spectrum of a 2D $N \times N$ uniform square array consists of $(N^2+2)/2$ distinct eigenvalues when N is even and $(N^2+2)/2$ distinct eigenvalues when N is odd. As we will see, this feature can be employed to simplify the reservoir structure. Finally, we note that in the absence of any applied gain, the combined laser and reservoir system is described by an equation similar to (2) except that the amplitude vector now contains the field amplitudes in the laser array as well as the reservoir chains. Additionally, the Hamiltonian of the total system H_{SR} will also contain information about the system, reservoir and their interactions. If the reservoir is made of M resonators, H_{SR} will have $N^2 + M$ different eigenmodes, each of which will vary as $exp(i\Omega_p t)$ with $p = 1, 2, ..., N^2 + M$. The real part of Ω_p represents the oscillating frequency while its imaginary part indicates the modal loss coefficient. As gain is applied to the system, the imaginary values of all Ω_p will be shifted upward and the mode with the minimum imaginary part will start to lase first. Without the reservoir, even when the fundamental mode is the first mode to lase, other modes follow suit shortly above its threshold, resulting in multi-mode lasing instead of single-mode lasing. The role

of the reservoir thus is to shift down the imaginary parts of all Ω_p before the gain is applied (Q-spoiling), except the fundamental mode. For simplicity, we will denote the complex eigenfrequency of that fundamental mode by $\Omega_f = \Omega_R + i\Omega_I$, where $\Omega_I < 0$ before lasing and $\Omega_I = 0$ at the lasing threshold.

In what follows we illustrate the power of our proposed method for eliminating the higher order lasing modes by considering two different examples of 2D uniform square laser arrays made of 3×3 and 4×4 coupled lasing elements respectively.

It is important to note that in all our studies we assume that only the optical resonators that comprise the main laser array are pumped. This configuration can be easily achieved in systems that rely on either optical pumping [24] or electric pumping [25].

Finally, and before we move to specific numerical examples, we note that in all the following, we have rounded all the resultant numbers for the frequencies and coupling coefficients that results from the procedure described in Figure. 5.2 to the first decimal points whenever appropriate.

5.2 Example I: 3×3 laser array:

Here we consider a square laser array made of nine identical resonators arranged on a square grid. At the lasing threshold, the system is linear and can be described by equation (5.2). We focus here on uniform arrays and we assume a normalized value

for the coupling and loss coefficients of $\kappa_{m,n} = \kappa = 1$ and $\gamma = 0.1$, respectively. This structure exhibits five distinct eigenvalues (see supplementary material) and thus, in principle only four auxiliary resonators are required in order to achieve single mode lasing. By applying the general recipe for achieving single mode operation as discussed above (see figure 5.2), we obtain two independent, one dimensional chains of optical resonators (one of them is just made of one element). However, by investigating the resultant structure, we found that it is necessary to include an additional resonator in order to achieve the single mode operation. This can be attributed to the fact that matching the eigenfrequencies of the laser array and the reservoir is not a sufficient condition to kill all the undesired states. The spatial overlap between the eigenmodes must also be taken into account.

By including the additional resonator (located to the right of the main array in figure 5.3 (a)) and carefully engineering the interaction between the reservoir and the main array, the fundamental mode indeed has the highest quality factor as evidenced by figure 5.3 (b), which indicates that it will lase first as the pump power increases. This is in contrast to the spectrum of the isolated array that shows that all modes will have the same lasing threshold. Thus based on our linear analysis, we indeed anticipate that our proposed structure will result in single mode operation within certain range of applied gain values. Interestingly, we also note that though the linear analysis indicate that the system will function as expected, the reservoir does not leave fundamental mode completely intact but rather shifts its complex eigenfrequency. This can

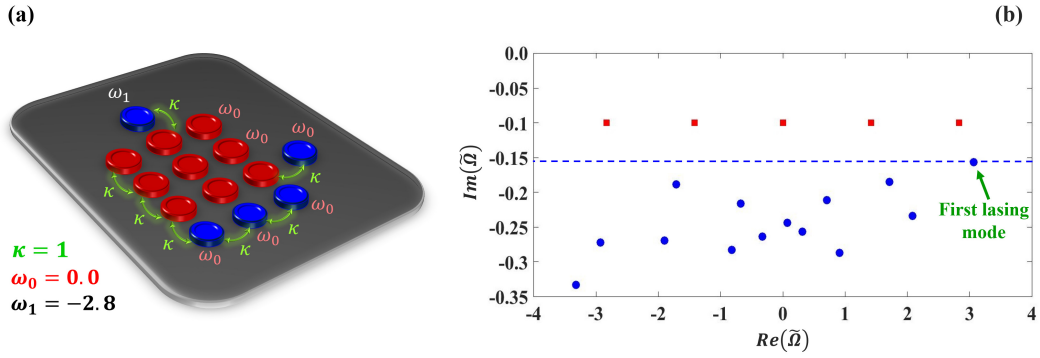

Figure 5.3: (a) Schematic illustration of a 3×3 laser array (red) coupled to a reservoir that consists of five optical cavities (blue). All the eigenfrequencies of the individual photonic resonators and the coupling coefficients which are all identical are depicted on the same figure. Note the procedure described in figure 2 yields only the reservoir chain at the bottom and the single resonator at the top. The extra cavity at the right side is added to optimize the performance. (b) Eigenvalue spectrum of the laser array alone in the absence of the reservoir (square red marks) as well as that of the combined system (blue circle marks). In (b) $\tilde{\Omega} = \omega_p/\kappa$, and as mentioned in the text ω_0 was taken to be zero. We have assumed that the optical loss coefficient of each cavity in the reservoir to be $\gamma_R = 0.5$.

be understood by noting that our recipe as described in figure 2 neglects off- resonant interactions [7] which is responsible for this shift. However, this is a smaller effect compared to the resonant coupling and thus does not affect the effectiveness of our approach. It important to note that the non-Hermitian engineering with additional loss in the reservoir only slightly perturbs the phase coherence of $a_{m,n}$ in the fundamental mode, with a maximum phase deviation 0.02π.

Before we move to the next example, we note that normalized value $\omega_1 = -2.8$ in the rotating frame means real value $\omega_1 = \omega_0 - 2.8\kappa$ in the nonrotating frame. Similar argument applies to all of the following discussions.

Example I: 4×4 laser array:

Having demonstrated our technique for a laser array that consists of nine elements, we now show that this method can be also applied to even larger systems by considering a 4×4 laser array. In this case, there are sixteen different eigenmodes, of which only nine are distinct (see supplementary material) and we find that a reservoir that consists of eight optical resonators is sufficient to suppress the higher order modes. By following the aforementioned procedure as described in figure 5.2, we obtain the structure shown in figure 5.4. Here, the optical loss coefficient is assumed to be $\gamma = 0.1$ for the main laser array and $\gamma_R = 0.8$ for the reservoir chains.

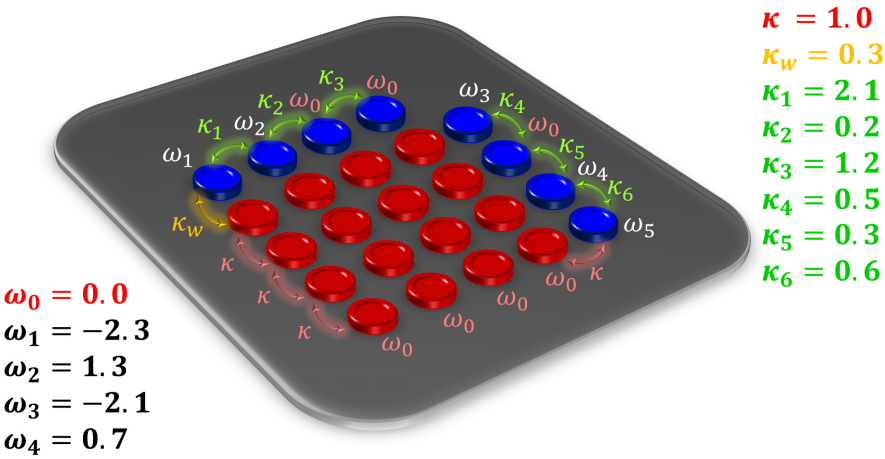

Figure 5.4: Schematic representation of a laser array (red cavities) coupled to a reservoir consists of eight resonators (blue resonators). The optical losses of the laser cavities and the reservoir are assumed to be $\gamma = 0.8$ and $\gamma_R = 0.8$, respectively. The normalized optical frequencies in the rotating frame are shown in the figure. The coupling profile of the reservoir and its interaction with the main array is also described in the same figure.

Similar to the previous scenario of nine elements array, here also the eigenvalue distribution (not shown) indicates that the fundamental mode exhibits the largest quality factor and thus will start to lase before any other mode as gain is applied.

An interesting observation here is that neither the structure of the reservoir nor its coupling profile to the main array are unique. In particular, due to the degeneracy of the main array, several different combinations for the reservoir chains can be obtained. Furthermore, for each reservoir structure, the coupling profile can be engineered in different fashions. For example in figure 5.4, the reservoir chains are assumed to be parallel to the main laser array with a uniform coupling coefficient κ and κ_w. Alternatively, one could connect the chain in a number of different ways or even use similar layout but with different coupling coefficients. Obviously this is an optimization problem with the optimal design defined by maximizing the single mode operation regime. Our strategy here is to demonstrate the basic idea and we carry out the optimization investigations in a different work. Throughout this work, the optimized designs were obtained by using the initial results of Householder and SUSY transformation in conjunction with trial and error parameter scanning. Employing specialized optimization algorithms is expected to yield devices with better performance and is a topic that we explore elsewhere.

5.3 Bosonic-inspired two dimensional laser arrays

In the previous examples of uniform square arrays, we have seen how the spectral degeneracy led to a simplified reservoir design with less optical resonators than those would have been needed in the absence of degeneracy. In these square uniform arrays, the multiplicity of the eigenvalues is a direct outcome of the spatial symmetry. In particular, the system exhibits a point symmetry group called D_4 that characterize its spectral feature.

Here we explore a different type of square arrays that do not have uniform coupling across the structure: the so called J_x arrays. These interesting configurations have been discovered in the context of spin networks [26] and later mapped to optical waveguides platforms [27]. While their behavior can be explained by using the angular momentum algebra, it was shown recently that their spectra and dynamics can be also understood by using bosonic algebra [28]. While the two different approaches (spin and bosonic algebras) for investigating J_x arrays are formally equivalent, the second picture proved more useful in building higher order networks that inherit most of the properties associated with the 1D J_x array [29].

The most pertinent feature of 1D J_x arrays in our context is their equidistant ladder of eigenvalues. Due to this property, a 2D discrete structure formed by taking the tensor product of two, 1D J_x array will possess additional accidental degeneracies beyond those arising from spatial symmetries for $N > 3$. As we show in the supplementary

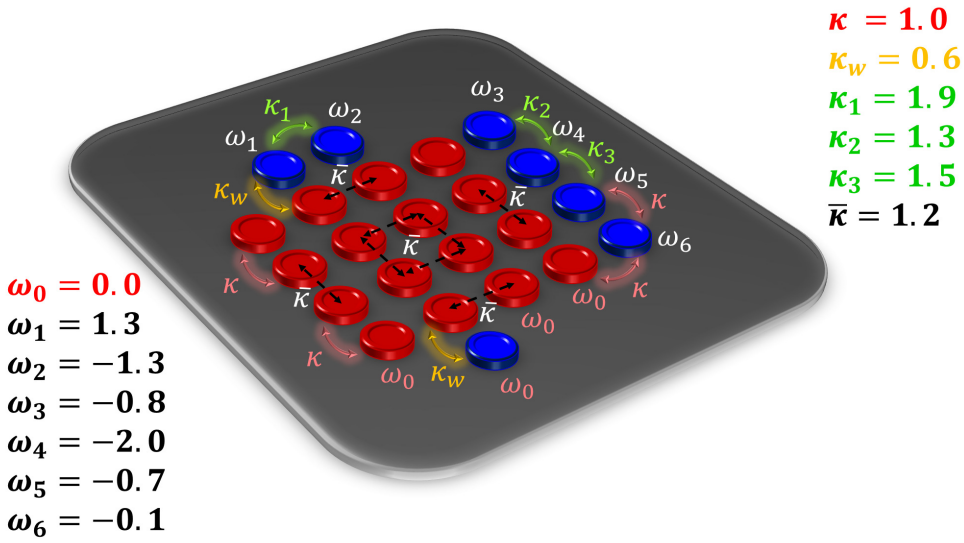

Figure 5.5: A schematic representation of a 4×4 bosonic J_x laser array (red cavities) interacting with reservoir made of seven resonators (blue). The normalized frequencies and coupling coefficients are depicted in the figure. Note that the coupling profile of the main array is no longer uniform. Here, the optical loss coefficients of the optical resonators associated with the laser array and the reservoir are assumed to be $\gamma = 0.1$ and $\gamma_R = 0.4$, respectively.

material, the number of distinct eigenvalues in an $N \times N$ bosonic array is given by $2N - 1$. Thus for example, while a uniform 4×4 structure has nine different eigenvalues, its counterpart array will have only 7 different eigenvalues. This in turn can lead to a further simplification of the reservoir design. We verify this for a bosonic laser array as shown in figure 5.5. Similar to the 3×3 case, here also we find that adding an extra resonator can enhance the single mode performance and we thus end up with 7 optical cavities in the reservoir instead of 6.

The eigenvalue distribution of the structure shown in figure 5.5 reveals that in this case also only one mode will start to lase as gain is applied. Again, similar to our previous discussion, there is more than one way of engineering the reservoir and its

coupling to the main array. An optimal design thus requires carrying out optimization analysis which we consider elsewhere.

We note that building 2D bosonic arrays similar to those discussed here is not fundamentally different from building uniform arrays. In the former, the separation between the resonators has to be carefully adjusted in order to produce the desired coupling profile which has been shown to be possible in 1D [27].

Finally, it would be of interest to compare the far field emission pattern from J_x and uniform laser arrays. However, this comparison cannot be carried out based on coupled mode analysis or laser rate equations, instead one has to consider a particular implementation and use full wave analysis which we plan to investigate in subsequent publication.

5.4 Emission dynamics

So far, we have investigate the single mode behavior of the engineered laser arrays below or at the lasing threshold where the system can be treated by using linear coupled mode theory. However, laser dynamics above threshold are intrinsically nonlinear [12, 30] and the lasing emission in this regime cannot be deduced from the linear analysis. Here we explore the nonlinear behavior of the laser structures proposed in this work in order to demonstrate that the single transverse mode emission persists in the existence of nonlinearity and quantify the range of single mode operation as

a function of the applied gain. While different models for laser nonlinearities do exist, here we consider a scenario where the carrier dynamics are very fast and can be integrated out of the laser rate equations. We thus consider a system of equations similar to Eq.(5.1) except that the linear gain coefficient is replaced by a nonlinear gain saturation term:

$$i\frac{da_{m,n}}{dt} = (\omega_0 - i\gamma + \frac{ig}{1+\alpha|a_{m,n}|^2})a_{m,n} + \sum_{m'.n'} \kappa_{m,n}^{m',n'} a_{m,n} \tag{5.3}$$

where α is the gain saturation coefficient. For the reservoir resonators, the coefficient γ is replaced by γ_R. To illustrate the nonlinear emission dynamics, we consider example of 3×3 laser array depicted in figure 3. By integrate equation (3) for that specific structure starting from random noise, we obtain the temporal evolution of the field intensities inside each resonator in the laser array as shown in figure 6. In this simulation, the gain coefficient was assumed to be $g = 0.4$ and the gain saturation coefficient was taken to be $\alpha = 1.0$.

In order to confirm that lasing mode is indeed the fundamental state with all the optical fields in different resonators oscillating in phase, we have also checked the phase dynamics (not shown here) of the field amplitudes and we observed in-phase oscillations with very small differences between the phases of the individual elements, which is consistent with the eigenmode analysis we have discussed in Sec. 2.1. This feature is crucial in order to ensure that light emitted from different cavities will add

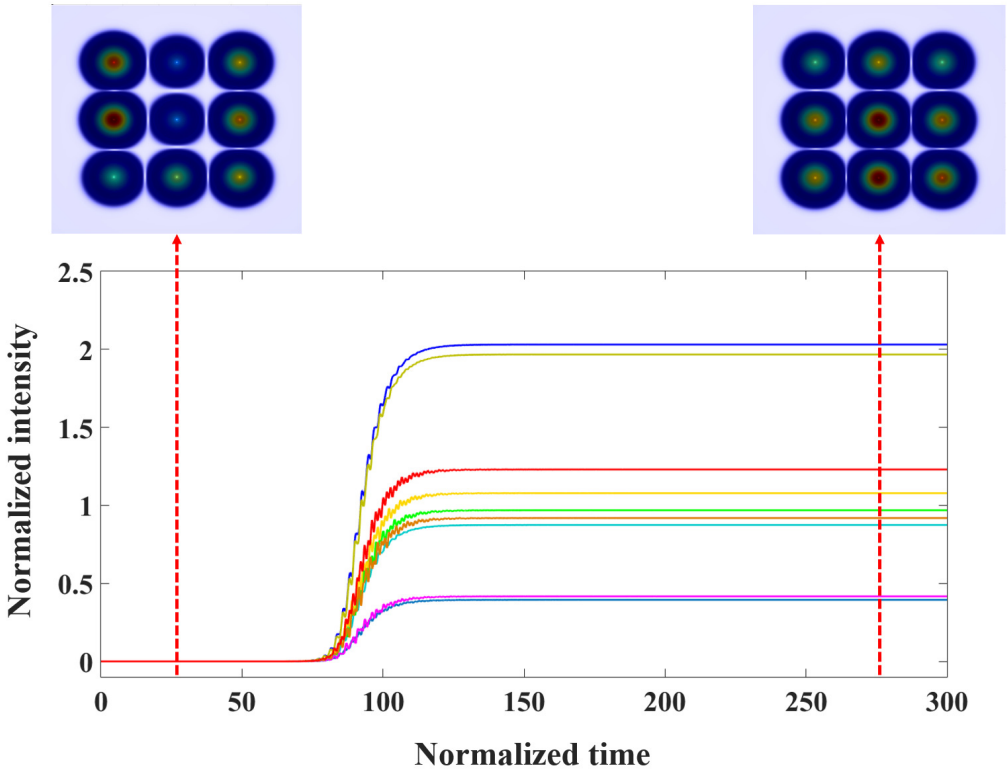

Figure 5.6: Nonlinear dynamics of optical intensities in the 3×3 laser array shown in figure 3 with the discrete reservoir taken into account. Here we also depict the temporal snapshots of the lasing pattern $|a_{m,n}|^2$ at different times where steady state single mode emission can be observed after a transient period.

constructively at the center of the far field emission plane. This in turn results in a far field bright spot that has an intensity proportional to the square of the number of elements in the array, i.e. $\sim N^4$. In practice however, due to the unequal amplitude distribution between the resonators (see figure 5.6), the intensity of bright spot will be less than N^4.

Our time-dependent simulations show that the single mode operation persists even when the gain is increased to more than two times its threshold value. To confirm

these results, we use techniques similar to those employed in the Stead-state Ab-initio Laser Theory (SALT) [31, 32] to calculate the steady state solutions which indeed confirms that the single mode operation extend in the range $0.18 \leq g \leq 0.5$. Interestingly, that range can be even significantly extended if the extra resonator on the right is removed and one of the coupling coefficients between the reservoir chain at the bottom is changed to $\kappa = -1.0$. While negative coupling is not common in microring and microdisk platforms, it can be engineered in photonic crystal cavities [33, 34]. We also note that if we had chosen to pump the laser array as well as the reservoir, we find a much narrower range of single-mode operating, i.e., $0.16 \leq g \leq 0.32$. We have also carried out similar simulations for the case of 4×4 arrays and Bosonic 4×4 and we have observed single mode operation for different range of the gain coefficient $0.13 \leq g \leq 0.25$ and $0.13 \leq g \leq 1.4$, respectively.

5.5 Appendix A: Householder Method

Householder method was introduced by A. S. Householder in 1985 [19] and has an extensive application in linear algebra such as carrying out of the QR decomposition in numerical algebra. In this section we present a Matlab code for Householder method and we use it to transform a given Hamiltonian matrix of a 2D laser array to a tridiagonal Hamiltonian.

Here, for any given input matrix A of size $n \times n$, one can perform Householder transformation as follows to achieve a tridiagonal matrix with the same eigenvalue spectrum.

```
[n,n]=size(A);
for k=1:n-2
    X=A(:,k);
    ss=0;
    for j=k+1:n
        ss=ss+X(j)^2;
    end
    S=sign(X(k+1))*sqrt(ss);
    R=sqrt(2*(S+X(k+1))*S);
    W=X;
    W(1:k)=0;
    W(k+1)=W(k+1)+S;
    W=(1/R)*W;
    V=A*W;
    c=W'*V;
    Q=V-c*W;
    A=A-2*W*Q'-2*Q*W';
end
```

Figure 5.7: MATLAB code for any given input matrix A of size $n \times n$.

Appendix B: Eigenvalue degeneracy in square arrays

The eigenstate degeneracy of uniform square arrays can be in general investigated by using the point group [8]. Other symmetry groups have to be considered for arrays having different topologies. However here, and since we focus on square arrays only, we discuss this feature by using an alternative straightforward algebraic method. At lasing threshold $\gamma = g$, equation (5.1) written in the rotating frame, takes the form: $i\frac{da_{m,n}}{dt} = (\kappa_{m,n}^{m-1,n}a_{m-1,n} + \kappa_{m,n}^{m+1,n}a_{m+1,n} + \kappa_{m,n}^{m,n-1}a_{m,n-1} + \kappa_{m,n}^{m,n+1}a_{m,n+1})$. By using separation of variable $a_{m,n} = \phi_m(t)\eta_n(t)$ and substituting back, it is straightforward to show that:

$$\begin{aligned} &\frac{1}{\eta_n}\{i\frac{d\phi_m}{dt} - (\kappa_{m,n}^{m-1,n}\phi_{m-1} + \kappa_{m,n}^{m+1,n}\phi_{m+1})\}+ \\ &\frac{1}{\phi_m}\{i\frac{d\eta_n}{dt} - (\kappa_{m,n}^{n-1}\eta_{m,n-1} + \kappa_{m,n}^{n+1}\eta_{m,n+1})\} = 0 \end{aligned} \tag{5.4}$$

In the most general case, the two terms in the brackets cannot be satisfied independently. However, for square arrays with identical rows and identical columns, i.e. $\kappa_{m,n}^{m\pm1,n} = \kappa_{m,n'}^{m\pm1,n'} = T_m^{m\pm1}$ and $\kappa_{m,n}^{m,n\pm1} = \kappa_{m',n}^{m',n\pm1} = J_n^{n\pm1}$, the two terms become independent and we obtain:

$$
\begin{aligned}
i\frac{d\phi_m}{dt} &= (T_m^{m-1}\phi_{m-1} + T_m^{m+1}\phi_{m+1}) \\
i\frac{d\eta_n}{dt} &= (J_n^{n-1}\eta_{n-1} + J_n^{n+1}\eta_{n+1})
\end{aligned}
\tag{5.5}
$$

Evidently if μ_m and μ_n are the eigenvalues associated with equations of (5.5), respectively, i.e. $\phi_m = \phi_0 exp(i\mu_m t)$ and $\eta_n = \eta_0 exp(i\mu_n t)$, it follows that the eigenvectors of full system satisfy $a_{m,n} = \phi_0 exp(i(\mu_m + \mu_n)t)\eta_0$ and the associated eigenvalues are given by $\mu_{m,n} = \mu_m + m_n$. Degeneracies thus occur whenever $\mu_m + \mu_n = \mu_{m'} + \mu_{n'}$ for any integer indices m, n, m' and n'.

Square uniform arrays

From the above analysis, it is clear that $\mu_{m,n} = \mu_{n,m}$. Also in the absence of any accidental degeneracy, the eigenvalues $\mu_{m,m}$ are unique. In addition, if one writes equations (5.5) in Hamiltonian forms, i.e. $i\frac{d\phi}{dt} = H_\phi\phi$ and $i\frac{d\eta}{dt} = H_\eta\eta$, it is easy to show that $\{\sigma_z, H_{\phi,\eta}\} = 0$ where $\sigma_z = \delta_{ij}(-1)^{i+1}$ and the brackets $\{\}$ denote anti-commutation. In other words, the Hamiltonians $H_{\phi,\eta}$ respects chiral particle-hole symmetry: each positive eigenvalue must be accompanied by a negative eigenvalue [9]. Consequently, the eigenspectrum is symmetric about the zero value. If the integer N is even, the eigenvalues of $H_{\phi,\eta}$ will not include any zero value and the null eigenvalues of the 2D system will be only of the form $\mu_{m,-m}$. As a result, the

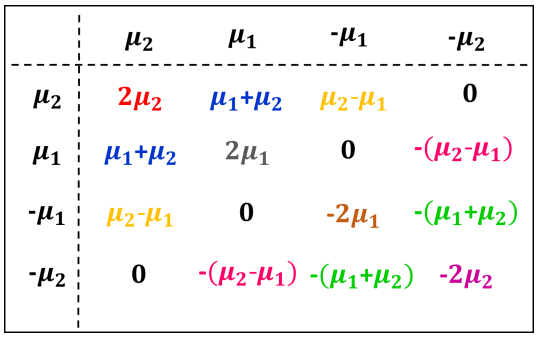

Figure 5.8: Eigenvalue structure of a 4×4 uniform square array. Nine distinct eigenfrequencies exist as highlighted by the different colors..

system will exhibit N unique eigenvalues of the form $\mu_{m,m}$, zero eigenvalues and doubly degenerate eigenvalues of the form $\mu_{m,n} = \mu_{n,m}$. The total number of distinct eigenvalues are thus given by $N + 1 + \frac{N^2-N}{2} = \frac{N^2+2}{2}$. We illustrate this results by the chart shown in figure 5.8 for the array where degenerate eigenvalues having the same values are highlighted with similar colors. Similar considerations applies for the case of odd value of N except that we must take into account that here the particle-hole symmetry forces one of the eigenvalues of $H_{\phi,\eta}$ to be zero and thus resulting in an additional accidental degeneracy. In that case, the total number of distinct eigenvalues turns out to be $\frac{N^2+2}{2}$. By applying these formulas for the two square arrays discussed in section two, we indeed find that the 3×3 and 4×4 arrays exhibit five and nine distinct eigenvalues, respectively.

We note that in the above analysis, we have assumed that apart from the zero eigenvalue dictated by the chiral symmetry in the case when N is odd, no other accidental degeneracy arises. Figure. 5.9 illustrates these degeneracy for the case of 4×4 array where only nine distinct eigenfrequencies exist.

	3Δ	Δ	−Δ	−3Δ
3Δ	6Δ	4Δ	2Δ	0
Δ	4Δ	2Δ	0	−2Δ
−Δ	2Δ	0	−2Δ	−4Δ
−3Δ	0	−2Δ	−4Δ	−6Δ

Figure 5.9: Eigenvalues of a 4×4 bosonic array where only seven distinct eigenfrequencies exist. Here we have an equidistant eigenvalue spectrum for J_x laser array and 2Δ corresponds to the eigenvalue ladder steps associated with the 1D Hamiltonians $H_{\phi,\eta}$.

Square bosonic arrays

The above discussion applies equally for the square bosonic arrays introduced in section 3. However, here in addition to the geometric induced degeneracies, accidental degeneracies also occur. In the other words, in bosonic arrays, the condition $\mu_m + \mu_n = \mu_{m'} + \mu_{n'}$ can be satisfied for a set of modes (characterized by the indices m, n, m' and n') that do not necessarily transform into one another under geometric operations such as reflection and rotation. In particular, due to the equidistant eigenvalue ladder of one dimensional bosonic arrays, the degeneracy condition $\mu_m + \mu_n = \mu_{m'} + \mu_{n'}$ in two dimensional configurations holds when $m + n = m' + n'$. By taking these accidental symmetries into account, we find that the total number of non-degenerate eigenstates in an $N \times N$ bosonic array is given by $2N - 1$. Figure. 5.9 illustrates these degeneracy for the case of 4×4 bosonic array where only seven distinct eigenfrequencies exist.

Appendix C: Absence of degeneracy in 1D discrete systems

As we have discussed in the main text, the eigenspectrum of one dimensional systems do not exhibit any degeneracies. For completeness, we present here a simple proof of this known fact. A 1D discrete system is described by a tridiagonal matrix. For any given eigenvalue, the elements of the corresponding eigenvectors can be expressed in terms of that eigenvalue, the matrix elements and the first component of that eigenvector which can be chosen arbitrarily. Now assume that there exist two different eigenvector that correspond to the same eigenvalue. Due to the linearity of the problem, we can scale the first component of the second eigenvector to match that of the first. But as a result, the rest of the components of the eigenvectors will be equal after the scaling. This in turn means that the original different eigenvectors were related by a constant multiplication factor and hence are basically the same. We note that these restrictions that lead to the impossibility of degeneracy in 1D systems are lifted in higher dimensions where degeneracy is allowed.

References

[1] Tatum, J. A. Evolution of VCSELs, Proc. SPIE 9001, 90010C-190010C-9 (2014).

[2] Fryslie, Stewart T. M. and Choquette, K. D. Breakthroughs in Photonics 2014: Coherent Vertical-Cavity Surface-Emitting Laser Arrays. IEEE Photonics Journal 7, (2015).

[3] Marciante, J. R. and Agrawal, G. P. Nonlinear mechanisms of filamentation in broad-area semiconductor lasers. IEEE Journal of Quantum Electronics 32, 590-596 (1996).

[4] Cheng, D.-L., Liu, E.-C. and Yen, T.-C. Single Transverse Mode Operation of a Self-Seeded Commercial Multimode VCSEL. IEEE Photonics Technol. Lett. 16, 278-280 (2002).

[5] Marino, F., Barland, S. and Balle, S. Single-mode operation and transverse-mode control in VCSELs induced by frequency-selective feedback. IEEE Photonics Technol. Lett. 15, 789-791 (2003).

[6] Hsu, C. P., Yen, T. C., Cheng, D.L. and Kuo, W. C. Multimode Suppression of a Vertical-CavitySurface-Emitting Laser by a Single-Mode Fiber Cavity. IEEE Photonics Technol. Lett. 22, 233-235 (2010).

[7] Chembo, Y. K., Mandre, S. K., Fischer, I., Elssser, W. and Colet, P. Controlling the emission properties of multimode vertical-cavity surface-emitting lasers via polarization- and frequency-selective feedback. Phys Rev. A. 79, 013817-10 (2009).

[8] Carroll, J.E., Whiteaway, J.E.A. and Plumb, R.G.S. Distributed Feedback Semiconductor Lasers (The Institution of Engineering and Technology, 1998).

[9] Shang, L., Liu, L. and Xu, L. Single-frequency coupled asymmetric microcavity laser. Opt. Lett. 33, 1150-1152 (2008).

[10] Feng, L., Wong, Z. J., Ma, R., Wang, Y. and Zhang X. Single-mode laser by parity-time symmetry breaking. Science 346, 972-975 (2014).

[11] Hodaei, H., Miri, M.A., Heinrich, M., Christodoulides, D.N. and Khajavikhan, M. Parity-timesymmetric microring lasers. Science 346, 975-978 (2014).

[12] Wang S. S. and Winful, H. G. Dynamics of phaselocked semiconductor laser arrays. Appl. Phys. Lett. 52, 17741776 (1988).

[13] Chumakov, S.M. and Wolf, K.B. Supersymmetry in Helmholtz optics. Phys. Lett. A, 193, 51-53 (1994).

[14] Miri, M.A., Heinrich, M., El-Ganainy, R. and Christodoulides, D.N. Supersymmetric optical structures. Phys. Rev. Lett. 110, 233902-1 233902-5 (2013).

[15] Heinrich, M. et al. Supersymmetric mode converters. Nature Communications 5, 3698 1-5 (2014).

[16] Longhi, S. Bloch oscillations in tight-binding lattices with defects. Phys Rev. A. 81, 195118-1 195118-6 (2010).

[17] Teimourpour, M. H., Christodoulides, D. N. and El-Ganainy, R. Optical revivals in nonuniform supersymmetric photonic arrays. Opt. Lett. 41, 372-375 (2016).

[18] El-Ganainy, R., Ge, L., Khajavikhan, M. and Christodoulides, D. N. Supersymmetric laser arrays. Phys. Rev. A 92, 033818-1033818-9 (2015).

[19] Householder, A.S. Unitary Triangularization of a Nonsymmetric Matrix. Journal of the ACM 5, 339342 (1958).

[20] Messiah, A. Quantum mechanics. 98-106 (Amsterdam: North-Holland Publishing Company, 1967).

[21] Hassan, A.U., Hodaei, H., Miri, M.A., Khajavikhan, M. and Christodoulides, D.N. Nonlinear reversal of the PT-symmetric phase transition in a system of coupled semiconductor microring resonators. Phys Rev.A. 92, 063807 (2015).

[22] Ge, L. and El-Ganainy, R. Nonlinear modal interactions in parity-time (PT) symmetric lasers. Sci. Rep. 6, 24889 (2016).

[23] Yu, S., Piao, X., Hong, J. and Park, N. Network-inspired design of broadband materials with reduced dimensionality. arXiv:1601.05635.

[24] Liew, S. F., Ge, L., Redding, B., Solomon, G. S. and Cao H. Pump-controlled modal interactions in microdisk lasers. Phys. Rev. A 91, 043828-1 043828-9 (2015).

[25] Aung, N. L., Ge, L., Malik, O., Treci, H. E. and Gmachl, C. F. Threshold current reduction and directional emission of deformed microdisk lasers via spatially selective electrical pumping. Appl. Phys. Lett. 107, 151106-1 151106-5 (2015).

[26] Christandl, M., Datta, N., Ekert, A. and Landahl, A. J. Perfect State Transfer in Quantum Spin Networks. Phys. Rev. Lett. 92, 187902-1 187902-4 (2004).

[27] Perez-Leija, A. P. et al. Coherent quantum transport in photonic lattices, Phys. Rev. A 87, 012309-1 012309-8 (2013).

[28] El-Ganainy, R., Eisfeld, A., Levy, M. and Christodoulides, D.N. On-chip non-reciprocal optical devices based on quantum inspired photonic lattices. App. Phys. Lett. 103, 161105-1 161105-3 (2013).

[29] Teimourpour, M. H., El-Ganainy, R., Eisfeld, A., Szameit, A. and Christodoulides, D. N., Light transport in PT -invariant photonic structures with hidden symmetries. Phys Rev. A. 90, 053817-1 053817-6 (2014).

[30] Siegman, A. E. Lasers. (University Science Books, 1986).

[31] Tureci, H. E., Ge, L., Rotter, S. and Stone, A. D. Strong interactions in multi-mode random lasers Science 320, 643-646 (2008).

[32] Ge, L., Chong, Y. D., and Stone, A. D. Steady-state ab initio laser theory: Generalizations and analytic results. Phys. Rev. A 82, 063824-1 063824-15 (2010).

[33] Caselli, N. et al. Antibonding ground state in photonic crystal molecules. Phys. Rev. B 86, 035133-1 035133-4 (2012).

[34] Haddadi, S. et al. Photonic crystal molecules: tailoring the coupling strength and sign. Opt. Express 22, 12359-12368 (2014).

[35] Tinkham, M. Group Theory and Quantum Mechanics. (Dover Publications, 2003).

[36] Ryu, S. and Hatsugai, Y. Topological Origin of Zero-Energy Edge States in Particle-Hole Symmetric Systems. Phys. Rev. Lett. 89, 077002-1 077002-4 (2002).

Chapter 6

Laser self-termination in trimer photonic molecules

Semiconductor lasers are playing an ever increasing role in a wide range of applications such as optical communication, medical diagnostics and sensing to just mention few examples. Current commercial on-chip semiconductor laser platforms which typically fall into one of two categories: edge or surface emitting devices have reached a high degree of maturity [1, 2, 3, 4, 5, 6, 7]. However, the increasing demand for new miniaturized laser sources having special emission characteristics, low pumping thresholds and fast response time scales has led to intense activities in engineering new micro and nano-laser geometries that can meet these requirements. In parallel with these efforts, various techniques to control laser emissions and mode selectivity have been

recently also pursued (see for example the recent work on using supersymmetry to engineer single mode laser arrays [8, 9]). An approach that was explored earlier [10] and gained more popularity recently is inhomogeneous pumping which demonstrates promising results in controlling emission from random lasers [11, 12, 13, 14, 15].

One of the most peculiar effects associated with laser operation under inhomogeneous pump is the process of laser self-termination in two coupled cavities which was theoretically predicted based on laser nonlinear models [16]. In this setup, when the first cavity is pumped while the second is kept passive, the system starts to lase after a certain pump threshold. When this pump level is kept fixed and the pump in the second cavity is increased adiabatically from zero, the lasing actions is terminated at certain pump value despite the increase in the total pump power. On first sight, this effect might seem to resemble the well-known phenomenon of oscillation death whereby two nonlinear oscillatory system come to a halt when coupled. However, careful investigations have shown that LST is a purely linear effect, usually associated with exceptional points or avoided crossings [17]. Experimental observations of LST in both photonics and electronics systems were reported in [18, 19] while the closely related effect of loss induced lasing was observed in [20]. Interestingly, an analogous effect has been also observed in transmission geometries outside the context laser physics [21]. We note that all the above cited work dealt with only two coupled cavities.

In this letter, we investigate LST in a more complex structure made of three coupled cavities. We show that here also LST is possible and is associated with avoided level crossing (ALC) where the eigenvalues only approach each others within a specific region in the parameter space before they divert again without crossing effect often called level repulsion. Our results indicate, that in contrast to the two identical cavities case, careful tuning is required to observe LST in three-cavity setup. Finally, we provide analytical insight into system's behavior by using adiabatic elimination. These results can be of importance for future investigations of complex non-Hermitian optical networks [23].

6.1 System and numerical results

To this end, we consider the system shown in Fig.6.1. It consists of three coupled optical cavities with coupling coefficients J and κ , respectively. Within temporal coupled mode formalism [17, 22], this system can be described by:

$$i\frac{d\vec{c}}{dt} = H\vec{c},\ H = \begin{pmatrix} i(g_1 - \gamma_1) & J & 0 \\ J & \Delta\omega - i\gamma_2 & \kappa \\ 0 & \kappa & \Delta\omega + i(g_3 - \gamma_3) \end{pmatrix} \tag{6.1}$$

where H is the Hamiltonian matrix, $\vec{c} = [c_1\ c_2\ c_3]^T$ is the electric field amplitude

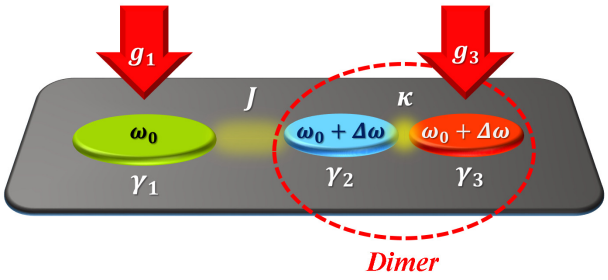

Figure 6.1: A schematic of the laser structure investigated in this work. It consists of three coupled optical cavities having coupling coefficients J and κ where $J << \kappa$. The cavity losses are denoted by $\gamma_{1,2,3}$. Both the middle and the right cavities are detuned by $\Delta\omega$ with respect to the first cavity. Finally, $g_{1,3}$ indicate the gain provided by the pumping in the first and third cavities, respectively.

vector and t is the time. We assume that the second and third cavities are identical and both have frequency detuning $\Delta\omega$ with respect to the first. We further denote the loss and gain coefficients of the cavities by γ_n and g_n with $n = 1, 2$ or 3 being an index referring to the different cavities. Note that Eq.(6.1) is written in a frame rotating with ω_0.

In what follows we consider a parameters regime where $J << \kappa$ and $0 < \sqrt{\kappa^2 - (\frac{\gamma_2 - \gamma_3}{2})^2} - \Delta\omega << 1$. The exact numerical values that we use are listed in the figure caption of Fig. 6.2. Our choice of parameters ensures that the resonant frequency of cavity 1 is close to the lower eigenfrequency of the dimer formed by the other two cavities when $J = 0$.

Figures 6.2 (a) and (b) depict the behavior of the real and imaginary parts of the three eigenfrequencies Ω_n of H as a function of the two pump powers of the first and third cavities as expressed in terms of gain coefficients $g_{1,3}$ when the middle

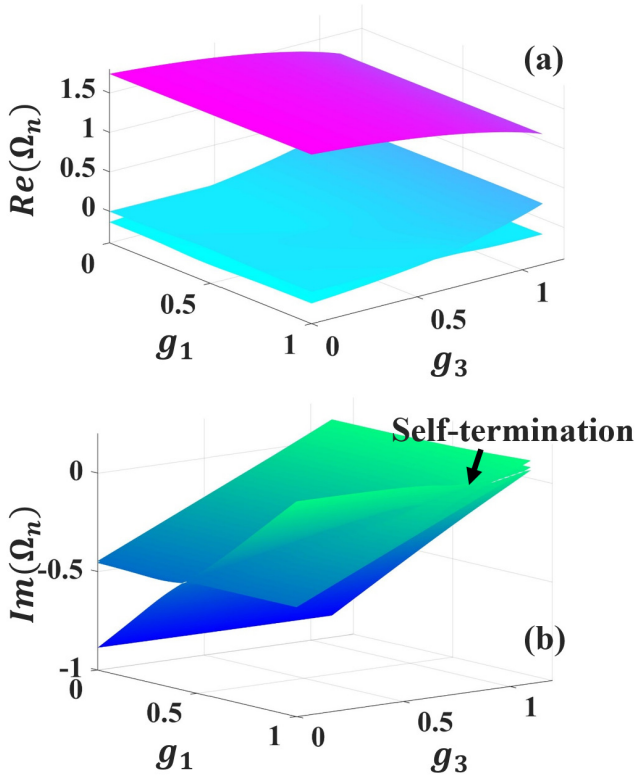

Figure 6.2: Real (a) and imaginary (b) parts of the eigenvalues of the structure shown in Fig.6.1 as a function of the gain parameters $g_{1,3}$. The other parameters are $\kappa = 1$, $J = 0.1$, $\gamma_1 = 0.9$, $\gamma_2 = 0.79$, $\gamma_3 = 0.1$ and $\Delta\omega = 0.8$. As g_1 is increased while keeping $g_3 = 0$, the system reaches the lasing threshold when one of the eigenvalues crosses the imaginary zero axis. At this value, when g_1 is kept fixed and g_3 is increased, we observe laser self-termination as indicated in the lower panel despite the absence of exceptional points.

cavity remains passive at all time, i.e. $g_2 = 0$. We first focus on trajectory along the line $g_3 = 0$, where we observe that at a certain threshold value of $g_1 = 0.912$, one eigenvalue crosses the imaginary zero axis, signaling the onset of laser action. Any further increase of g_1 pushes the imaginary part of that eigenvalue upward. This however does not happen in reality since gain saturation effects lead to eigenvalue

clamping. We consider these nonlinear effects later.

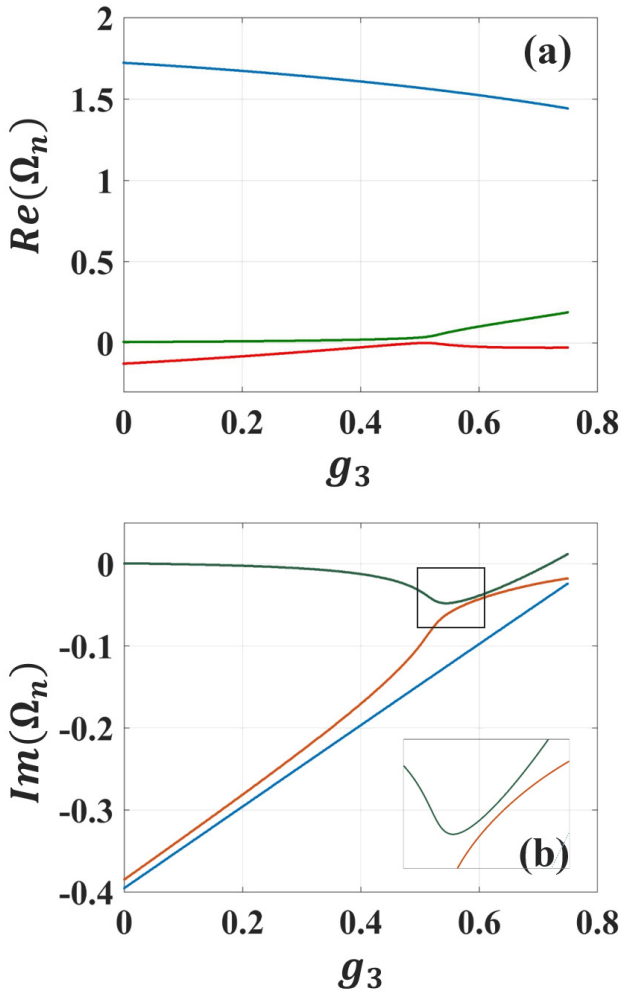

Figure 6.3: Real (a) and imaginary (b) parts of the eigenvalues of the structure shown in Fig.6.1 for $g_1 = 0.912$ as a function of the gain parameters g_3. The other parameters are the same as Fig.6.2. Insect provides a better view for avoided crossing level around $g_3 \approx 0.6$.

By fixing the value of g_1 slightly above its lasing threshold and increases g_3 gradually from zero, we observe a region along this trajectory where avoided level crossing takes place. Near this regime at $g_3 \approx 0.3$, the laser action is terminated as the imaginary

part of the eigenvalue ω_1 becomes negative. This is exactly the phenomenon of LST studied in [**?**] except that here it does not occur as a result of crossing exceptional points but is rather associated with avoided level crossing. As the pumping power of the third cavity is further increased, laser action starts again at $g_3 \approx 0.75$. In contrast to its counterpart effect in symmetric photonic molecules, the lasing revival here is a direct outcome of level repulsion and not due to exceptional points crossing. In order to further illustrate our results, we present plots of the real and imaginary parts of Ω_n as a function of g_3 across a section defined by $g_1 = 0.91$ (see Fig. 6.3). The inset in (b) depicts the details of the avoided crossing of imaginary part of the eigenvalues. Interestingly, along other cross sections, either the real or the imaginary parts of two eigenvalues might cross (not shown here). This is however still represents avoided crossing since for EP's, both the real and imaginary parts have to coalesce at the same point.

6.2 Reduced model via adiabatic elimination

The results presented in the previous section demonstrate clearly that some of the intriguing effects that has been previously associated with exceptional points can still survive when the system exhibit avoided level repulsion. Given the recent volume of work on the physics of exceptional points, we would like to develop more insight into our results beyond the numerical simulations. In this respect, Hamiltonian H can

be diagonalized analytically but that does not provide much insight either. Instead, here we adopt a different strategy that treats the interaction between cavity 1 and the dimer formed by cavities 2 and 3 perturbatively. This is facilitated by the fact that $J << \kappa$. This can be directly achieved via the similarity transformation

$$\tilde{H} = \begin{pmatrix} 1 & 0 \\ 0 & S^{-1} \end{pmatrix} H \begin{pmatrix} 1 & 0 \\ 0 & S \end{pmatrix} \approx \begin{pmatrix} i(\gamma_1 - g_1) & \frac{J}{\sqrt{2}} & \frac{J}{\sqrt{2}} \\ \frac{J}{\sqrt{2}} & \Omega_+ & 0 \\ \frac{J}{\sqrt{2}} & 0 & \Omega_- \end{pmatrix} \tag{6.2}$$

where the 2×2 block diagonal matrix $S = [\vec{V}_+, \vec{V}_-]$ and $\vec{V}_\pm = [1 \ \pm e^{\mp i\theta}]^T$ are the eigenvectors associated with the dimer when $J = 0$, with $\tan\theta = \gamma_0/\sqrt{\kappa^2 - \gamma_0^2}$ for $\kappa > |\gamma_0|$ and $\gamma_0 = \frac{\gamma_2 - \gamma_3 + g_3}{2}$. Furthermore, $\Omega_\pm = \Delta\omega + i(\gamma_2 - \gamma_0) \pm \sqrt{\kappa^2 - \gamma_0^2}$ are the eigenfrequencies associated with $\vec{V}_\pm$. The right hand side of Eq.(6.2) indicates that cavity 1 is now coupled to the complex supermodes of the dimer with renormalized coupling coefficients $J/\sqrt{2}$. If the frequency detuning between cavity 1 and any of the supermodes $\Omega_\pm$ is large, the effect of this mode can be adiabatically eliminated. For the chosen set of parameters, this is indeed the case for supermode Ω_+ as represented schematically in Fig.6.4.

From this analysis, and by inspecting the expression for Ω_-, it is clearly that the effect

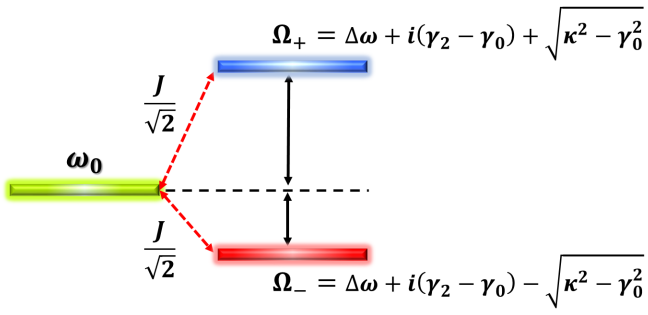

Figure 6.4: A schematic of the coupling profile as represented by the transformed Hamiltonian $\tilde{H}$ of Eq.(6.2) where the eigenstate of cavity 1 is coupled to the two supermodes of the dimer (having eigenfrequencies of $\Omega_\pm$) with an effective coupling of $J/\sqrt{2}$

of increasing g_3 from zero is to increase Ω_-. As the value of Ω_- approaches that of ω_0, the two modes interact stronger. Since mode Ω_- exhibits a net loss, it leads to laser self-termination (around $g_3 \approx 0.3$ in our simulations). On the other hand, the small effect of the adiabatically eliminated mode on the rest of the system prevents the formation of an exceptional point. As g_3 is further increased, the strcuture starts to lase again after a second threshold given by $g_3 \approx 0.82$. This behavior is also similar to the photonic molecule case studied in [**?**] but without any exceptional points.

6.3 Nonlinear gain saturation effect

So far we have focused only on a linear model for the laser system and we have investigated its spectral features. For sake of completeness, we now treat the more general case of laser rate equations that involves nonlinear gain saturation effects. We do this by modifying the gain coefficient in Eq.(6.1) according to $g_n/(1+\alpha|c_n|^2)$,

where α is the gain self saturation factor whose normalized value we take to be 0.1.

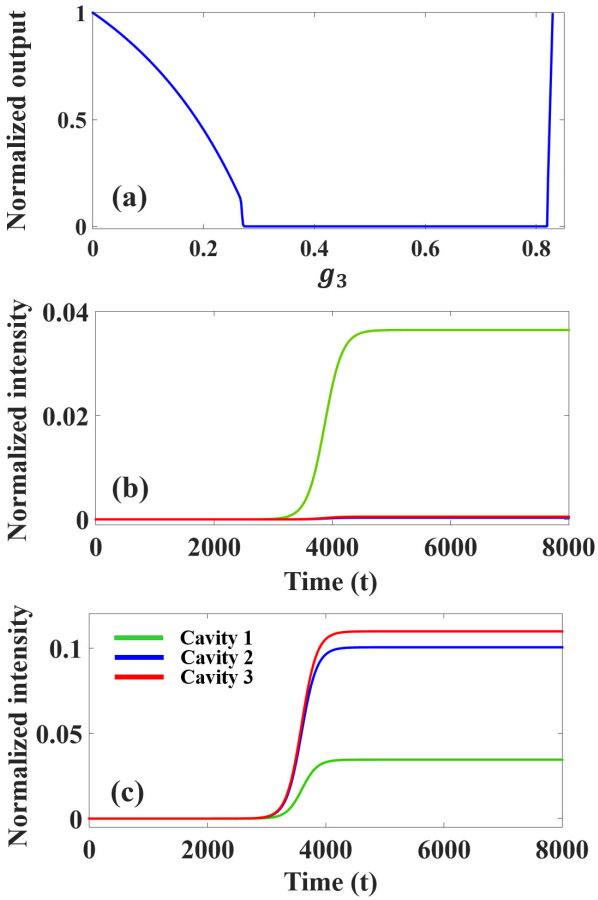

Figure 6.5: (a) Normalized output power of the first cavity before and after LST versus g_3, clearly self termination occurs for $0.2 \leq g_3 \leq 0.8$. Dynamics of the normalized intensity before ($g_3 = 0.1$) and after ($g_3 = 0.82$) self termination is depicted in (b) and (c) respectively.

Figure 6.5 (a) shows a plot of the normalized lasing intensity as a function of g_3 for the same parameters used previously. Evidently, the gain saturation terms do not alter our conclusion about the LST effect which occurs almost in the range of g_3 ($0.2 \leq g_3 \leq 0.8$) as predicted by the linear model. Figures 6.5 (b) and (c) depict the nonlinear lasing dynamics for two points on the curve in (a) when $g_3 = 0.1$ (before

the self-termination) and $g_3 = 0.82$ (after the self-termination). In the former case, only cavity 1 mainly participates in the lasing action while in the latter, the intensity distribution is more uniform.

As a final remark, we note that the effect of LST in the studied system occurs for a wide range of parameters. The particular values used here in this work were chosen best illustrate our results.

References

[1] G. P. Agrawal and N. K. Dutta, *Semiconductor Lasers*, (Springer Science and Business Media, 2013).

[2] J. Ohtsubo, *Semiconductor Lasers: Stability, Instability and Chaos*, (Springer Berlin Heidelberg, 2005).

[3] E. Kapon, *Semiconductor Lasers I: Fundamentals*, (Academic Press, 1999).

[4] H. Ghafouri-Shiraz, *Distributed Feedback Laser Diodes and Optical Tunable Filters*, (John Wiley and Sons, 2004).

[5] J. Faist *Quantum Cascade Lasers*, (Oxford University Press, 2013).

[6] H. Dalir and F. Koyama, "29 GHz directly modulated 980 nm vertical-cavity surface emitting lasers with bow-tie shape transverse coupled cavity," Appl. Phys. Lett. 103, 091109 (2013).

[7] H. Dalir and F. Koyama, "High-speed operation of bow-tie-shaped oxide aperture VCSELs with photonphoton resonance," *Appl. Phys. Express* 7, (2014).

[8] R. El-Ganainy, L. Ge, M. Khajavikhan, and D. N. Christodoulides, "Supersymmetric laser arrays," *Phys. Rev. A* **92**, 033818 (2015).

[9] M. H. Teimourpour, L. Ge, D. N. Christodoulides, R. El-Ganainy, "Non-Hermitian engineering of single mode two dimensional laser arrays," *Sci. Rep.* **6**, 33253 (2016).

[10] E. Kapon, C. Lindsey, J. Katz, S. Margalit, and A. Yariv, "Chirped arrays of diode lasers for supermode control," *Applied Physics Letters* 45, 10.1063/1.95209, (1984).

[11] X. Wu, J. Andreasen, H. Cao, and A. Yamilov, "Effect of local pumping on random laser modes in one dimension," *J. Opt. Soc.Am. B*, 24, A26 (2007).

[12] J. Andreasen, C. Vanneste, L. Ge, and H. Cao, "Effects of spatially nonuniform gain on lasing modes in weakly scattering random systems," *Phys. Rev. A*, 81, 043818 (2010).

[13] L. Ge, Y. D. Chong, S. Rotter, H. E. Tureci, and A. D. Stone, "Unconventional modes in lasers with spatially varying gain and loss," *Phys. Rev. A*, 84, 023820 (2011).

[14] T. Hisch, M. Liertzer, D. Pogany, F. Mintert, and S. Rotter, "Pump-Controlled Directional Light Emission from Random Lasers," *Phys. Rev. Lett.*, 111, 023902 (2013).

[15] S. F. Liew, B. Redding, L. Ge, G. S. Solomon, and H. Cao, "Active control of emission directionality of semiconductor microdisk lasers," *Applied Physics Letters*, 104, 231108 (2014).

[16] M. Liertzer, L. Ge, A. Cerjan, A. D. Stone, H. E. Treci, and S. Rotter, "Pump-induced exceptional points in lasers," *Phys. Rev. Lett.* **108**, 173901 (2012).

[17] R. El-Ganainy, M. Khajavikhan, and L. Ge, "Exceptional points and lasing self-termination in photonic molecules," *Phys. Rev. A* **90**, 013802 (2014).

[18] M. Brandstetter, M. Liertzer, C. Deutsch, P. Klang, J. Schberl, H. E. Treci, G. Strasser, K. Unterrainer and S. Rotter, "Reversing the pump dependence of a laser at an exceptional point," *Nat. Commun.* **5**, 4034 (2014).

[19] M. Chitsazi, S. Factor, J. Schindler, H. Ramezani, F. M. Ellis, and T. Kottos, "Experimental observation of lasing shutdown via asymmetric gain," *Phys. Rev. A* **89**, 043842 (2014).

[20] B. Peng, . K. zdemir, S. Rotter, H. Yilmaz, M. Liertzer, F. Monifi, C. M. Bender, F. Nori, L. Yang, "Loss-induced suppression and revival of lasing," *Science* **346**, 328 (2014).

[21] A. Guo, G. J. Salamo, D. Duchesne, R. Morandotti , M. Volatier Ravat, V. Aimez , G. A. Siviloglou and D. N. Christodoulides, "Observation of PT-Symmetry Breaking in Complex Optical Potentials," *Phys. Rev. Lett.* **103**, 093902 (2009).

[22] W. Suh, Z. Wang anf S. Fan, "Temporal Coupled-Mode Theory and the Presence of Non-Orthogonal Modes in Lossless Multimode Cavities," IEEE JOURNAL OF Quantum Electronics, **40**, 1511, (2004).

[23] M.H Teimourpour, R. El-Ganainy, A. Eisfeld, A. Szameit, D. N. Christodoulides, "Light transport in PT-invariant photonic structures with hidden symmetries", *Physical Review A* **90**, 5 053817 (2014).

Chapter 7

Conclusion

In conclusion, this thesis is comprised of three main parts. In the forth chapter, we have investigated two different aspects of PT symmetric lasers: that of the robustness of their single mode operation and the possibility of a more versatile mode selectivity based on generalized loss engineering scheme [1]. We have shown that in general, multimode operation can be triggered by instabilities arising from nonlinear modal interactions. By performing linear stability analysis and presenting the stability map under different conditions, we found that PT symmetry can provide superior performance and robust single mode operation (compared to single cavities) in systems made from microcavities having relatively large FSR. For systems made of long resonators with large optical path between roundtrips, the situation might be different. For example, consider a microring resonator having a radius of $R = 10\mu m$ and a

typical waveguide-based edge emitting laser having a length of say $L = 1mm$. Rough estimations based on simplified models gives: $F \equiv FSR_{ring}/FSR_{strip} = \frac{L}{\pi R} \sim 30$. As a result, the optical modes in edge emitting lasers are more densely packed than those of microrings, resulting in larger r values and consequently stronger mode competition which eventually can lead to instabilities (see large r regimes in figures 3 and 4 in chapter four). Future experimental work using these platforms will definitely shed more light on performance of these systems. It will be also interesting to investigate nonlinear laser dynamics in complex laser networks having higher order exceptional points [2].

Additionally, we have investigated the possibility of controlling the lasing modes by employing a more general scheme of loss engineering. Our analysis shows that by carefully engineering the modal loss in the passive cavity independently from that associated with the active one, a secondary mode can be enhanced at the expense of fundamental mode. This can be achieved for instance by depositing meta-absorbers whose dispersion properties are tailored to match the frequency of the desired mode. The advantage of this approach is the possibility of tuning the absorption spectrum by means of geometric design of the absorbers. However, this can work only if the free spectral range of the cavity is larger than the bandwidth of th meta-absorbers. Another alternative is to use dopant material with narrow absorption bandwidth. However, this is a material-dependent approach and may not provide much flexibility.

A different possibility is to exploit the modal intensity distribution to design meta-absorbers that target only certain modes. This strategy has been employed recently in [3, 4]. This latter approach also opens the door for dynamically controlling the laser emission by using meta-absorbers made of material platforms whose electric properties can be tuned by carrier injection [5]. We explore some of these possibilities in future work.

Finally we note that even though we focused here only on two lasing modes, additional modes (longitudinal or transverse) can be treated exactly in the same manner after extracting their physical parameters (resonant frequencies, quality factors and coupling coefficients) using full electromagnetic simulations. Given that these modes will experience smaller gains, their effect is not expected to alter our results dramatically. In particular, they will change the boundaries between the different lasing regimes without affecting their existence.

In chapter five, we have proposed a new approach for building single mode two dimensional laser arrays based on engineering a discrete reservoir whose functionality is to suppress higher order lasing modes while leaving the fundamental mode almost intact [6]. Our approach builds on our recent work for one dimensional laser arrays [7] except that here we cannot use discrete supersymmetry directly. Instead we first apply the Householder algorithm to laser array in order to generate an isospectral 1D discrete structure which can be then used in conjunction with supersymmetry

to achieve single mode operation. Using the linear analysis at lasing threshold, we have shown that this technique indeed predicts single mode emission for 3×3 and 4×4 uniform arrays. We also demonstrated that using a special type of non-uniform arrays whose properties are derived by using bosonic algebra can result in a higher dimensional degenerate landscapes which in turn can lead to a simplified reservoir design. Additionally, we have confirmed the single mode operation of the proposed laser structures and studied their nonlinear dynamics under gain saturation for arbitrary initial conditions as noise. Our numerical investigations shows that a reasonable range of single mode operation is achievable in the 3×3 and 4×4 arrays.

While the approach proposed in this work can be applied in principle to any laser array system (microrings, microdisks, VCSELs or photonic crystals), general considerations must be taken into account during implementation. In particular, in order for the proposed structures to function as intended, the coupling coefficients between the different elements of the main array should be large compared to the bandwidth enhancement factor. Otherwise, the nonlinear evolution of the system can still result in chaotic emission. Another practical advantage for operating in the strong coupling regime is fabrication tolerances in the following sense. All the parameters of the auxiliary array (the reservoir) in the previous examples including the frequency detuning from ω_0 (the resonant frequency of the cavities the main array) are calculated in terms of some coupling coefficient which was taken to be unity. If this coupling coefficient is very small compared to ω_0, it will require a very high fabrication precession in order to

implement the new resonators with these small detuning values. On the other hand, if say $\kappa/\omega_0 \in [10^{-3}, 10^{-2}]$, we can roughly estimate that for an optical cavity with a characteristic length scale (radius of microring cavity for example) of $10\mu m$, the necessary change in the cavity dimension to produce the required frequency detuning will be of in the range between $10 - 100\ nm$ which can be achieved by using todays fabrication techniques. We note that the above discussion implies a coupling factors in the order of $0.1 - 1\ THz$ which has been already observed experimentally in transversely coupled VCSELs [8, 9] and in photonic crystal platforms [10]. Furthermore we note that the non-uniformity in the physical parameters (resonant frequencies, coupling coefficients, etc.) due to limited fabrication precision can be an important factor in determining the device performance. In our previous study of 1D SUSY laser arrays [7], we have shown that even with 10% disorder, single mode operation can be still achieved. We have confirmed here also that in the 2D case, single mode operation can be still obtained for different realizations with few percent of disorder. Finally we comment on the scalability of our approach. For any $N \times N$ square array (uniform or bosonic), the total number of resonators is N^2 but the number of resonators on the four edges is $4N - 4$. In the case of uniform arrays, despite the fact that the number of supermodes having distinct eigenvalues scales as $\sim N^2/2$ for large N (see appendix A), these modes can be still accessed and influenced by the reservoir since they are extended all over the array with finite intensity contribution at the edge elements. In the case of bosonic array, the number of modes with different

eigenfrequencies scales as $2N$ can be also accessed via the edge resonators. However it is important to note that for large N, disorder induced localization can render some of the modes inaccessible through the edge cavities- a limitation that persists in all systems made of large number of coupled oscillators. It is thus clear that this current work presents several opportunities as well as challenges that merit more theoretical and experimental investigations which we plan to carry elsewhere.

Finally, in chapter six, we have studied a photonic molecule laser structure made from three coupled optical cavities and shown that under certain condition, the process of laser self-termination can take place near avoided crossing as opposed to exceptional points [11]. In addition, we have also analyzed our results by employing a simple reduced model by using adiabatic elimination. Finally, we have demonstrated that the predicted effect survives after including the gain saturation nonlinearity. Our work complements the earlier work on the laser behavior around exceptional points and provides an insight into the behavior of non-Hermitian system.

References

[1] M. H. Teimourpour, M. Khajavikhan, D. N. Christodoulides, R. El-Ganainy, Robustness and mode selectivity in parity-time (PT) symmetric lasers, Scientific Reports 7 (1), 10756 (2017).

[2] Teimourpour, M.H., El-Ganainy, R., Eisfeld, A., Szameit, A., and Christodoulides, D. N. Light transport in PT-invariant photonic structures with hidden symmetries. Physical Review A **90**, 5 053817 (2014).

[3] Schlehahn, A. *et al.* Mode selection in electrically driven quantum dot microring cavities. Optics express **21**(13), 15951-15958 (2013).

[4] Feng, L. Wong, Z. J., Ma, R. M., Wang, Y., and Zhang, X. Single mode laser by parity-time symmetry breaking. *Science* **346**, 972-975 (2014).

[5] Gao, Z., Fryslie, S.T. M., Thompson, B. J., Carney, P. S., and Choquette, K. D. Parity-time symmetry in coherently coupled vertical cavity laser arrays. *Optica* **4**, 323-329 (2017).

[6] MH Teimourpour, L Ge, DN Christodoulides, R El-Ganainy, Non-Hermitian engineering of single mode two dimensional laser arrays, Scientific reports 6, (2017).

[7] El-Ganainy, R., Ge, L., Khajavikhan, M. and Christodoulides, D. N. Supersymmetric laser arrays. Phys. Rev. A 92, 033818-1033818-9 (2015).

[8] dalir

[9] Dalir, H. and Koyama, F. High-speed operation of bow-tie-shaped oxide aperture VCSELs with photonphoton resonance. Appl. Phys. Express 7, 022102-1 (2014).

[10] Majumdar, A. et al. Design and analysis of photonic crystal coupled cavity arrays for quantum simulation. Phys. Rev. B 86, 195312 (2012).

[11] M. H. Teimourpour, R. El-Ganainy, Laser self-termination in trimer photonic molecules, Journal of Optics 19 (7), 075801, (2017).